Naval Research Reviews

Office of Naval Research
Three/1982
Vol XXXIV

Special Issue On
Naval Environmental Sciences

The late Dr. Maurice Ewing (third from left) preparing to take a large water sample of deep Atlantic water from Woods Hole's **R/V Atlantis,** *circa 1952. Using the carbon 14 dating method, these samples were used to measure the residence time of the deep ocean water from sinking in the high latitudes to upwelling in the lower latitudes. The residence time was of the order of 500 years. This was the first measurement of the cycling time of these deep water masses.*

Dr. Ewing, who founded the Lamong-Doherty Geological Observatory of Columbia University, was one of the first scientists the Office of Naval Research funded. He is recognized as an important pioneer in the field of marine geology and geophysics.

Naval Research Reviews

Office of Naval Research
Three/1982
Vol XXXIV

Chief of Naval Research	RADM L. S. Kollmorgen, USN
Technical Director	Dr. J. A. Smith
Scientific Editor	Dr. G. A. Neece
Associate Scientific Editor	Dr. J. T. Lester
Associate Scientific Editor	Dr. D. A. Patterson
Managing Editor	M. J. Whetstone
Chief Writer/Editor	W. J. Lescure, III
Art Editor	Edward Bailey

ARTICLES

3 Sources and Transport of Arctic Pollution Aerosol: A Chronicle of Six Years of ONR Research
by Kenneth A. Rahn and Glenn E. Shaw

28 On the Use of Dissolved Oxygen Concentration as an Indicator of Winter Convection
by Joseph L. Reid

41 "FRONTS-80"—A Study of The North Pacific Subtropical Front
by Pearn Niiler

52 Finestructure: Oceanic "Kinks and Wiggles"
by Michael C. Gregg

DEPARTMENTS

27 Profiles in Science
Valentine Worthington

51 Conrad Award
Dr. Alan Berman

73 Research Notes

About Our Cover

Infrared image from NOAA-7 satellite on 4 November 1981 of Ra's al Hadd on the Eastern tip of the Arabian Peninsula showing cold core eddie and upswelled deep water at the entrance to the Gulf of Oman. Satellite imagery is becoming increasingly important as a basic research tool in oceanography.

Naval Research Reviews publishes articles about research conducted by the laboratories and contractors of the Office of Naval Research and describes important naval experimental activities. Manuscripts submitted for publications, correspondence concerning prospective articles, and changes of address, should be directed to Code 732, Office of Naval Research, Arlington, Va. 22217. Requests for subscription should be directed to the Superintendent of Documents, U.S. Government Printing Office, Washington, D.C. 20402. For this quarterly publication a yearly domestic subscription is $11.00 and foreign is $13.75. A single domestic copy is $3.75 and foreign is $4.70. *Naval Research Review* is published from appropriated funds by authority of the Office of Naval Research in accordance with Navy Publications and Printing Regulation P-35. Controlled circulation postage paid at Washington and additional mailing offices.

Model of an air deployable oceanographic mooring.

Alvin (submersible research vehicle)

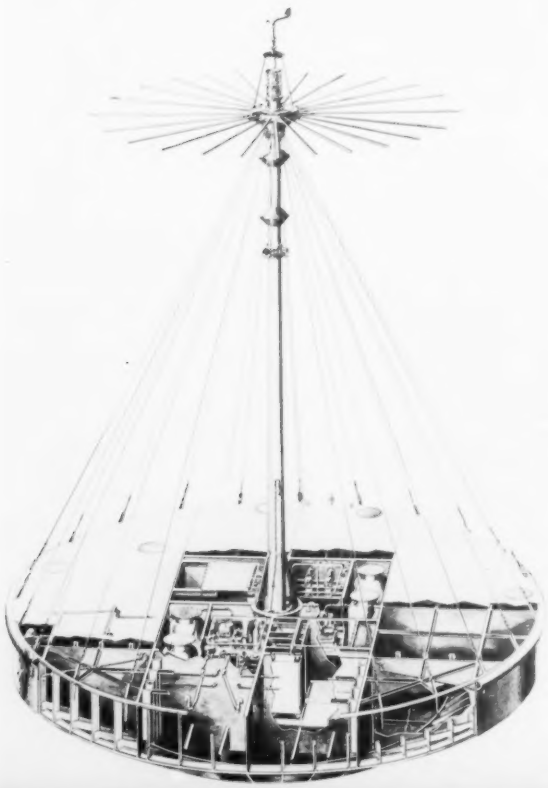

Monster buoy transmits and stores oceanographic data.

Introduction

by Louis Goodman
Office of Naval Research

The Office of Naval Research, since its establishment in 1946, recognized the critical role that the marine environment plays on naval operations and communications. Through funding and directing research in oceanography over the years, ONR is not only a recognized pioneer in the field but an important force in present day research. A reorganization at ONR has brought under one management (The Environmental Sciences Directorate) the disciplines of oceanography, geophysics, underwater acoustics, atmospheric science, and the Arctic program. This will allow better interdisciplinary research and exchange of ideas regarding the environmental programs.

Environmental research tends to be observationally oriented with theoretical, numerical and laboratory modelling usually following rather than preceding indicators or tracers of phenomena rather than of the phenomena directly. The four articles presented in this issue reflect this viewpoint.

Drs. Rhan and Shaw use chemical tracers to examine the source of Arctic haze. This research is an interesting blend of meteorology and marine chemistry and is a good perspective on the evolution and modification of hypotheses in environmental research as new observational evidence emerges.

The remaining three articles are from the field of physical oceanography and cover widely disparate scales of phenomena. Dr. Reid's article is a description of the large scale structure of the upper ocean and how oxygen may play an important role in understanding winter time convection. Dr. Niiler's article discusses the Fronts 80 Experiment. The phenomena of this experiment are intermediate or mesoscale and may in fact play a role in cascading energy and momentum downscale to Dr. Gregg's review of ocean finestructure. These reviews have the common theme of an indirect, often fragmentary, type of measurement. This occurs not because the scientists have purposedly avoided measurements, but because the state of the art in observations is not spacially three dimensional and simultaneous with temporal measurement over the wide range of scales and variables necessary. The research reported here is detective work by clever scientists who have a limited set of observational tools.

Sources and Transport of Arctic Pollution Aerosol: A Chronicle of Six Years of ONR Research

by

Kenneth A. Rahn
University of Rhode Island
and
Glenn E. Shaw
University of Alaska

Arctic Air Is Not Clean

The polar regions are universally considered to be desolate, remote regions whose air and water are still clean and pure. From the earliest explorers to modern travellers, all visitors to the polar regions attest to this view. After all, are not the poles literally the ends of the earth, far removed from the last traces of civilization's products?

In many respects the polar regions are indeed still pristine. The air over Antarctica, for example, shows some of the lowest concentrations of pollutants yet measured on this planet. Snow and ice from Antarctica fail to show any evidence of global pollution in their content of trace substances.

But cracks are beginning to enter this picture. More than a decade ago, snow and ice of Greenland were alleged to show increasing concentrations of certain trace contaminants dating back a century. Further analysis has confirmed this. As a result, it is now generally acknowledged that global air pollution affects both gases and particles throughout the Northern Hemisphere.

During the past six years, the authors, under long-term sponsorship of the Office of Naval Research, have been able to discover and carefully document a major crack in the above picture—the phenomenon known as Arctic haze. Arctic haze is the end product of massive transport of air pollution from various midlatitude sources to the northern polar regions, on a scale and with an intensity that could have never been imagined, even by the most pessimistic observer. The road from initial observation to first hypothesis to final explanation to critical acceptance by the scientific community as a whole has been long, sometimes arduous, and often marked by controversy as new and unexpected ideas were put forth. In this article, we recount how some forgotten observations of 30 years ago eventually led to a whole new field of research—Arctic air chemistry.

First Scientific Observations of Arctic Haze

Perhaps no one will ever know the identity of the first person who knowingly sighted Arctic haze. It probably wasn't an Eskimo, even though they are surrounded by it all winter and spring, because the haze is only barely discernible to a ground observer, even one trained in atmospheric optics. But from the air, it can't be missed. The first description of Arctic haze was in an article on visibility in the polar regions by Dr. J. Murray Mitchell, Jr., then a young climatologist, in 1957[1]. He summarized observations from the "Ptarmigan" weather reconnaissance flights, which from the late 1940's flew from Alaska northward over the Arctic Ocean in an effort to remove the meteorological blind spot in the Arctic which had existed until then. From talks with various observers and from scrutiny of their records, Mitchell was able to systematize the existing knowledge, however scanty, of Arctic haze.

Mitchell found that the haze, which he defined as diffuse bands of tropospheric aerosol (an aerosol is a collection of solid and/or liquid particles suspended in the atmosphere) occurring northward of about 70° and at altitudes of up to 9,000 meters (30,000 feet), was sighted a surprising fraction of the time. Vertical visibility was unaffected by Arctic haze; horizontal and slant visibility could be reduced to as little as 3-8 km (2-5 miles) in a layer, however. This is hardly to be expected for a pristine area. Although light haze can be sighted occasionally in the Antarctic, there is no real counterpart to Arctic haze there.

Mitchell summarized the then-known characteristics of Arctic haze as follows:

> "The haze is found during a very high percentage of the time that the weather of the Arctic Ocean is otherwise clear and, being encountered at all normal flight altitudes (700-500-300-mb levels), appears to have considerable vertical depth. Owing to the widely varying conditions of illumination, nothing can confidently be said about the seasonal variation in its frequency. The horizontal extent of the haze is usually limited to segments of the air route which are 500-800 miles (800-1300 km) long, but sometimes stretches over the entire 2000 miles of the reconnaissance track. A curious fact about the haze is that it is seldom found over land, as in the vicinity of Greenland. A ground observer can rarely detect the presence of Arctic haze, just as thin cirrostratus layers encountered by jet aircraft in middle latitudes are often indistinguishable from clear sky to an earth-bound observer. But the similarity between Arctic haze and thin cirrostratus seems to end there: (1) Whereas the cirrostratus appears milky-white from the air, Arctic haze possesses a grey-blue hue in antisolar directions and a reddish-brown hue in the direction of the sun. (2) Whereas the cirrostratus is confined to a definite layer in the atmosphere, Arctic haze possesses very diffuse and indistinct upper and lower boundaries and occupies, in the vertical, a considerable fraction of the Arctic troposphere. And finally, (3) Whereas the cirrostratus is obviously crystalline when viewed at

close range from an aircraft ('You can reach out and touch it'), and produces sun pillars, parhelia, halos and similar optical phenomena in sunlight which are characteristic of ice crystals, the Arctic haze seems completely amorphous to the eye and is almost always without optical effects, at least those which are sufficiently bright to be seen through aircraft windows. The color effects in the haze suggest that, like the low-tropospheric haze of middle latitudes, the constituent particles are no larger than about 2μ. This size is so small that, should the haze be made up of ice, the crystals would be very rudimentary. Since ambient temperatures in the haze are normally in the range of -30 to $-35\,^{\circ}C$, it is yet possible that supercooled water could be present although, to the writer's knowledge, no aircraft icing has ever been reported in Arctic haze."[1]

Alaskan Air Was Too Turbid

After Mitchell's article, Arctic haze was forgotten for 15 years, until one of us, Glenn E. Shaw (G.E.S.), rediscovered it. During the 1972 AIDJEX (Arctic Ice Dynamics Joint Experiment) pilot study near Barrow, Alaska, supposedly routine measurements of atmospheric turbidity with a sun photometer revealed unexpectedly high values, i.e., the local atmosphere contained larger-than-expected amounts of aerosol. These measurements were confirmed during the AIDJEX Lead Experiment of 1974. Numerous flights over the pack ice north and northwest of Barrow showed that much of the anomalous turbidity originated with distinct haze layers at altitudes of a few kilometers. When viewed edge-on, these layers appeared brownish-yellow in color, similar to the more familiar urban haze layers. Occasionally, horizontal visibility through the layers was reduced to only a few kilometers. The similarities between these haze layers and those of Mitchell were so striking that they must have been one and the same phenomenon—Arctic haze[2].

This established that Arctic haze was real and persistent. But the foremost question, its origin, was quite another matter, and was not to be answered easily. Both the visual observations and the optical measurements had shown that the haze was composed of true aerosol, that is, was predominantly very tiny suspended particles. Except for the size, sunphotometer measurements could offer no further information on the aerosol. The issue of greatest concern was whether Arctic haze was natural in origin, i.e., represented some previously unrecognized feature or process of the Arctic atmosphere, or whether it could possibly be pollution-derived. A pollution origin would have great implications for global air pollution, because sources of Arctic haze would have to be at greater distances than were then recognized for transport of pollution aerosol.

Dr. Shaw realized that chemical measurements were needed to determine the origin of the haze. But neither he (an atmospheric physicist) nor his institution (the Geophysical Institute of the University of Alaska) was prepared to carry out the specialized measurements that were required. A compatriot was needed. In May 1975, GES met Kenneth A. Rahn (K.A.R.) at a workshop in Polar Meteorology in Reno, Nevada. KAR's background in trace-element analysis of remote aerosols and interest in the north seemed to make him an ideal candidate for a partner. The subject was broached, a joint proposal for a pilot study was submitted and accepted by ONR in 1976, and the association has continued through the present.

Asian Desert Dust Over Alaska

Our approach to Arctic haze was to combine optical, chemical, physical and meteorological techniques to get the broadest possible information. The chemical composition of the haze was to be used to deduce whether it was natural or pollution-derived. If pollution-derived, an idea of its age was to be obtained from its optical and physical properties, primarily from its particle-size distribution. An idea of its source area was to come from backwards airmass trajectories. Things didn't work out at all this way in practice, however.

Our first experiment consisted of equipping a light airplane for aerosol sampling, then collecting samples directly from haze bands over Barrow. This experiment was under the direction of Mr. Randolph D. Borys, now a graduate student at Colorado State University, and took place in April-May 1976. It was based at the Naval Arctic Research Laboratory in Barrow, and used one of their single-engine Cessna 180's. Overall, it was a huge success. Ironically, however, a chance encounter with an atypical aerosol threw us off the track for several months.

During the early sampling, no distinct haze bands were seen, and the flights proceeded routinely. Towards the end of the experiment, however, pronounced haze bands appeared, associated with winds from the south. It seemed that a period of intense Arctic haze had been caught by luck. Just before the end of the experiment, the bands disappeared. Back at the University of Rhode Island, analysis of the

aerosol samples caught us completely by surprise: particles of the early period showed distinct traces of pollution products, whereas those of the later (banded) period showed large amounts of soil-derived dust. In other words, the haze bands had been soil dust!

The chemical basis for this conclusion is illustrated in Figure 1 which shows concentrations of the elements aluminum (Al) and vanadium (V) for the nine samples that were taken. These two elements are extremely useful in studies of aerosol from remote regions, because of their sources. Atmospheric Al comes primarily from soil dust. V, on the other hand, has two main sources: soil dust and combustion of oils, particularly the less-refined residual oil (which is too heavy and viscous to be burned in the Arctic). The V/Al ratio of soil-derived aerosol is very well-known and reproducible from place to place, and similar to that of the bulk crust. Aerosol with a soil-like V/Al ratio can be considered as strongly natural in origin. In and around polluted areas, however, particularly those where large amounts of oil are burned, the V/Al ratio is much higher and can reach extremes of more than 100 times the crustal ratio. In these circumstances, V is said to be enriched relative to the crust. The degree of enrichment is usually expressed by calculating the aerosol-crust enrichment factor of V, defined as

$$EF_V = (V/Al)_{aerosol}/(V/Al)_{crust},$$

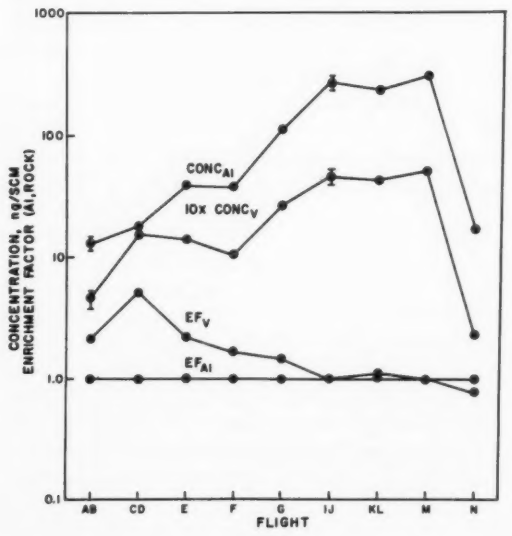

Figure 1. Concentrations and enrichment factors of V and Al in aerosol over Barrow, Alaska, April-May 1976.[7]

where Al and rock serve as the reference element and reference material, respectively, for the crust. We normally use Mason's mean composition of global rock as our reference material[3]; other workers sometimes use other mean rocks or mean soils.

The enrichment factor of vanadium (EF_V) provides an extremely sensitive test of the pollution vs. natural character of an aerosol. When its values are below 1.5 or so, the aerosol may be considered natural. When the value exceeds 1.5, the aerosol is showing definite influences of pollution. Our first Barrow experiment had two distinct phases: Flights A through G where pollution aerosol was seen, and Flights I through N where the aerosol was soil-derived. The soil-derived nature of the latter aerosol was seen clearly when the filters were examined with an electron microscope: angular mineral particles were abundant in samples I through M and nearly absent earlier.

As noted above, the soil dust came to Barrow with south winds. But the North Slope was still frozen and completely snow-covered, and could not have been the source of this material. The rest of Alaska was probably not the source either, for it too was mostly snow-covered. Furthermore, the very small size of the soil particles indicated that they had travelled long distances in the atmosphere, farther than from some other part of Alaska.

The source was finally revealed by backwards air-mass trajectories, as shown in Figure 2. Those samples with the most soil dust had passed over the great deserts of eastern China and Mongolia (Gobi, Takla Makan, Ordos, Loess Plateau) a few days earlier. (By contrast the earlier, slightly polluted, samples had come from the north.) Each spring, these deserts give rise to huge dust storms whose soil particles can travel far over the Pacific. In the deep-sea sediments of the Pacific, east-west bands of quartz and certain clay minerals can be found extending from Asia nearly to North America[4,5]. Short events of desert dust reaching North America, called "ice-nucleus storms," have been detected in Washington State and even in Fairbanks[6]. So it perhaps should have come as no surprise to find Asian desert dust over Barrow, but we were nevertheless taken aback. To confirm the Asian origin of our desert dust, we checked the weather records during our experiment, and found that there had indeed been a major dust storm in eastern Asia from 22-24 April 1976, which could be followed from its generation in the Gobi Desert through its transport southward, then northeastward past Japan and Korea out over the Pacific, where it was lost until part of the cloud was observed a few days later over Barrow (see Figure 3)[7].

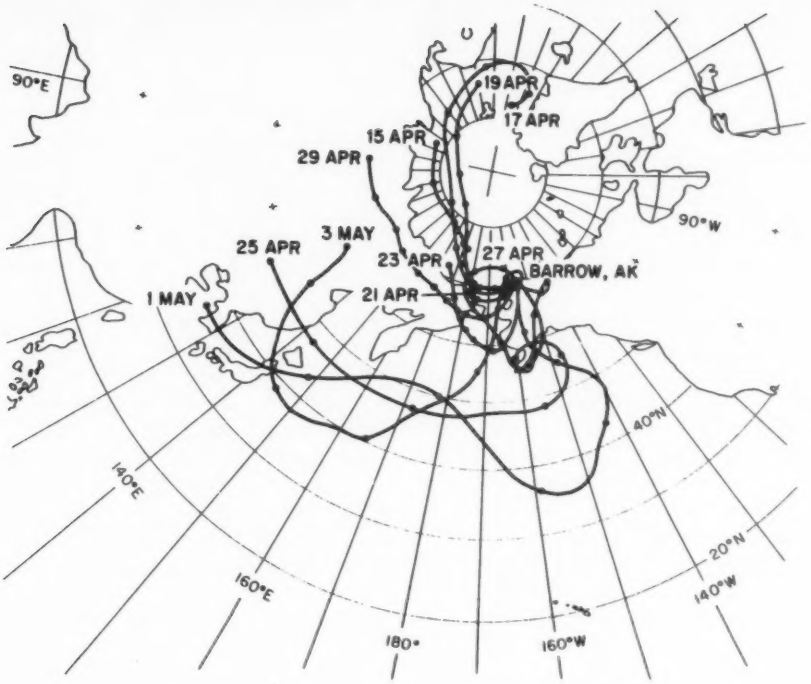

Figure 2. 700-mb isobaric trajectories of air to Barrow, spring 1976[7]. Numbers refer to date of arrival at Barrow; solid circles each 24 hours.

In short, our first experiment had found a little pollution and a lot of soil dust over Barrow. Furthermore, the banded nature of the dust clouds matched the two earlier reports on Arctic haze. For these reasons, we concluded that Asian desert dust might be responsible for much or most of Arctic haze. Consequently, Arctic haze was a natural phenomenon.

Arctic Haze is Pollution Aerosol, Not Desert Dust

Within a year or so, however, this idea had to be abandoned. The first inkling that something was wrong came from sun-photometer data of this experiment, which showed that there had been just as much turbidity before the soil-dust bands arrived as when they were over Barrow in full force. In the first flushes of discovering the longest known transport of Asian dust, we had failed to face this observation squarely; only several months later did its true meaning become fully evident. The very low concentrations of pollution-derived vanadium, nearly as low as had been measured anywhere else in the Northern Hemisphere, also failed to alert us to the potential link between pollution aerosol and Arctic haze. We now know one very important reason for this, namely that our experiment was unwittingly performed at the very end of the pollution season at Barrow, just before pollution aerosol disappears for the summer. Had we done our experiment several months earlier, we would have been hit with such high concentrations of vanadium that their significance could not have been missed.

The real blow to the desert-dust hypothesis and a natural explanation for Arctic haze came with the initiation of ground-based aerosol sampling at Barrow the following fall. Ironically, we started this ground project as a cheap alternative to year-round aircraft experiments, whose cost and logistics were both prohibitive. But we were still looking for desert aerosol, and were quite unprepared for what was about to happen.

The ground-based experiment almost never

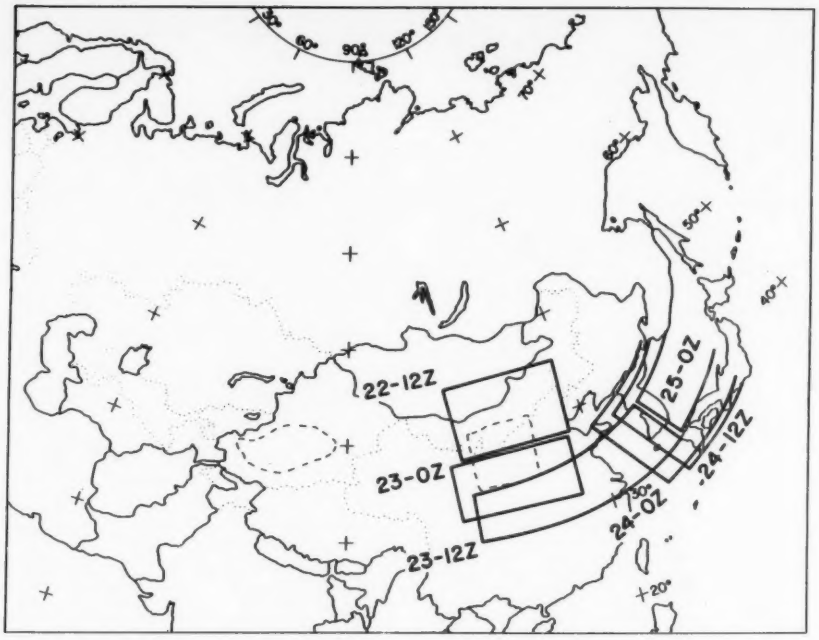

Figure 3. Progression of the dust cloud for the storm of 22 April 1976.[1]

started. We knew that ground-level sampling wasn't a very good way to look for bands of aerosol which are usually found aloft, and so did our program manager Dr. G. Leonard Johnson, Group Leader of ONR's Arctic Program. But we argued that ground sampling was better than nothing, was inexpensive, and had a reasonable chance of picking up some traces of dust layers aloft. In any event, it would tide us through the winter until we could perform another aircraft experiment the following spring. Dr. Johnson relented, the experiment went forward, the next spring's aircraft experiment never happened (for a variety of other reasons), and Arctic air chemistry hasn't been the same since.

In September 1976, KAR visited Barrow and set up a high-volume aerosol-sampling system at the GMCC Baseline Observatory. The GMCC (Geophysical Monitoring for Climatic Change) program is a branch of the National Oceanic and Atmosphic Administration (NOAA) which is dedicated to monitoring long-term changes in the chemistry and physics of the atmosphere that may affect world climate. The GMCC program also operates observatories at Mauna Loa (Hawaii), American Samoa, and the South Pole. At Barrow, their two full-time observers changed filters for us and mailed them to Rhode Island, thereby greatly reducing the costs of our experiment, and making long-term sampling at Barrow feasible.

The first few samples from Barrow were very light in color, and contained little besides sea salt. About the first of November, however, the entire character of the Barrow aerosol changed suddenly. The samples were dark gray in color, and contained much higher concentrations of Al, V and Mn, in proportions more like urban samples than clean-area samples. For example, the enrichment factor of vanadium jumped from 1 to 10, indicating that 90 percent of the aerosol was pollution-derived. When all these facts were considered (together with data for a much larger number of elements that we later determined), it was obvious that we were dealing with a pollution-derived aerosol.

Throughout that first winter, concentrations of Al, V, Mn and carbon remained at roughly an order of magnitude above their September-October values. During spring, the traditional period of most intense haze at Barrow, the elemental concentrations increased by another factor of 2-3. Near the end of April, all concentrations decreased abruptly, and the aerosol remained nearly pure sea salt for the rest of the summer. The monthly mean concentrations of vanadium during the first year of sampling are shown in Figure 4. No desert dust was seen that winter or

spring!

The Winter Pollution Did Not Come from Barrow

Where had the pollution aerosol of winter come from? We realized immediately that it could not have had Barrow as a source, for several reasons. First, no vanadium is emitted by Barrow. As mentioned above, vanadium comes from heavy oils, and the fuels at Barrow are primarily natural gas (which is free of trace elements like V and Mn) and highly refined jet fuels, which are also extremely low in impurities. Second, our samples were sector-controlled, that is, air was sampled only from directions other than Barrow. The GMCC observatory is east of everything else around Barrow, so that air coming from the east off the Arctic Ocean (the predominant wind direction during winter) is free of local influences. Third, as a test, we had taken four of the initial samples deliberately out-of-sector, i.e., from the direction of Barrow. No significant differences from the in-sector samples were seen. This indicated that Barrow was a weak source of pollution, which was reasonable considering that Barrow had only 3,000 inhabitants, mostly Eskimos, who follow a simple lifestyle. (While these ideas were proof enough for us, it would be several more years before we would be able to convince the last skeptics that our samples were something other than Barrow contamination.)

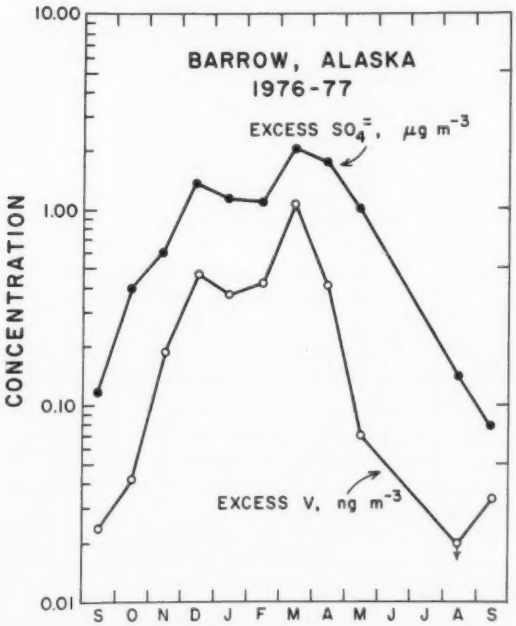

Figure 4. Monthly mean concentrations of excess (nonmarine) sulfate and excess (noncrustal) vanadium at Barrow, Alaska, 1976-77.[24]

Abnormal Amounts of Sulfate Required to Explain the Intensity of the Haze

On balance, the outstanding feature of that first year's record from Barrow was the 10- to 30-fold higher concentrations of pollution aerosol during winter than during summer. (We now have taken five years of aerosol samples from Barrow. The first four years have been analyzed, and confirm the seasonality and absolute concentrations of the first year). We thus began to consider very seriously whether pollution aerosol could be responsible for Arctic haze. Although the timing seemed right, a problem remained: the concentrations of vanadium, manganese, etc., seemed much too small to account for the haze. Whereas the intensity of the haze (as measured by optical depth, or turbidity) was only 3-5 times less than in regionally polluted areas such as the northeastern United States, manganese and vanadium were 20-40 times lower. In other words, there was an order of magnitude "too much" haze for the pollution aerosol.

At this point, various possible explanations were proposed but none seemed very reasonable. Perhaps some major constituent of the haze was enriched by an order of magnitude compared to urban aerosols. This explanation (which later turned out to be the correct one) was dismissed at the time because of the great similarities among many different aerosols shown by previous studies. A strong effect of relative humidity (which causes hygroscopic particles to take up water and swell, and hence scatter light more efficiently) in the Arctic was suggested but also considered unlikely. A layer of concentrated aerosol aloft was also considered improbable and *ad hoc*.

Without a great deal of hope, we undertook to measure the amount of sulfate in the haze. Sulfate is a major constituent of most aerosols, and is often the single most abundant species. To our great surprise, sulfate turned out to be an order of magnitude higher at Barrow than we had expected, and easily concentrated enough to explain the turbidities. Its monthly means for 1976-77 are shown in Figure 4. The absolute concentrations of sulfate are strikingly high at Barrow: mean winter values for 1976-77 were 1-2 $\mu g\ m^{-3}$, and the mean for March 1977 (and subsequent Marches as well) was about 2.5 $\mu g\ m^{-3}$. (We had anticipated concentrations of 0.1–0.3 $\mu g\ m^{-3}$.) To put

these values in perspective, consider that sulfate concentrations in the northeastern United States during winter are roughly 6 $\mu g\ m^{-3}$, only twice as high as those at Barrow during March. Our first Barrow samples were roughly a week in duration; we have since found that individual days can have sulfate concentrations as high as 5 $\mu g\ m^{-3}$. This means that on some days, sulfate is higher in Barrow than it is in the northeastern United States!

Other things being equal, it is harder to understand the sources of sulfate than of vanadium, because there are significant natural sources of sulfur to the atmosphere, at least when averaged over the globe. The high sulfate concentrations, coupled with their parallelism to pollution-derived vanadium, suggested to us from the beginning that the sulfate was also pollution-derived, and nothing since then has changed our minds. It truly seemed that Arctic haze stemmed largely from a pollution-derived, sulfate-rich aerosol of distant origin.

Source of the Pollution Haze Is Outside the Arctic

We then began to focus on the area of origin of the haze. Certain colleagues had suggested that we were detecting nothing more than North Slope contamination, from the oil-related activities in Prudhoe Bay. We did not accept this explanation because, by this time, aerosol very similar to that of Barrow had been detected by other scientists in the Northwest Territories of Canada (at Mould Bay) and around the northern edge of Greenland, and at Spitsbergen and Bear Island in the Norwegian Arctic. To eliminate the North Slope as a major source, Mr. Thomas J. Conway of our project carried out an experiment on Narwahl Island in April 1979. Narwahl Island lies about 25 miles NW of Prudhoe Bay, so that air coming to it from the north-to-east quadrant is unaffected by the Alaskan mainland. A series of samples taken at Narwahl Island concurrently with samples at Barrow showed very similar concentrations of manganese, vanadium and sulfate, and were indistinguishable to the eye from the Barrow samples (had equal concentrations of carbon). This showed once and for all that pollution aerosol observed at Barrow represents that found over much of the polar cap during winter, not just the North Slope. The sources of this aerosol must lie outside the Arctic. To localize these sources, we turned (unsuccessfully) to trajectory analysis.

Air-mass Trajectories Not Useful

The most common meteorological technique for tracing the history of an air mass is to calculate back-trajectories for it. Using the speed and direction of wind at the time of sampling, the position of the air is calculated for some previous time, say 12 hours earlier. Observations at that time and place are then used to calculate where the air had been another 12 hours earlier, and so on. At Barrow, one may precede this process with the observation that the most polluted air comes from the north, i.e., from over the polar cap. Air masses from the south are up to an order of magnitude cleaner. (This situation is just the opposite of what is normally found in midlatitudes, where north is the clean direction.) Severe problems arise almost immediately when one attempts to calculate back-trajectories for the northern (polluted) air masses at Barrow, however. First of all, it typically takes four days for air masses to cross the ice cap. As a rough rule of thumb, trajectories become quite uncertain after two days and of little meaning after five days, except when flow patterns are extremely well-defined. Thus, it is difficult to determine where an air mass first encountered the ice cap, to say nothing of where it had been earlier. This problem of distance is compounded by the sparsity of meteorological data in the Arctic—very often there are no data at all from the entire ice cap. As a result, trajectories calculated for the Arctic are less reliable than those for other locations. When this is coupled with the long distances from the Arctic to major pollution sources (5,000-10,000 km), it should perhaps not be surprising that trajectory calculations have been unable to localize the source areas of aerosol of the North American Arctic, even though we and others have tried both forward and backward trajectories[8-10]. As an alternative, we tried using air-mass analysis, where characteristic properties such as temperature, relative humidity, or stability were used as tracers, but this didn't work either, because of the tendency for air masses to become aged and similar in properties by the time they reached the Arctic. Still other meteorological approaches, some quite inventive, have been tried to explain the origin of the aerosol of the North American Arctic[11,12]. Results have been mixed at best.

Thus we reluctantly concluded that presently available meteorological techniques cannot satisfactorily resolve the source areas of Arctic aerosol. It remains an important question, however. For some years, we sought the answer by assembling all relevant evidence, however indirect and circumstantial. Fortunately, there are quite a few pieces of relevant

evidence; in the paragraphs below, we review a few of the most important. A fuller discussion has recently been given elsewhere[13].

Likely Sources and Pathways of Pollution

At the beginning of this project, we felt intuitively (and probably naïvely) that eastern North America was the most likely source of Arctic haze. Shortly thereafter, as we began to measure distances on a globe and evaluate potential transport pathways, we were forced to broaden our outlook to three large polluted areas: eastern North America, Europe (including the western USSR) and eastern Asia (China, Japan, Korea, etc.). By knowing the prevailing winds near each source area, one can rather easily propose the most likely pathway(s) from each to the Arctic. Figure 5 shows these sources and pathways as

Figure 5. Possible sources and pathways for transport of pollution aerosol between midlatitudes and the Arctic.[13]

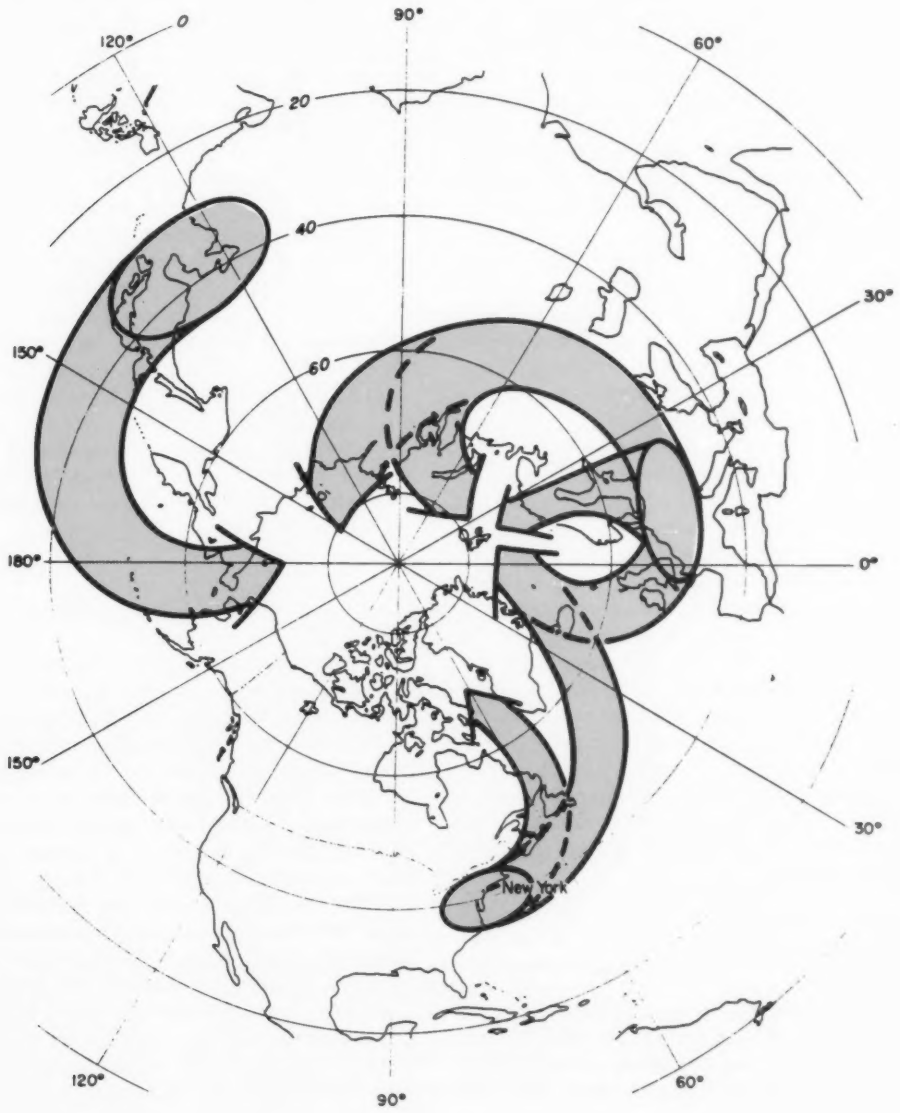

they were conceived in 1979. From eastern North America, the most likely pathway would be via the North Atlantic Ocean, Iceland and the Norwegian Sea, following the dominant storm track for that region. Another possible pathway would be via the west side of Greenland, but this should be less important, because the normal flow of air there is southward, not northward (northeastern Canada is the great exit area for air leaving the Arctic). From the beginning, we felt that the most important pathway(s) had to be active a large fraction of the time during winter, because polar air at Barrow inevitably had high concentrations of aerosol. A pathway with the wrong basic directionality, such as the one along the west side of Greenland, could probably not play a major role in Arctic air chemistry. The pathway from eastern Asia over the Pacific was similar to that from eastern North America, being also based on a storm track. Air flow near the ends of the Atlantic and Pacific pathways would be controlled by the Icelandic and Aleutian low-pressure areas, respectively.

On observational grounds alone, it was easy to eliminate eastern Asia as a major source of Arctic aerosol: air from the Pacific pathway, approaching Barrow from the south, is the cleanest observed there. The reason for these low concentrations is probably the storminess of this path because abundant precipitation cleanses the air efficiently. Analogous reasoning would imply that the North American source via the Atlantic pathway ought not to be important for the Arctic. For a long time we lacked direct observations along this pathway to confirm or reject this idea, but we now have them from both southern Greenland and Iceland. Near southern Greenland, concentrations of aerosol are very low in winter, as expected from an inefficient pathway. At Iceland, from which we now have abundant year-round data, air masses approaching from the west are very clean. High concentrations of aerosol are occasionally observed at Iceland, to be sure, but only in air masses coming from Europe. A study off the coast of western Ireland confirmed the cleanliness of Atlantic air masses. We have never observed high concentrations of aerosol in air masses that have crossed the Atlantic.

Europe the Likely Source

This reasoning left Europe as the only source area for Arctic pollution aerosol. By late 1978, the basis for this conclusion was strong enough that we began to speak about it publicly. Again, there were many skeptics, including those who chose to read scientific nationalism into the contention of Americans that Europe, not North America, was the source of Arctic haze. But this conclusion has stood the test of time (with modifications discussed below), and is now supported by abundant evidence. The first strong piece of evidence we had, and one which is still solid, is the geographical distribution of sulfate aerosol during winter. Figure 6 is a map of winter-mean concentrations of nonmarine sulfate in and around the Arctic, with data available as of 1979. It shows that concentrations are low over the North Atlantic (data from southern Greenland and several cruises in the mid-Atlantic) and, indirectly, that concentrations are low over the Pacific (2½-fold lower concentrations in interior Alaska, which receives Pacific air, than at Barrow). Furthermore, the map shows that Europe is indeed connected to the Arctic by a broad tongue of high sulfate concentrations stretching northward through Scandinavia into the Norwegian Arctic. From southern Scandinavia through Spitsbergen, a north-south distance of 2,000 km, sulfate remains constant at about 2 $\mu g\ m^{-3}$. Another observation from Figure 6 that is consistent with a European source is the slight decrease in sulfate from the Norwegian to the North American side of the Arctic, from 2 to 1.5 $\mu g\ m^{-3}$, which suggests that the sources for both regions are on the Norwegian side of the Arctic.

Convincing as these arguments are, however, they are still indirect and circumstantial, and hence not completely satisfying, even as a package. Direct evidence is needed.

Tracer Evidence of Sources—Mn/V

For a long time, we have believed that the only truly direct evidence on sources of Arctic aerosol was going to come from the composition of the aerosol itself acting as a tracer. According to this idea, there must be regional differences in pollution aerosol stemming from regional differences in fuels, basic economies, etc. But no one had ever found such differences. On the contrary, the major impression from trace-element studies in Europe and North America was the similarity, not the difference between aerosols. If an element was nonenriched in one city, it was nonenriched in all other cities. If an element was enriched in one city, it was enriched in all other cities, and to surprisingly similar degrees. To a limited extent, we had looked for regional differences, but to no avail. By the late 1970's, we had nearly given up on ever finding them, and had even

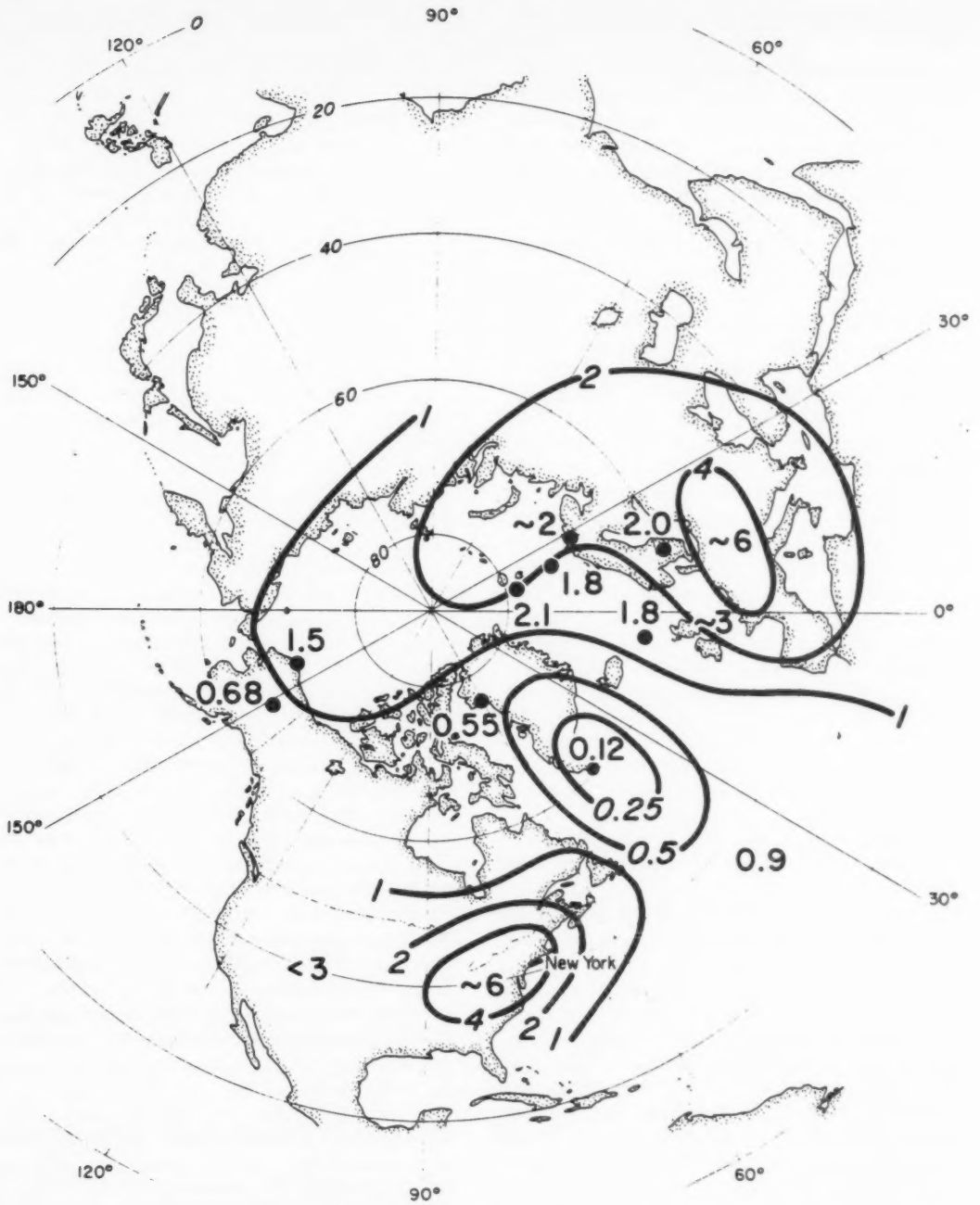

Figure 6. Mean winter concentrations of nonmarine sulfate (μg m⁻³) in surface aerosol of the Arctic and environs.[13]

looked into the feasibility of using pollution gases instead.

Then in April 1980, in a chance conversation between KAR and Dr. L. Barrie of Atmospheric Environment Service, Canada, the subject of manganese in the European aerosol arose. Both had lived and worked in Europe a few years earlier, and had independently found more Mn in European cities than they were accustomed to in North America. That conversation led KAR to try to construct a tracer from the Mn/V ratio (more precisely, the ratio of noncrustal Mn to noncrustal V). This ratio had the prospect of being considerably larger in value in Europe than in eastern North America, because Mn was high in Europe and V was high in eastern North America. In principle, the ratio of two elements would have distinct advantages as a tracer, because its value should change much more slowly during transport than would the concentration of either element alone, especially if the two elements were on similar particle sizes in the aerosol. A properly chosen elemental ratio could thus approach conservative behavior during transport. Mn and V were good candidates for a ratio because they are both enriched, pollution-derived elements, and hence associated with the submicron fraction of the aerosol. Earlier attempts to use the enrichment factor of pollution elements as tracers had been abandoned because of the great disparity in size between the pollution-derived elements (usually submicron) and the reference element aluminum (supermicron). As a result, enrichment factors changed too much during transport.

The Mn/V ratio worked. On a plot of Mn vs. V, European samples separated cleanly from those taken in the eastern United States (Figure 7). Mean Mn/V ratios were 5 ± 1 times greater in Europe than in the eastern United States. Although the reasons for this are still not known fully, the tracer can be used with confidence. In addition, values from various Arctic sites on the same plot, showed that the Norwegian Arctic and North American Arctic regions were separated by a factor of two in ratio. We had not realized that there were such large regional differences in the Arctic aerosol. Like Europe, the North American Arctic had Mn/V ratios greater than unity, and like eastern North America, the Norwegian Arctic had ratios less than unity.

Did this mean that Europe was the source of aerosol for the North American Arctic and eastern North America for the Norwegian Arctic? Not necessarily, for there is both theoretical and observational evidence that the Mn/V ratio decreases systematically during long-range transport by factors of up to 3-4.

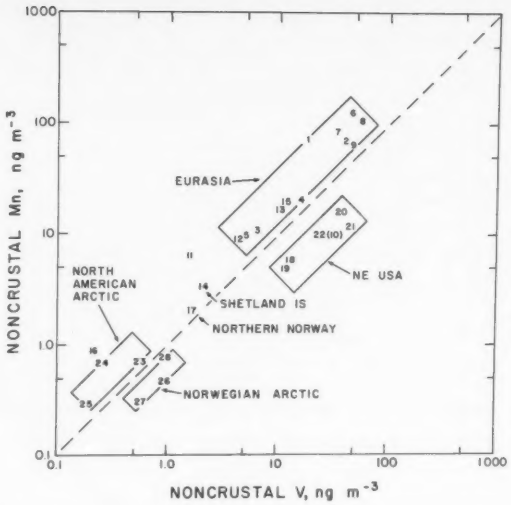

Figure 7. Atmospheric concentrations of noncrustal Mn and V in Eurasia, the northeast U.S.A., and the Arctic.[14]

The reasons for this are not completely understood. In part, they seem to be related to particle size, for Mn is often found on somewhat coarser particles than is V and thus should be removed faster during transport[14]. But the decreases predicted from particle size alone are more like a factor of two at most. The reasons for this discrepancy are not yet known. Applying the operational decrease of 3-4 times during transport brings a great deal of order to Figure 7: aerosol of the Norwegian Arctic becomes compatible with a European precursor, as so much other evidence indicates; aerosol transported from eastern North America takes on a Mn/V ratio much lower than is ever found in the Arctic, which is consistent with the rapid washout of North American aerosol by Atlantic storms noted above. But another puzzle is created: the source area for aerosol of the North American Arctic (Barrow and Mould Bay) must have a higher Mn/V ratio than any site depicted in Figure 7.

The Central Soviet Union a Potent Source

What could this source be? We feel that it is most likely the central Soviet Union. There are at least two reasons to expect a very high Mn/V ratio in aerosol from this region: much steel is produced there (which favors the release of large amounts of Mn), and the economy of the area is based strongly on coal (coal-burning areas have high Mn/V ratios).

Huge quantities of pollution aerosol are released in the central Soviet Union—some of the highest pollution levels in the entire Soviet Union are found here[15]. Furthermore, as discussed below, there is a very efficient transport path from this region that went unrecognized for a long time. A great variety of circumstantial evidence now points to the central Soviet Union as the major source of aerosol for the North American Arctic. Ironically, it was not one of our original three candidate-areas.

Pathways

What about pathways to the Arctic? Here we have to consider Europe and the central Soviet Union separately. For Europe, there is a broad body of basic knowledge concerning northward transport which has come from the decade-long systematic study of acidity in Scandinavia. Sponsored first by OECD (Organisation for Economic Cooperation and Development) and now by ECE (Economic Commission for Europe), the transport and deposition of sulfur and acidity have been thoroughly investigated by large-scale cooperative studies within Europe. The deposition of acidity in Scandinavia normally occurs in a series of episodes each winter, all associated with strong northward air flow from the more populated and industrialized countries to the south, such as Great Britain, France, Germany, Poland and the western Soviet Union. The most common vehicle is the "black episode," so named for the dark appearance of the aerosol on filters[16]. A black episode is created when a high-pressure area centered over or east of Europe combines with a low-pressure area approaching from the Atlantic to create a narrow but intense zone of northward transport in between. When the low and high are positioned so that this transport zone begins in central Europe and passes over Scandinavia, much of Scandinavia is blanketed by black, acidic aerosol in concentrations several times the norm and for periods of up to a few days.

It is now known that black episodes can occasionally continue all the way into the Norwegian Arctic. As such, they become an important source of pollution aerosol for this region. There are at least two variations on the basic northward pathway: one west of Norway (when the Asiatic high is westward of its normal position), and one over the Baltic Sea between Sweden and Finland. According to Dr. B. Ottar of the Norwegian Institute for Air Research, who has directed these European studies for the last several years, there is a tendency for the northward air flow to avoid the mountainous Scandinavian Peninsula. Because of their relatively straight pathways, we refer to these periods of northward flow to the Norwegian Arctic as "direct" episodes.

For a long time, we thought that direct episodes were the key to understanding air pollution in the Norwegian Arctic. In 1979, however, we were surprised to learn that they are only a small part of the story. In a cooperative study of air pollution at Bear Island with the Norwegian Institute of Air Research, we discovered that the most frequent pathway of SO_2 (the gaseous precursor to sulfate aerosol) into Bear Island is from the northeast, not from the south as would be expected for direct episodes. During the winter of 1977-78 for example, 10 of 13 pulses of SO_2 at Bear Island were from the northeastern quadrant[17].

These northeastern air masses are much colder than are those of direct episodes from the south. The basic explanation for this second type of episode can be seen easily from meteorological maps: the cold-air pulses from the northeast are inevitably associated with low-pressure areas centered over open water south of Bear Island, and are really the tail end of a cyclonic pathway that originated far to the south, moved eastward and northeastward around the leading edge of the advancing low, then recurved southward and westward around the north side of the low. Because of this 180° curvature, we coined the term "return-flow" pathway. Figure 8 shows five examples of actual return-flow pathways for SO_2 coming to Bear Island; Figure 9 is an idealized version of this path as it was envisaged in 1979, and shows how aerosol might continue from the Norwegian Arctic into the North American Arctic. We have recently confirmed the existence of this pathway to Barrow. It seems to be particularly active during spring, for reasons discussed below.

The main transport pathway from the central Soviet Union to the Arctic can be seen quite readily, together with the meteorological mechanism responsible for it, from meteorological maps. As noted above, we had missed this pathway until recently, because we didn't have the right source area in mind (it was only in 1980 that we realized that the central Soviet Union was the key source for Barrow, after we had come upon the Mn/V tracer. Previously, we had sought repeatedly and unsuccessfully to correlate episodes of flow from Europe with pulses of aerosol at Barrow.)

It should be noted perhaps that we use the term "central Soviet Union" in a vague, operational sense since the exact source areas of aerosol in this region are not yet clear. Originally, we focused on the southern Urals, where heavy industry is abundant. There are other potential sources nearby, however, including adjoining parts of Kazakhstan, western Siberia, and possibly also the European Soviet Union.

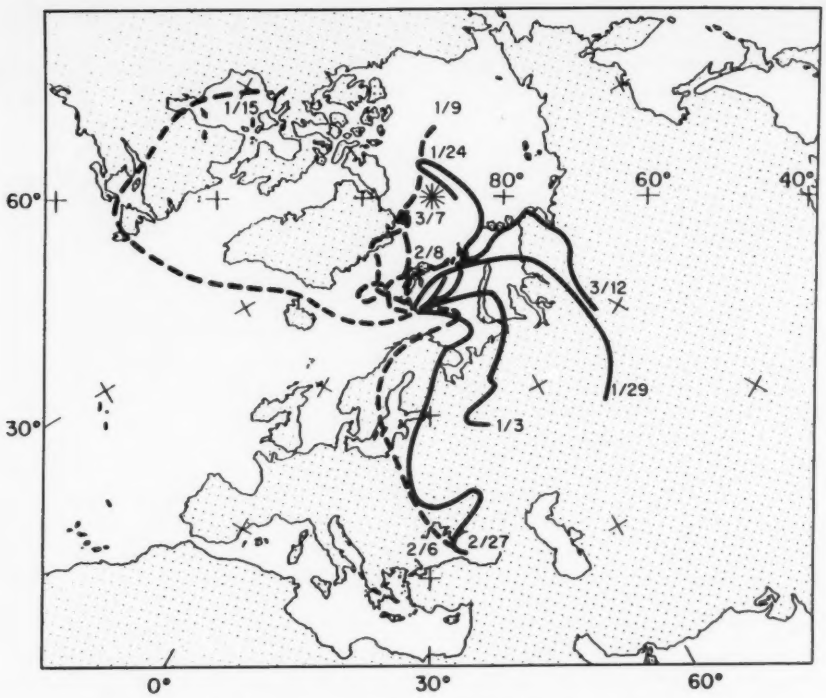

Figure 8. Five-day surface geostrophic back-trajectories of return-flow episodes (solid lines) and periods of low concentrations (broken lines) of SO_2 at Bear Island during winter 1977-78. Dates of arrival at Bear Island are indicated.[17]

Noril'sk, a copper-nickel smelting complex in Northern Siberia, may also be important.

Meteorological Features of Pollution Transport

The meteorological maps showed that, once again, the leading edge of a low-pressure area is involved with transport to the Arctic, normally but not always in combination with a high-pressure area. The low-pressure areas involved are later stages of the same systems discussed earlier for Bear Island. In this case, however, they are centered near Novaya Zemlya. They are often quite large, and their area of influence can extend as far south as 50 °N, easily encompassing the important source areas at roughly 55 °N. The high-pressure area involved is the Asiatic high, which is very strong during winter and is normally centered in Mongolia. In addition to dominating the pressure patterns over much of interior Asia, it often has a lobe which extends through the northeastern Soviet Union into the Arctic. The combination of the low over Novaya Zemlya and the high over Mongolia produces a very strong region or northward air flow centered roughly on the eastern Taymyr Peninsula. Pressure patterns at the surface during January are shown in Figure 10.

Several interesting aspects of this flow pattern should be noted. Perhaps the most significant of these stems from the fact that the lows rarely penetrate beyond Novaya Zemlya. This is because they depend on the warm open sea for their energy. But the open water, which extends over the top of Norway in response to a branch of the warm Gulf stream (which creates the ice-free Arctic port of Murmansk, so important to the Soviet Union), ends before Novaya Zemlya. The migrating lows, which are traceable all the way back to North America, pass rapidly over the North Atlantic and Iceland, then follow the warm water over the top of Norway, past Bear Island and into the Novaya Zemlya area. Upon encountering the pack ice west of Novaya Zemlya and the ridge of high pressure on the other side of the Taymyr, they stagnate and eventually die, to be replaced a few days later by the next low. With certain variations, this pattern repeats itself throughout the winter.

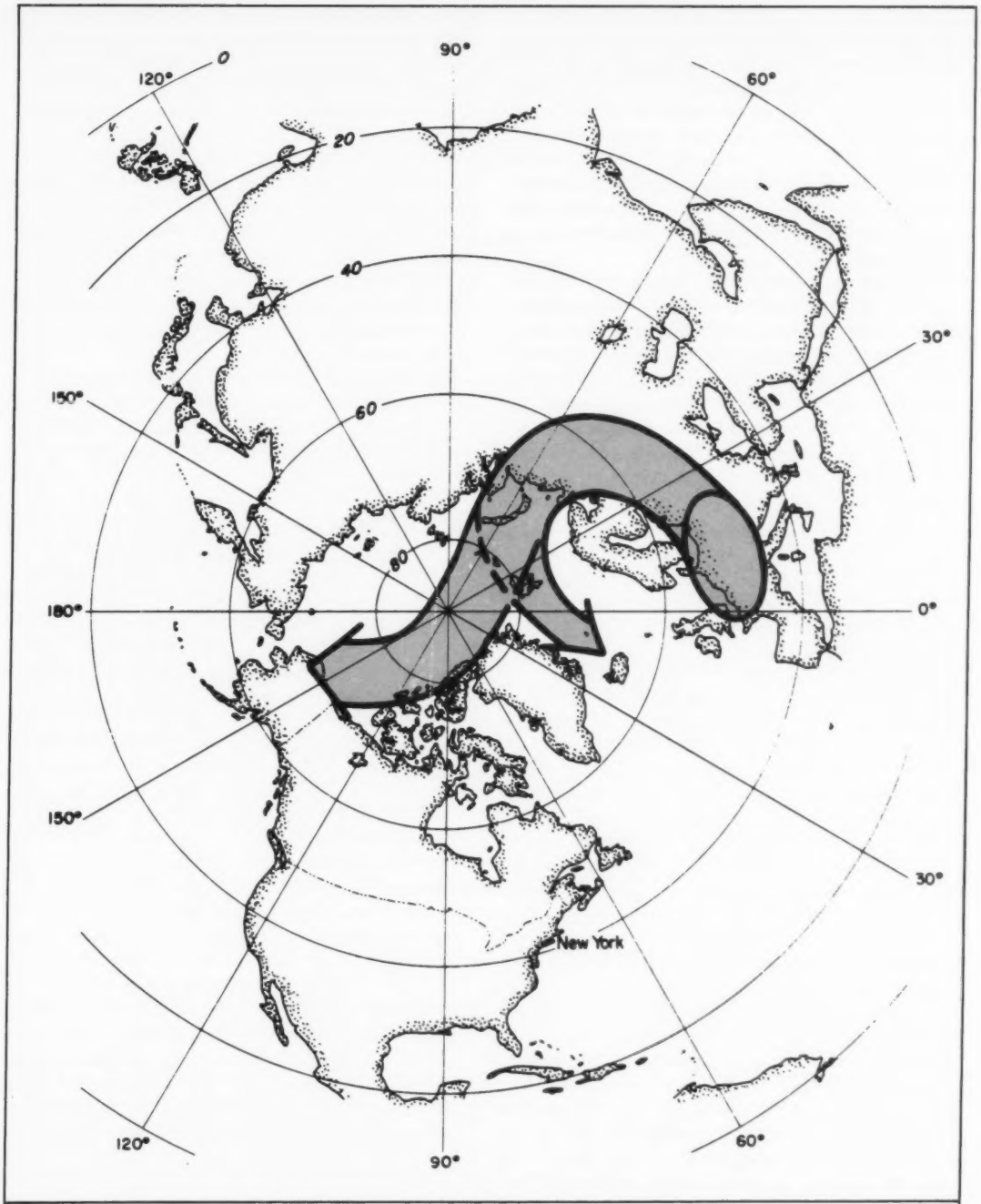

Figure 9. Idealized return-flow pathway from Europe to the Norwegian Arctic, with continuation to the North American Arctic.[27]

The net result is to create a semi-permanent zone of east-west pressure gradient centered on the eastern Taymyr Peninsula. Because the migrating lows do not pass the peninsula, this pressure gradient varies in intensity (depending on the proximity of the nearest low) but not in direction. This creates a zone of flow to the Arctic which we call the Taymyr pathway, whose intensity pulsates but whose direction is nearly always the same—northward. The close relation between the Taymyr and return-flow pathways is shown in Figure 5.

The contrasts between the Taymyr pathway and the return-flow pathway are very important to Arctic air chemistry. Because the low-pressure areas pass completely by Bear Island, the return-flow pathway from Europe is only in place for 1-3 days before it is replaced with an entirely different kind of trajectory. As a result, the concentrations of pollutants in the Norwegian Arctic are "noisy," i.e., vary greatly and with a rapid periodicity. But the Taymyr area has some of the least changeable winds in the Eurasian Arctic. As a result, concentrations of pollutants near Barrow are much steadier than at Bear Island, and have more of their variation associated with longer periodicities.

The meager precipitation in the interior of Asia during winter (nearly the lowest in the Northern Hemisphere), combined with the intensity and constancy of the winds along the Taymyr pathway, make it ideal for transporting pollution aerosol. Strong pollution sources in the central Soviet Union lie near the beginning of this path, and make it the dominant one for much of the Arctic, in particular for the North American Arctic.

(The scanty precipitation in the Arctic itself is one of the major reasons for Arctic haze. Because precipitation scavenges aerosol efficiently, regions of abundant precipitation have low concentrations of

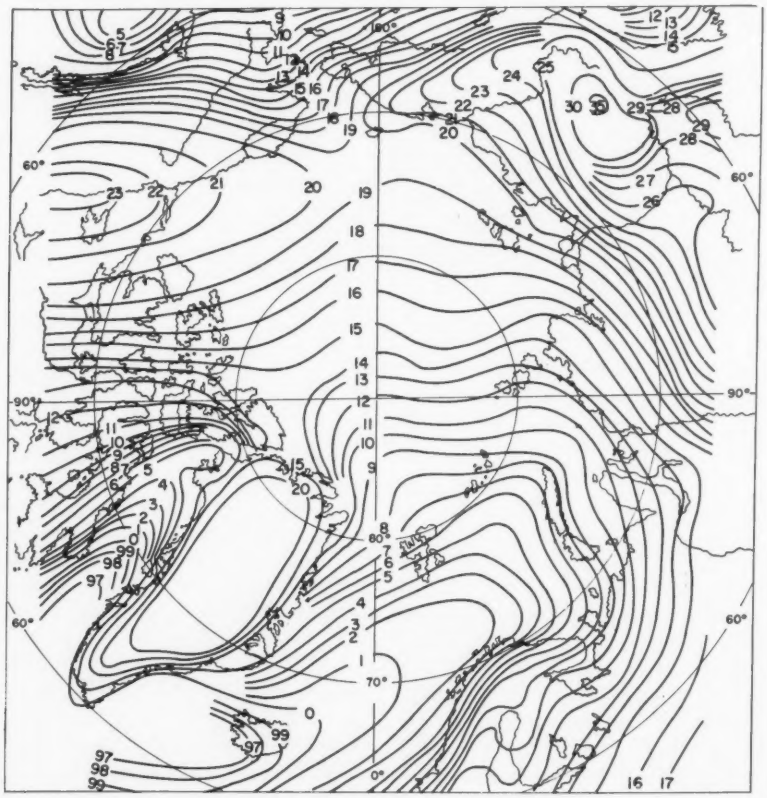

Figure 10. Mean surface pressure (mb) in January.[28,29]

aerosol. We feel that this is the reason why the seasonalities of aerosol and precipitation in the Arctic are inversely correlated.)

Because of its location, the Taymyr pathway is more difficult to verify by actual observation than is the return-flow pathway. We have been able to verify it to our satisfaction, though, with aerosol samples provided by the Air Force from routine Arctic flights. This has established that aerosol emerging from the Taymyr pathway matches the Barrow aerosol in composition, and is different from that of the Norwegian Arctic. Back-trajectories for the Taymyr samples, which are numerous enough to allow statistically valid conclusions to be drawn, pass through the central Soviet Union.

It is interesting to note that all the major pathways from Eurasia to the Arctic discussed above have one feature in common—the same migrating low-pressure areas. Because the importance of these lows to Arctic air chemistry has not been fully appreciated before, we summarize the above discussion by following the progress of a given low as it creates each of the pathways in turn.

Consider a low-pressure area fresh from the North American mainland. It first follows the North Atlantic storm track, which is basically the path of the Gulf Stream, i.e., from the Canadian Atlantic Provinces toward Iceland. As the low approaches Europe, it may combine with a high over Europe to produce a black episode into Scandinavia. The low then advances northward along the Norwegian coast. If conditions are right, it may extend the black episode to the Norwegian Arctic, where it would appear as a direct episode. As the low passes between Bear Island and Norway, on its way to Novaya Zemlya, it creates a brief, but strong, return-flow episode into the Norwegian Arctic. As it reaches Novaya Zemlya, the flow around the leading edge of the low combines with the Asiatic high to bring aerosol from the Soviet Union to the Arctic via the Taymyr pathway. By this time, the next low is already near Europe, and in a few days it will have arrived at Novaya Zemlya to replace the first one, which in the meantime has filled and disappeared. And so it goes throughout the winter, with successive pulses of aerosol to Scandinavia, the Norwegian Arctic, then the eastern Arctic, each type of pulse being a little slower and steadier than the one preceding it.

Movement of Pollution in the Arctic

Where does pollution aerosol go after it enters the Arctic? This depends on location and season. During early winter, from roughly November through January-February, the answers are very different for the Norwegian Arctic and for the Taymyr area. In the Norwegian Arctic, there is little tendency for deeper penetration into the Arctic, for the return-flow pathway is already heading south. At this time of year, aerosol from the Norwegian Arctic is not seen near Barrow. In the Taymyr area, however, air flows (in the mean) straight across the ice cap to the North American Arctic (see Figure 10). This penetration is facilitated by the lack of a high-pressure area over the pole at this time. This pressure pattern is at odds with the traditional picture of semi-permanent high pressure centered on the pole, and is a feature of Arctic meteorology whose importance to Arctic air chemistry has only recently been appreciated. Of course, not every pulse of air from the Taymyr flows to Barrow, but the distinct tendency is there, and each winter there are few events, typically of several days duration, that can be very strong. When the Asiatic high is well developed at the same time, the flow can come from deep inside the Soviet Union.

The situation during spring is quite different. By March and April, the classical polar high has formed, and is centered on the Alaskan side of the pole near the center of the pack ice (see Figure 11). This air mass blocks direct flow from the Taymyr to Alaska, and diverts it westward along the Eurasian coast into the Norwegian Arctic and thence past Greenland and along the Canadian Arctic Islands to Alaska. The portion of this pathway from the Norwegian Arctic is shown in idealized form in Figure 9. As far as the North American Arctic is concerned, the presence of the polar high favors nearer sources of aerosol along this path, i.e., Europe rather than the central Soviet Union. When conditions are right, (European) aerosol from the Norwegian Arctic can be transported *en masse* to Barrow. An example of this is given in Figure 12, which shows Mn and V in daily samples from Barrow during the winter of 1979-80. Throughout the early part of the winter, the Mn/V ratio remained between 1 and 2, i.e., near its winter-mean values. But in early March, aerosol with a Mn/V ratio of about 0.6 appeared suddenly and remained for nearly 6 weeks. Meteorological maps for this period revealed that there had been a prolonged direct episode northward from Europe beginning a few days before the new aerosol appeared at Barrow, and that there had been a strong polar high to divert the flow from the Norwegian Arctic toward Barrow. Because the low Mn/V ratios of this episode corresponded so closely to the winter mean at Bear Island (see Figure 7), there could be little doubt that this aerosol had, in fact, come from Europe, via the Norwegian Arctic. Events such as this seem to be a regular feature of spring

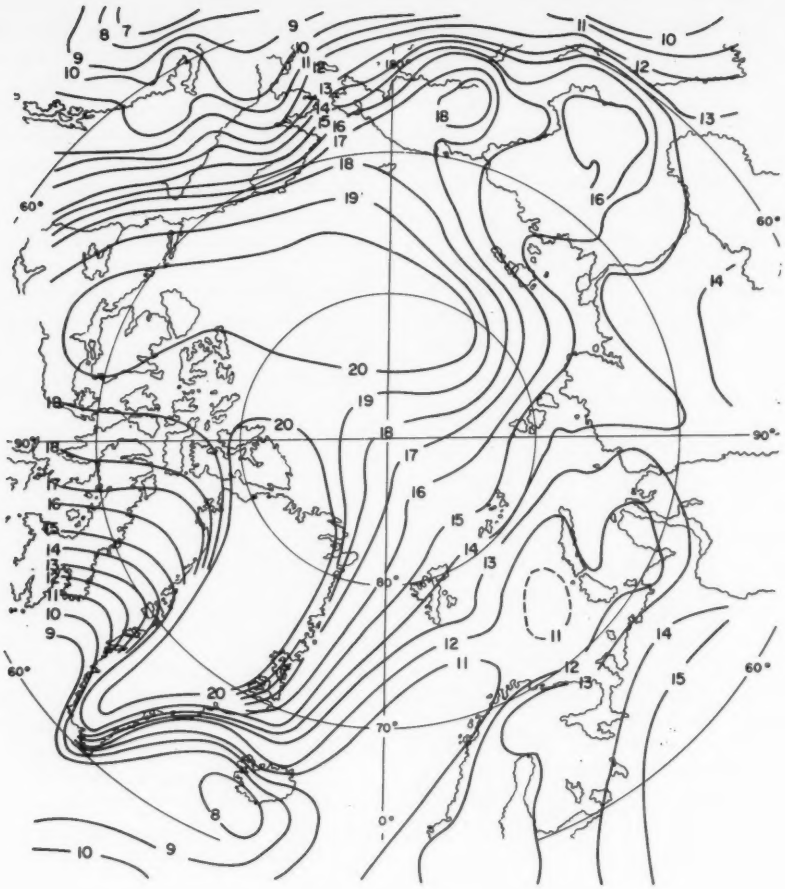

Figure 11. Mean surface pressure (mb) in April.[28,29]

at Barrow.

During March and April, the intensity of the general circulation decreases rapidly. Consequently, the migrating lows and the Asiatic high weaken, and transport to the Arctic declines rapidly. By May, nearly all the aerosol of winter is gone. The North American Arctic remains nearly free of pollution for the rest of the summer, until September or October when the cycle starts over again. On the Eurasian side, however, sources are nearer, and weak events of transport appear sporadically throughout the summer, but are curiosities rather than being of real significance. Between pulses, the air is extremely clean.

Altitude of Transport

One of the most interesting questions concerning transport of aerosol to the Arctic is its altitude. Long-range transport of aerosol is often regarded as occurring primarily in the mid-troposphere, where air moves faster and contaminants are removed more slowly than in the surface boundary layer below 1-2 km elevation. Transport aloft seems to be the rule for Saharan dust crossing the Atlantic, as well as for Asian desert dust over the Pacific Ocean. For this reason, it has been suggested at various times that long-range transport of pollution aerosol to the Arctic should take place well above the surface. While the last word is certainly not in on this subject, primarily because there have been so few measurements

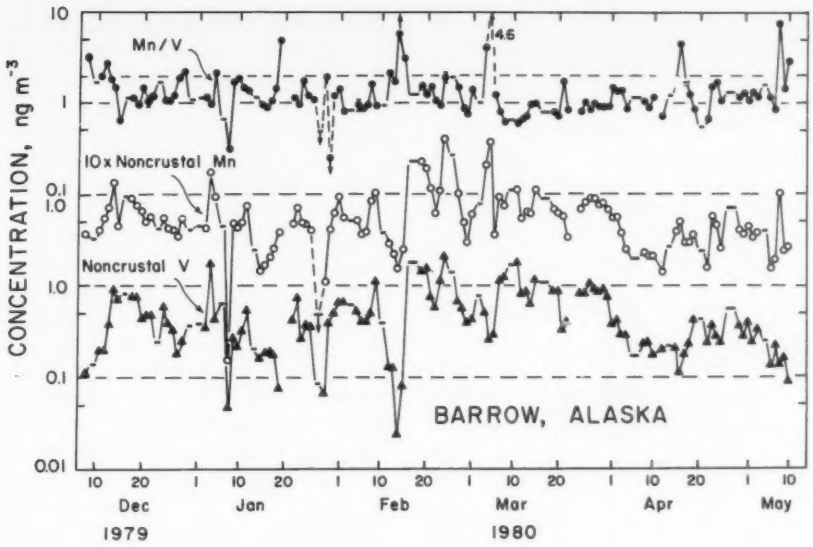

Figure 12. Noncrustal Mn, noncrustal V, and the Mn/V ratio in daily samples from Barrow, Alaska, winter 1979-80.

aloft, the facts do not seem to support this supposition. Rather, the transport seems to be concentrated at unusually low altitudes, normally below 3 km (10,000 feet) and often at or below 1.5 km (5,000 feet). Because these observations "break all the rules" of long-range transport, they have been treated with considerable skepticism. But we have repeatedly found the haze at Barrow to be concentrated below 3 km or so. Although the Ptarmigan observers occasionally reported haze to the Arctic tropopause (8-9 km), the great majority of their sightings were below 5 km. (Lacking reference points in the upper troposphere, visual observations often overestimate the amount of haze.) Earlier balloon-based measurements of light scattering in the Alaskan Arctic by the University of Wyoming showed the bulk of the haze particles to be below 5 km. Various other aircraft measurements have suggested that the effective ceiling may be closer to 3 km.

There are good reasons why aerosol should be transported to the Arctic at lower elevations than elsewhere. The principal one is the lack of a driving force to lift the aerosol. The Arctic atmosphere is extremely stable during winter, when the ice cap is at its maximum and there is negligible direct solar radiation to destabilize the surface layer. The smooth surface of ice and snow minimizes mechanical turbulence as well. Low-pressure areas, which are a great destabilizing force in midlatitudes, are weak and ineffective by the time they reach the Arctic. Nearer the sources there is also little tendency to mix aerosol aloft, for most of Eurasia is snow-covered during winter. In the central Soviet Union source area, temperatures are commonly −20 °C and below. It should be remembered that the Eurasian population in general is located 10° farther north than is the North American population, and hence receives much less sunlight during winter. Even when aerosol is transported from central Europe to Scandinavia (50-60 °N), it is held below 2 km altitude[18].

Thus, it would seem that transport to the Arctic takes place at lower elevations than is common in other parts of the world. One fortunate side effect of this low-level transport is that measurement at the surface, which is often the only practical way to accumulate regular samples, may be considerably more representative of the transport as a whole in the Arctic than in areas where the surface layer is cut off from transport aloft.

Environmental Effects of Arctic Haze

No discussion of Arctic haze would be complete without mention of its environmental effects, which may be classified as radiative, nucleational, or depositional. Radiative effects include scattering and absorption of visible light by the aerosol, and the conse-

quent alteration of the local radiation balance. In most aerosols scattering dominates absorption, and Arctic haze is no exception. Sulfate and the associated water are the major scatterers. Other than creating the visible haze, however, scattering is a relatively unimportant feature of the Arctic aerosol; it merely lengthens the path of the light rays as they pass through the Arctic atmosphere. Absorption is far more important, in spite of its smaller magnitude. The primary absorber in most aerosols, and in the Arctic aerosol as well, is black carbon, or soot. Arctic haze contains much more black carbon than expected—orders of magnitude more than found over the Pacific Ocean, for example, and 2-3 times more than predicted based on pollutants such as sulfate, vanadium or manganese. Measurements by Dr. Edward M. Patterson of the Georgia Institute of Technology show that carbon is higher in concentration at Barrow than at Bear Island. We are tentatively ascribing these high concentrations to some feature of air pollution in the central Soviet Union source area that we do not understand. It may be from a general lack of pollution controls there, from the predominant use of coal as an energy source, or it may have some entirely different explanation.

Whatever the reason, there is a great deal of carbon in the aerosol of the North American Arctic. It has been estimated that during spring, this carbon can heat the local lower atmosphere by as much as 1 °C per day[19]. More recent estimates have tended to revise this figure downward, but it still remains unexpectedly high relative to the nature of the area. This topic is currently undergoing extensive further study, because any effect of man that tends to heat the polar regions is well worth monitoring closely.

Another aspect of Arctic carbon is its deposition onto the pack ice, where is continues to absorb solar radiation throughout the summer, long after atmospheric carbon has disappeared[20,21]. Clearly, this can greatly extend the influence on Arctic climate and preliminary evidence indicates that carbon in Arctic snow can indeed increase the latter's absorption of visible radiation by several percent[21].

The nucleational aspect of Arctic haze may be one of its most important environmental effects. In general, three kinds of nuclei are recognized: condensation nuclei (CN), such as are measured by an Aitken counter at several hundred percent supersaturation; cloud-condensation nuclei (CCN), particles which nucleate water at the much lower supersaturations actually found in clouds (a few tenths of a percent); and ice nuclei (IN), particles which nucleate ice crystals in clouds. CN counts give the total numbers of particles in the atmosphere, rather than information on their nucleational properties, and hence will not be considered further here. CCN and IN are environmentally meaningful quantities, and are presently the subject of a Ph.D. thesis by Mr. Randolph D. Borys of Colorado State University (under ONR sponsorship). His preliminary data are most interesting—they show that Arctic haze increases the numbers of CCN but seems to decrease the numbers of IN. The increase of CCN is tentatively linked to elevated sulfate concentrations in Arctic haze, whereas the decrease of IN concentrations is more puzzling. One proposal is that the surfaces of IN (often soil or mineral particles) may be poisoned by secondary material such as sulfate or organics deposited during transport. In one completed study by Mr. Borys, an episode of aerosol transport from Europe to Iceland was observed in August 1979. During this event, concentrations of both CCN and pollution aerosol were temporarily elevated[22].

Depositional effects of Arctic aerosol have not been studied as much as its radiative and nucleational effects have. Carbon deposited on pack ice has already been mentioned. But many other elements and ions can be detected in Arctic snows; the relation between the trace compositions of snows and parent aerosol is not at all clear, however, and may be very complex. In one now-classic case, trace elements in a series of snow samples near Barrow were measured; from their ratios, it was concluded that the aerosol near Barrow was primarily natural in origin[23]. But these same elements in the Barrow aerosol reveal an overwhelming anthropogenic influence. Part of this discrepancy may be from the methods used to interpret the snow data, but part of it may also be due to selective scavenging of aerosol by snow. This aerosol-snow dichotomy is worthy of considerable further study, for it is central to the interpretation of trace-element data from the Greenland Ice Sheet, which are used to derive historical trends of air pollution in the Northern Hemisphere.

Ecological aspects of deposition to the surface of the Arctic may also be important. It has recently been calculated that more lead enters the Arctic Ocean from the atmosphere than from the influx of North Atlantic water or from rivers[24]. The situation may well be the same for other metals of ecological interest. These metals and other substances such as organic compounds are also deposited on the tundra, where they enter the Arctic food chain. The ramifications of this remain completely unexplored. The Arctic aerosol is also very acidic, particularly during spring. The effects of this acidity on the tundra biome need to be investigated.

Further Studies—International Cooperation

The ONR Arctic haze project has stimulated the creation of several other programs: The Canadian Atmospheric Environment Service is now operating three sampling stations in the Canadian Arctic, at Mould Bay, Igloolik, and Alert. Denmark has five sampling sites around the perimeter of Greenland. Iceland is engaged in a long-term cooperative study of their aerosol with URI. The winter and summer aerosol of western Ireland was studied with the aid of University College, Galway. The Norwegian Institute for Air Research has conducted several years of air sampling at both Bear Island and Spitsbergen, and is about to expand its program during the next five years. One of the major scientific goals of the summer 1980 Arctic expedition of the Swedish icebreaker *Ymer* was an international study of air pollution in the Norwegian Arctic. As a result of the *Ymer* cruise, the Johannes Gutenberg University in Mainz, W. Germany has begun its own study of the Arctic aerosol.

Several countries and laboratories interested in Arctic air pollution have formed the Arctic Air-Sampling Network[25]. From its inception in 1977 (at a meeting sponsored by ONR), the network has grown until it now includes approximately 15 sampling sites. Figure 13 shows the locations of these sites as of 1980.

Two international conferences have been held on Arctic air chemistry, the first at Oslo in April 1977 and the second at Rhode Island in May 1980. The proceedings of the Rhode Island symposium comprised the August 1981 issue of the international journal *Atmospheric Environment*. A third conference is tentatively scheduled for October 1983 in Toronto.

The current surge of interest in Arctic air pollution has caused the GMCC Program to upgrade its activities at Barrow. Of its four baseline observatories, Barrow now receives the most attention. Last spring, GMCC sponsored a special series of accelerated measurements there, aimed primarily at further documenting the radiative aspects of Arctic haze.

Without a doubt, the greatest disappointment in our six-year term with Arctic haze was our failure to induce the Soviet Union to participate. Repeated overtures have been made to various individuals and departments, all without success. This is most unfortunate in light of the evidence for the central Soviet Union as the major source of aerosol to the North American Arctic.

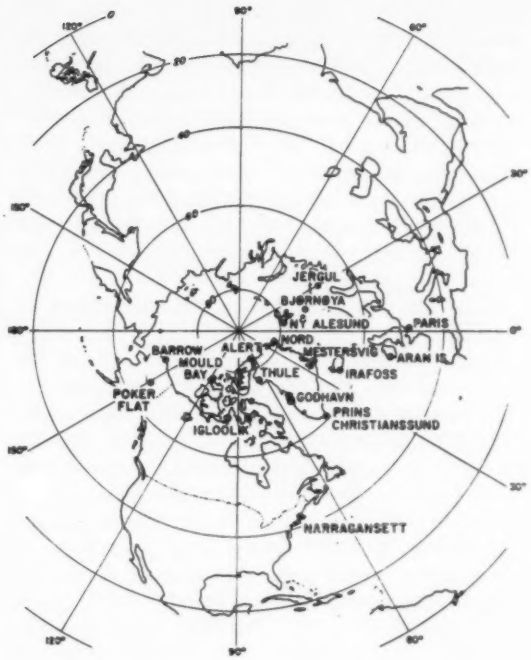

Figure 13. Sites of the Arctic Air-Sampling Network in 1980.[25]

Broader Outgrowths of This Research

There have been important spinoffs into other areas from the ONR Arctic Haze Program. One of these is the development of a general system of elemental tracers for source areas of pollution aerosol, which is sure to find application in various regions and atmospheric problems. This system is still in its infancy. A major effort to develop it into a full-fledged system involving many tracer elements is now under way at URI for Europe, via a collection of cooperative local efforts called the European Aerosol-Sampling Network. Aerosol samples are being collected in Belgium, West Germany, Austria, Hungary, Sweden, Finland, and eventually also Poland, we hope, and are sent to the University of Rhode Island for analysis. Compositional patterns over Europe will be correlated with similar observations on both sides of the Arctic; from these correlations, we hope to be able to deduce which elements make the best tracers, and which subregions of Europe are the most important sources of Arctic aerosol. From this, it should be possible to go more deeply into meteorological aspects of transport to the Arctic.

Another major spinoff, just developing, is the

construction of a similar set of elemental tracers for the eastern United States and its application to the problem of sources and transport of acidity to the Northeast. This project is particularly noteworthy because acid precipitation is the number-one environmental issue in the United States today. The sources of acid rain in the Northeast are not at all clear; it is our hope that the tracer techniques first developed for the Arctic can be expanded and refined for the Northeast, and will shed some light on the true sources of acid rain there.

In conclusion, the ONR-sponsored research of the last six years on Arctic haze has shown that it is strongly pollution-derived, that its sources are primarily Eurasian but differ from one part of the Arctic to another, that it is transported in the lower troposphere by major synoptic systems, primarily the migratory lows and the polar high, and that it may have important radiative, nucleational and depositional effects. These conclusions are only broad generalizations, however—much work remains to be done providing details for each area. In the future, we hope to use elemental tracers to delineate the sources more precisely, to develop more appropriate meteorological techniques to better understand the transport, to fill in the third dimension with more aircraft-based observations, and to look further into the various environmental effects. We hope to continue to stimulate other groups to join us, in order to broaden the range of studies. But one thing is sure: no matter what the total effort devoted to Arctic haze, and no matter what the eventual mix of laboratories and projects involved, the study of air pollution in this area will continue to be fascinating and stimulating.

Acknowledgments

We are most grateful for the long-term support of ONR's Arctic Program, which has made this work possible. Throughout this investigation, Dr. G. Leonard Johnson and Mr. Ronald K. McGregor of ONR encouraged us to be broad and interdisciplinary, and gave us the scientific freedom that was indispensable in dealing with the many and varied unknowns of Arctic haze. Additional support was provided by the National Science Foundation. Messrs. Randolph D. Borys and Thomas J. Conway designed and carried out many of the field experiments, and analyzed samples in the laboratory as well. More recent analyses were performed by Ms. Noelle F. Lewis and Mr. Douglas H. Lowenthlal. The GMCC program, in Boulder, Colorado, has been continually supportive of our efforts. A long series of their observers in Barrow, Alaska, have changed samples for us and cared for our equipment. Elemental analyses were performed using facilities of the Rhode Island Nuclear Science Center. ■

References

1. Mitchell, J. M., "Visual Range in the Polar Regions with Particular Reference to the Alaskan Arctic," *Journal of Atmospheric and Terrestrial Physics,* Special supplement, (1957), p. 195.

2. Holmgren, B., G. Shaw and G. Weller, "Turbidity in the Arctic Atmosphere," *AIDJEX Bulletin,* Vol. 27, (1974), p. 135.

3. Mason, B., *Principles of Geochemistry,* 3rd Edition, Wiley & Sons, Inc., New York (1966).

4. Rex, R. W., J. K. Syers, M. L. Jackson and R. N. Clayton, "Eolian Origin of Quartz in Soils in Hawaiian Islands and in Pacific Pelagic Sediments," *Science,* Vol. 163, (1969), p. 277.

5. Griffin, J. J., H. Windom and E. D. Goldberg, "The Distribution of Clay Minerals in the World Oceans," *Deep-Sea Research,* Vol. 15, (1968), p. 433.

6. Isono, K., M. Komabayasi, T. Takeda and others, "Concentration and Nature of Ice Nuclei in Rim of North Pacific Ocean," *Tellus,* Vol. 23, (1971), p. 40.

7. Rahn, Kenneth A., Randolph D. Borys and Glenn E. Shaw, "Asian Desert Dust over Alaska: Anatomy of an Arctic Haze Episode," *Desert Dust: Origin, Characteristics, and Effects on Man,* Ed. Troy L. Pewe, Geological Society of America, Special Paper 186, (1981), p. 37.

8. Miller, J. M., "A Five-year Climatology of Five-day Back Trajectories from Barrow, Alaska," *Atmospheric Environment,* Vol. 15, No. 8, (1981), p 1401.

9. Barrie, L. A., R. M. Hoff and S. M. Daggupaty, "The Influence of Mid-Latitudinal Pollution Sources on Haze in the Canadian Arctic," *Atmospheric Environment,* Vol. 15, No. 8, (1981), p. 1407.

10. Patterson D. E., and R. B. Husar, "A Direct Simulation of Hemispherical Transport of Pollutants," *Atmospheric Environment,* Vol. 15, No. 8, (1981), p. 1479.

11. Reiter, E. R., "Planetary-wave Behavior and Arctic Air Pollution," *Atmospheric Environment,* Vol. 15, No. 8, (1981), p. 1465.

12. Carlson, T. N., "Speculations on the Movement of Polluted Air to the Arctic," *Atmospheric Environment,* Vol. 15, No. 8, (1981), p. 1473.

13. Rahn, K. A., "Relative Importances of North America and Eurasia as Sources of Arctic Aerosol," *Atmospheric Environment,* Vol. 15, No. 8, (1981), p. 1447.

14. Rahn, K. A., "The Mn/V Ratio as a Tracer of Large-scale Sources of Pollution Aerosol for the Arctic," *Atmospheric Environment,* Vol. 15, No. 8, (1981), p. 1457.

15. Komarov, Boris, *The Destruction of Nature in the Soviet Union,* (M. E. Sharpe, Inc., White Plains, NY, 1980), p. 150.

16. Brosset, C., "Black and White Episodes," *Ambio,* Vol. 5, (1976), p. 157.

17. Rahn, Kenneth A., Einar Joranger, Arne Semb and Thomas J. Conway, "High Winter Concentrations of SO_2 in the Norwegian Arctic and Transport from Eurasia," *Nature,* Vol. 287, No. 5785, (1980), p. 824.

18. "Organisation for Economic Cooperation and Development," *The OECD Programme on Long Range Transport of Air Pollutants—Measurements and Findings,* (Paris, 1977).

19. Shaw, Glenn E. and Knut Stamnes, "Arctic Haze: Perturbation of the Polar Radiation Budget," *Annals of the New York Academy of Sciences,* Vol. 338, (1980), p. 533.

20. Wiscombe, Warren J. and Stephen G. Warren, "A Model for the Spectral Albedo of Snow. I: Pure Snow," *Journal of the Atmospheric Sciences,* Vol. 37, No. 12, (1980), p. 2712.

21. Warren, Stephen G. and Warren J. Wiscombe, "A Model for the Spectral Albedo of Snow. II: Snow Containing Atmospheric Aerosols," *Journal of the Atmospheric Sciences,* Vol. 37, No. 12, (1980), p. 2734.

22. Borys, R. D. and K. A. Rahn, "Long-Range Atmospheric Transport of Cloud-active Aerosol to Iceland," *Atmospheric Environment,* Vol. 15, No. 8, (1981), p. 1491.

23. Weiss, H. V., M. M. Herron and C. C. Langway, Jr., "Natural Enrichment of Elements in Snow," *Nature,* Vol. 274, (1978), p. 352.

24. Rahn, K. A., "Atmospheric, Riverine and Oceanic Sources of Seven Trace Elements to the Arctic Ocean," *Atmospheric Environment,* Vol. 15, No. 8, (1981), p. 1507.

25. Rahn, K. A., "The Arctic Air-Sampling Network in 1980," *Atmospheric Environment,* Vol. 15, No. 8, (1981), p. 1349.

26. Rahn, Kenneth A. and Richard J. McCaffrey, "On the Origin and Transport of the Winter Arctic Aerosol," *Annals of the New York Academy of Sciences,* Vol. 338, (1980), p. 486.

27. Rahn, Kenneth A., "On the Causes, Characteristics and Potential Environmental Effects of Aerosol in the Arctic Atmosphere," *Proceedings of the Conference on the Arctic Ocean, London, 11-12 March 1980* (In press).

28. Vowinckel, E. and S. Orvig, "The Climate of the North Polar Basin," *Climates of the Polar Regions* (ed. S. Orvig), *Vol. 14 World Survey of Climatology,* Elsevier, Amsterdam, (1970), p. 129.

29. Prik, Z. M., "Mean Position of Surface Pressure and Temperature Distribution in the Arctic," *Tr. Arkticheskogo Nausch.-Issled,* Vol. 217, (1959), p. 5.

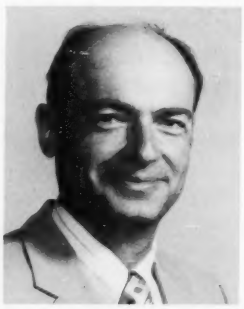

Dr. Kenneth A. Rahn is Associate Research Professor at the Graduate School of Oceanography, University of Rhode Island, Narragansett. His research specialty is using the trace-element content of remote aerosols as indicators of their origins and transport. He has been an ONR contractor studying Arctic haze since 1976.

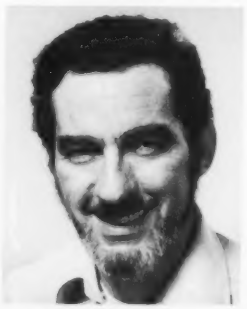

Dr. Glenn E. Shaw is Professor of Geophysics at the University of Alaska's Geophysical Institute; he teaches astronomy and atmospheric physics. He received his Ph.D from the University of Arizona in 1971. During the last decade, Dr. Shaw has investigated the chemical, optical and physical properties of particles in the air and ice of the polar regions.

profiles in science

Mr. Valentine Worthington was Chairman of the Department of Physical Oceanography at the Woods Hole Oceanographic Institution; he retired this past spring. For 38 years Worthington was on the staff of Woods Hole and was a contractor for the Office of Naval Research since its establishment in 1946. He is known for important research in the areas of deep ocean circulation and water mass formation.

Typical of his work on deep ocean water masses were the results of 1951 and 1952 expeditions to the Arctic ice pack to obtain deep water salinity and temperature data from the Arctic Basin. Because of differences of the data in the deep water off Alaska and off Eurasia, he inferred the existence of a submarine ridge, which was subsequently confirmed by Soviet oceanographers.

The comprehensive data from surveys of the North Atlantic waters inspired Worthington to undertake a fine-scale volumetric census of water masses. This work lead to the publication in 1976 of his monograph, *On the North Atlantic Circulation,* which contains an analysis, layer by layer, of the deep water sources and flows. His extensive knowledge of the thermohaline, oxygen, and silicate fields in the North Atlantic enabled Worthington to postulate a two-gyre circulation east of the Grand Banks, to infer links between Gulf Stream intensity and formation of 18°C water in the Sargasso, and to continue speculation about deep water formation and renewal.

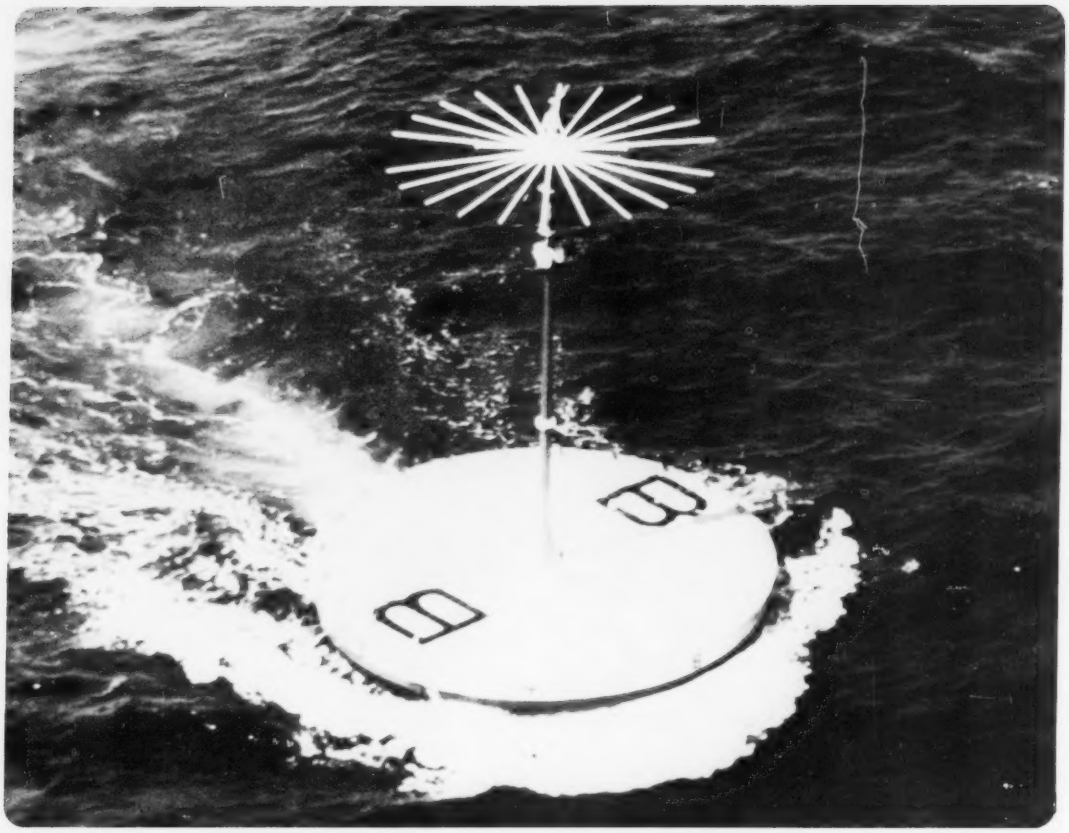

On the Use of Dissolved Oxygen Concentration as an Indicator of Winter Convection

by

Joseph L. Reid
Scripps Institution of Oceanography

Introduction

There exists a rough concordance in the upper layer of the North Pacific Ocean between the patterns of saturation of dissolved oxygen and the depth of winter convection as determined from temperature structure. While this should not be surprising, when the general physical and chemical processes are considered, two of its features are novel and interesting. One is that the observations in high latitudes in winter indicate substantial undersaturation in the upper layer. This may result from the water being cooled faster than the oxygen can equilibrate, or from the fall and winter mixing of deeper, undersaturated water into the upper layer. The other is that in winter the depth to which saturated or nearly saturated water extends, may indicate the depth to which convection has taken place previously. Even though the convection may have ceased for a while, and the vertically uniform temperature and salinity associated with the convection may have been interrupted, leaving no unique signal of the depth of previous penetration, the high saturation value of oxygen may provide such a record.

Some of us may be concerned with the maximum depth of convective overturn, at whatever time in winter it occurs. This will clearly be important in studies of heat budget, where we want to know how thick a layer may have been in contact with the atmosphere.

The determination of the depth of a winter convective layer is not difficult if proper measurements are made at the time of convection. However, convection may not be continuous throughout the winter, but interrupted between the passages of storms, and determination of the maximum depth of convection during some earlier winter event depends upon some trace being left of such previous penetration.

Values of temperature and salinity may not suffice if some restructuring has occurred, that is, if an area of convection has been covered over by layers of less dense waters from adjacent regions. The structure, if altered, may not leave a clear record of an earlier, deeper, convection, and the specific temperature and salinity during the previous convection may not be known. Thus, the maximum depth of convection, which may be an important quantity in calculations of the heat budget, may be known, but poorly.

It is possible that the degree of saturation of the dissolved oxygen concentration may leave a record of the depth of penetration of previous convection.[1] Although the winter data for examining this concept are not yet so numerous as we should like, nor perhaps all of such high quality, there does seem to be enough material to discuss the proposition and to make it seem plausible at least, if not yet proven.

Saturation of Dissolved Oxygen in the Upper Layer

Over most of the North Pacific the water at the sea surface (sampled by bottles at 1- or 2-m depth) has a concentration of dissolved oxygen that in summer is at or slightly above the value expected if it were in equilibrium with the atmosphere.[2] A map of the depth at which the saturation ratio (for atmospheric pressure) has decreased to 100 percent in summer (Figure 1) has been prepared by Shulenberger and Reid.[3] In the far north and west the values are irregular but mostly shallower than 75 m. Near the equator in the east, upwelling brings up undersaturated waters and the 100 percent isopleth outcrops. South of about 35 °N this map bears some resemblance to the maps of the depth of the winter mixed layer prepared by Bathen[4] and Robinson[5]; north of 35 °N it is more nearly like their mixed-layer maps for summer.

Both of their maps are based upon temperature data alone. Robinson[5] chose as a criterion the depth at which temperature is 1.11 °C (2 °F) below the surface temperature. Because of the various inversions in the higher latitudes that make this criterion questionable, she chose not to map the northern areas for winter. Bathen[4] used various criteria for estimating the depth from the thermal structure, and his maps include the entire North Pacific Ocean.

Winter Conditions

Why should there be such a similarity in the fields of density in March and oxygen saturation in July-August south of 35 °N, and no such fit farther north? And in areas where there is such a fit in winter, can we make any use of it?

One proposition might be that the oxygen concentration in the well-mixed layer reaches equilibrium with the atmosphere during winter mixing and retains its value through much of the following summer. Gaseous oxygen from the atmosphere dissolves in sea water, and its solubility is greatest in the coldest, least saline waters. It is measured in sea water by the Winkler method, from discrete samples. Since the accuracy is about plus or minus one percent, any saturation ratio between 99 and 101 percent will be treated here as 100 percent. The solubilities determined by Weiss[6] have been used in all of these calculations. The saturation has been calculated as if the

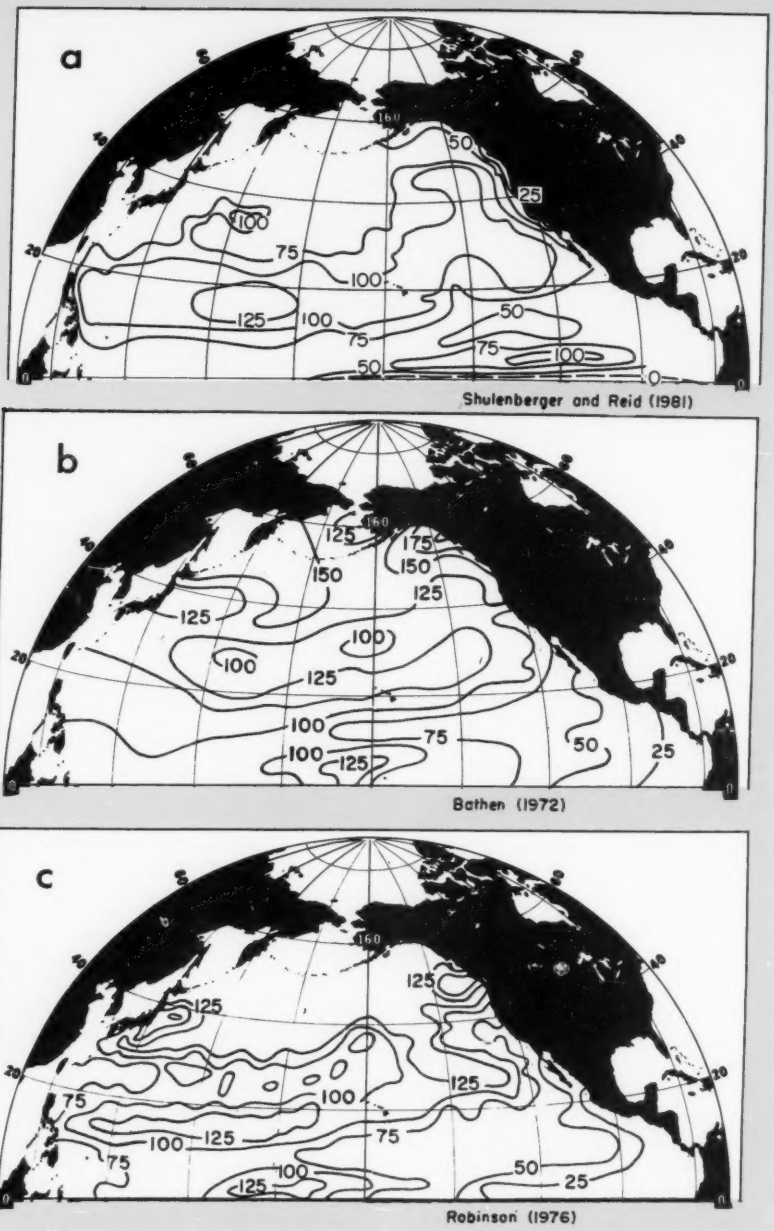

Figure 1a. Depth (in meters) at which the oxygen saturation ratio is 100% in summer.[3]

Figure 1b. Depth (in meters) of the mixed layer in March, adapted from Bathen.[4]

Figure 1c. Depth (in meters) of the mixed layer in March, adapted from Robinson.[5]

sample were at the sea surface and in contact with the atmosphere (at one atmosphere of pressure) and the saturation ratio is expressed in percent, to avoid confusion with other quantities.

A station in the northern North Pacific in mid-ocean illustrates the winter conditions (Figure 2). Temperature, salinity, dissolved oxygen concentration and oxygen saturation ratio are uniform to a little more than 100-m depth.

Similar conditions exist at Station Papa even in late winter (Figure 3). In the following summer at Station Papa (Figure 4) the depth of saturation is still within a few meters of the winter depth, though the overlying waters have changed in structure and the oxygen concentration is well above the saturation value.

However, this situation does not obtain everywhere during winter. In the northwestern area, in particular, where the North Pacific water is coldest in winter, quite a number of stations show surface layers which, though well-mixed in temperature and salinity, are not in equilibrium with the atmosphere in terms of oxygen. This could mean either that the water is still cooling, and equilibrium cannot quite keep up, or that convection is still bringing in the deeper undersaturated water.

This is illustrated by data from a station in the far northwest (Figure 5). Uniform conditions extend to 200-m depth in all quantities, but the upper layer has not yet come to equilibrium in oxygen concentration: it is undersaturated. As the coldest waters of the open North Pacific are found in the far northwest in winter, surface layer concentrations of dissolved oxygen are highest there, as might be expected. Even so,

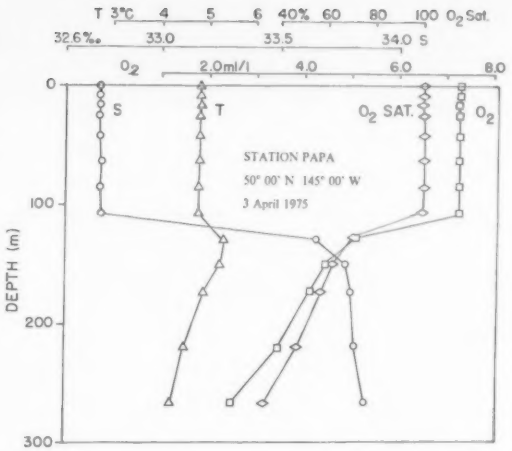

Figure 3. Temperature (°C), salinity (°/oo), dissolved oxygen (ml ℓ^{-1}), and oxygen saturation (%) on a Papa Station.[8]

the waters there (Figure 6) are substantially undersaturated in February and March.[11] It has been proposed that under violent storm conditions bubbles of air carried down might dissolve and lead to supersaturation, but the data show no effect of such a process. The stormiest domains are lowest in saturation in these winter data.

Furthermore, in some areas in the north, the oxygen concentration decreases substantially in summer below the upper few meters (possibly the result of respiration), and cannot serve in summer as a

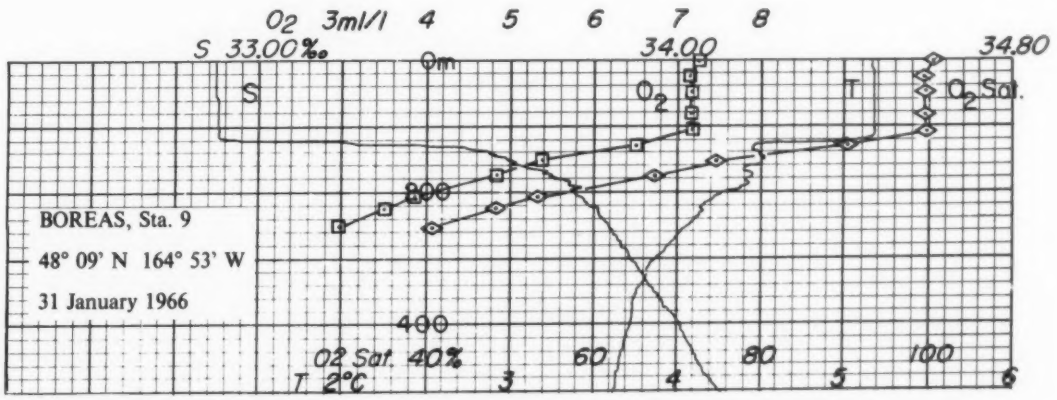

Figure 2. Temperature (°C), salinity (°/oo), dissolved oxygen (ml ℓ^{-1}), and oxygen saturation (%) on Boreas Station 9.[7] *Temperature and salinity were measured by a continuously-recording STD, oxygen was measured from water samples.*

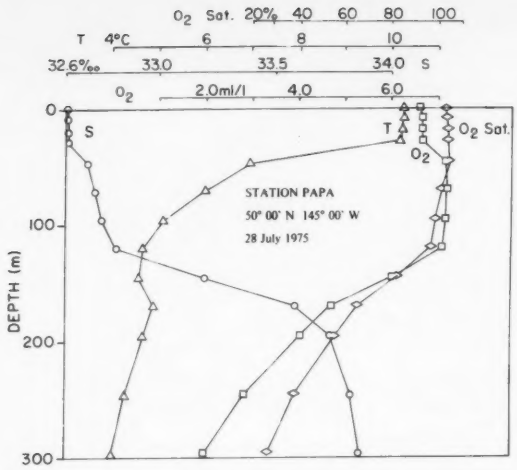

Figure 4. Temperature (°C), salinity (°/oo), dissolved oxygen (ml l^{-1}), and oxygen saturation (%) on a Papa Station.[9]

record of previous winter convection (Figure 7). Farther south, photosynthesis in summer actually increases the oxygen concentration down to the approximate depth of winter convection, though the increase does not seem to extend below that depth (Figure 8). In these lower latitudes the depth of the 100% isopleth in summer appears to correspond quite well to the depth of winter convection.[3]

Mixed-layer Depth in the Northwest

In substantial areas of the northern North Pacific Ocean the upper layer is undersaturated in oxygen. The equilibrium value (a saturation ratio of 100 percent) is not found anywhere in the column, and therefore is not available to serve as an indicator of convection. However, the saturation ratios in these areas (Figure 6) are fairly uniform vertically, even though they may be quite low (Figures 5 and 7). In such situations the break in saturation ratio beneath the uniform layer may serve as such an indicator. We can choose a saturation ratio that is 1 percent or 2 percent below the surface value, which seems to apply very well on stations that are uniform in all characteristics (Figures 5 and 7). We can compare a map prepared from the direct measurements of temperature and salinity in winter (Figure 9a) with a corresponding map, showing the depth of the 94 percent isopleth (Figure 9b) based upon the more limited number of oxygen measurements from the same expedition. Except that many of the measurements did not include oxygen, the two maps show good agreement in major features, though there are some notable differences.

In particular, six of the stations that are in the hatched areas on the map (Figure 9a), where the temperature and salinity structure give no indication of a convective layer, have oxygen saturation ratios that give clear records of the depth of a previous convection. Some of these (Figure 10), from February and early March, do not show deep, uniform convective

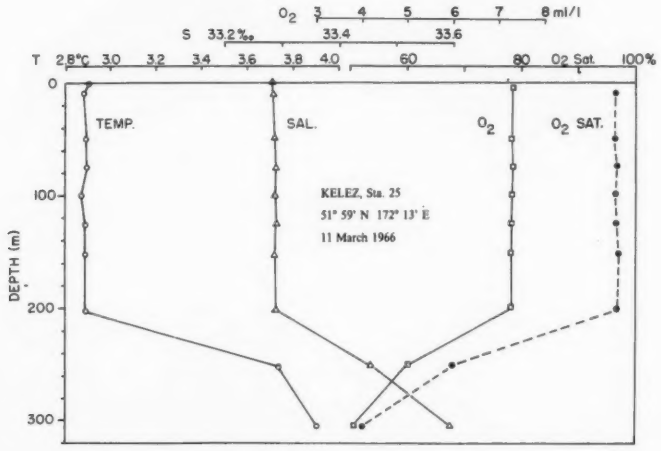

Figure 5. Temperature (°C), salinity (°/oo), dissolved oxygen (ml l^{-1}), and oxygen saturation (%) on Kelez Station 25 on 11 March 1966 at 50°59'N, 172°13'E (J.O.D.C.[10]*).*

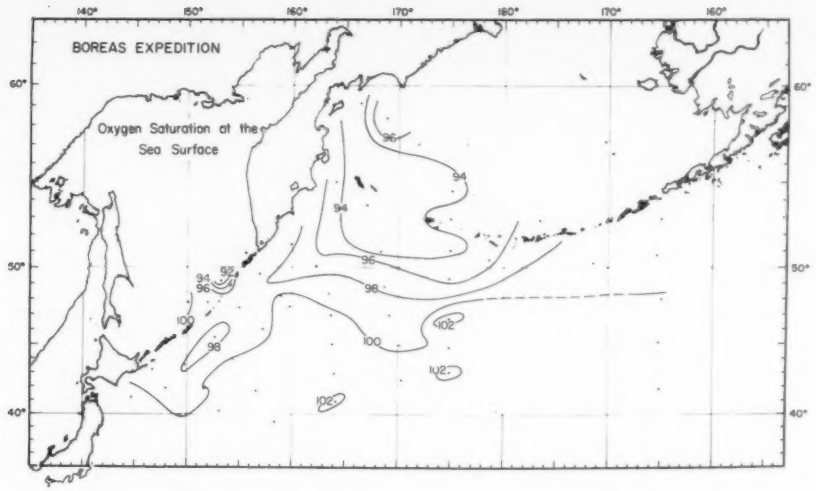

Figure 6. Saturation ratio (%) of dissolved oxygen at the sea surface, from the Boreas data.[11]

layers such as are seen on Figures 2-5; these may be examples of the transient restructuring that occurs between storms. Others, late in March in the far west (Figure 11), seem to reveal also the effect of the beginning of the warming season (Figure 11a) and interleaving with the warmer, more saline waters from the southwest (Figure 11b).

In the case of Boreas Station 175 (Figure 10b), it is worthwhile to note that, though temperature and salinity vary strongly in the upper layer, the density (σ_t, not shown) is almost uniform down to 117 m. This structure must result from horizontal exchange of waters of only slightly different density.

Mixed-layer Map for the North Pacific Ocean in Winter

From the available winter oxygen data a map of the estimated maximum depth of convection has been prepared (Figure 12). In the far northwest the depth is defined by the saturation ratio of 94 percent (though in the area with less than 94 percent seen on Figure 6, a value of 92 percent or 93 percent had to be used). In the extreme northeast a value of 97% was used, and south of about 50°N values of 97 to 100 percent were used.

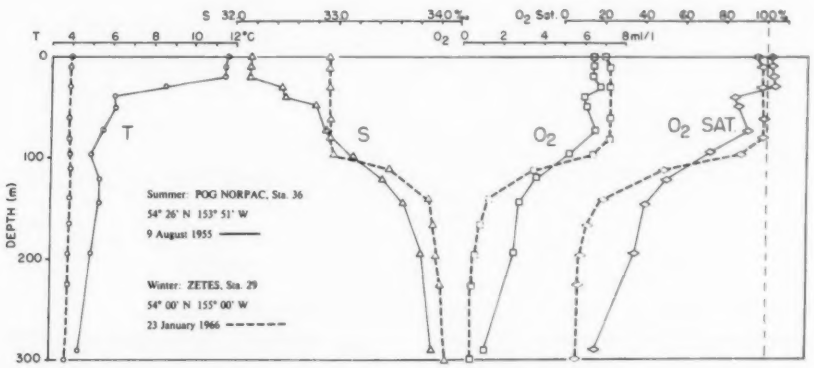

Figure 7. Temperature (°C), salinity (°/oo), dissolved oxygen (ml ℓ^{-1}), and oxygen saturation (%) in summer and in winter in the northern North Pacific Ocean.[12,13]

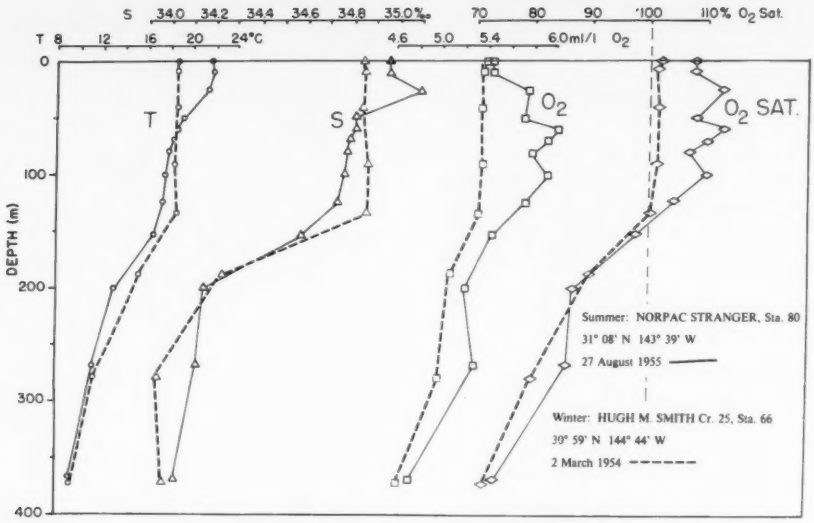

Figure 8. Temperature (°C), salinity (°/oo), dissolved oxygen (ml l^{-1}), and oxygen saturation (%) in summer and in winter near 30°N.[13,14]

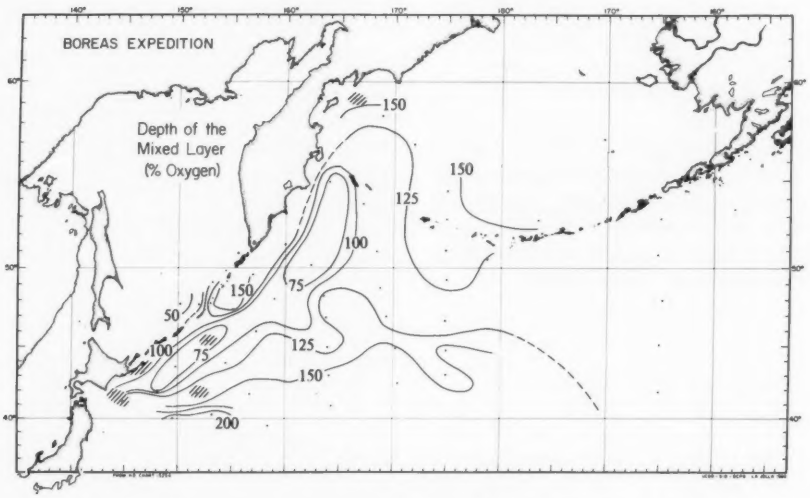

Figure 9a. Mixed-layer depth (in meters) estimated from the temperature and salinity structure.[11] *Shaded areas here and in Figure 9b indicate stations where a convective layer could not be defined.*

The data are not nearly so complete as one would like, nor is their accuracy known in all cases. And as the data, though few, include materials from different years, and are too few to be averaged, the map may show some irregularities that are not representative of an average condition but of a particular year, month, or storm.

In particular, the details near 50°N, 170°E are different from those of the Boreas map (Figure 9b) because the Kelez data (J.O.D.C.[10]) have been included, and these show clear evidence of a small area of deep convection as seen on Figure 5. Also, on Ken-

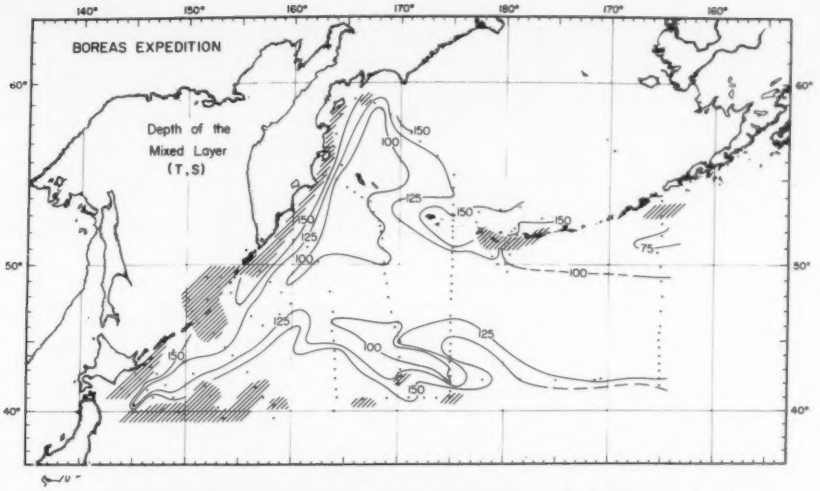

Figure 9b. Mixed-layer depth (in meters) estimated from the saturation-ratio of dissolved oxygen.

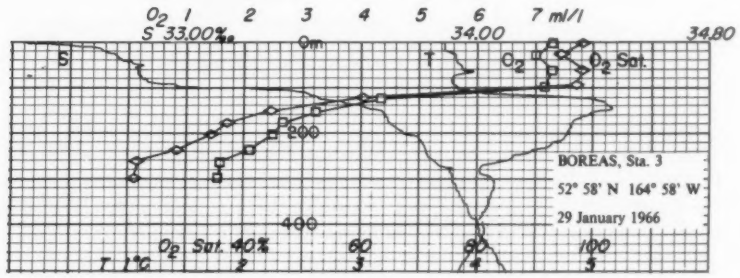

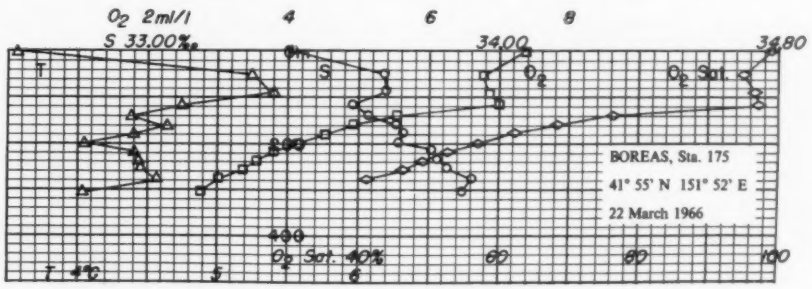

Figure 10a. Temperature (°C), salinity (°/oo), dissolved oxygen (ml l^{-1}), and oxygen saturation (%) at Boreas Station 3.' Temperature and salinity were measured from a continuously-recording STD. Oxygen was measured from discrete samples.

Figure 10b. Temperature (°C), salinity (°/oo), dissolved oxygen (ml l^{-1}), and oxygen saturation (%) at Boreas Station 175' in late winter.

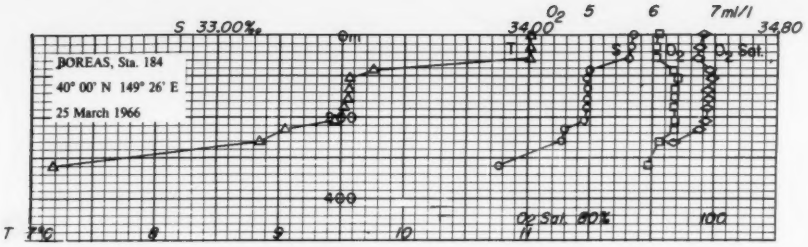

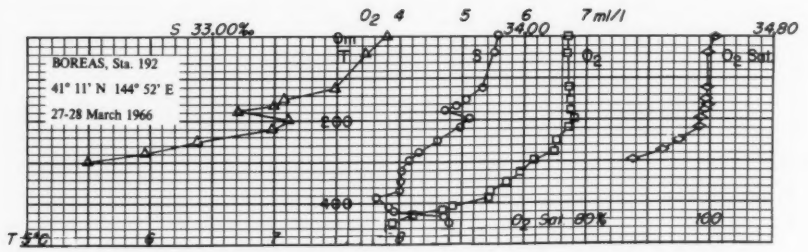

Figure 11a. Temperature (°C), salinity (°/oo), dissolved oxygen (ml l^{-1}), and oxygen saturation (%) at Boreas Station 184[7] in late winter.

Figure 11b. Temperature (°C), salinity (°/oo), dissolved oxygen (ml l^{-1}), and oxygen saturation (%) at Boreas Station 192[7] in late winter.

yon's[15] line of closely-spaced stations along 35 °N, the presence of large eddies west of 170 °E gives alternating shallow and deep upper layers, some reaching more than 200 m in depth. These features cannot be illustrated completely on a map of this size, but their presence is noted. They have been illustrated in a study by Kenyon[15]. How to treat these in terms of convection over the rather large areas where they ob-

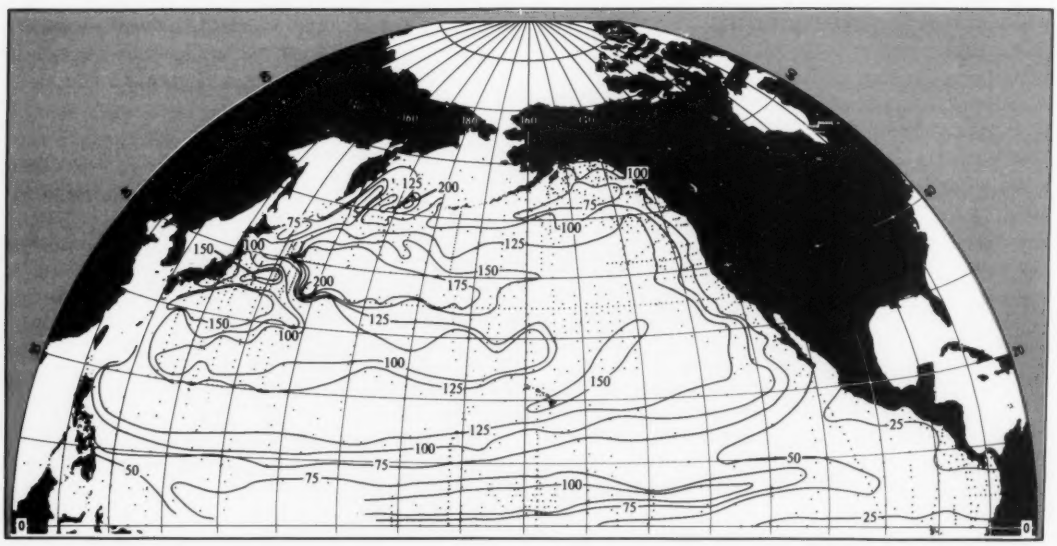

Figure 12. Mixed-layer depth (in meters) from the saturation-ratio of dissolved oxygen.

tain is uncertain, and the problem should be considered carefully when estimates of the heat budget are attempted.

However, there is a fairly clear pattern over much of the area that can be compared to earlier maps and examined in terms of the processes that contribute to the pattern.

One of the processes that might contribute to the pattern of winter mixed-layer depth is the large-scale flow pattern. The relative geostrophic flow in the upper ocean might be balanced in part by horizontal pressure gradients associated with variations in the thickness of the mixed layer. On maps of geopotential anomaly of the North Pacific Ocean (Reid[16]; Wyrtki[17]; Reid and Arthur[18]) the long east-west high in geopotential anomally defining the anticyclonic gyre extends from about 15 °N to 20 °N in the far west eastward past the Hawaiian Islands to about 25 °-30 °N at 140 °W. This shape is matched roughly by the trough defined by the 125-m isobath on Figure 12, and appears on Robinson's[5] map also (Figure 1b). In Bathen's[4] map the trough is somewhat farther north in the far west, but matches well in the central and eastern areas (Figure 1c).

South of the 15 °N-20 °N trough the system of zonal flows might be reflected in mid-ocean by a ridge near 10 °N, and (southward across the North Equatorial Countercurrent) by another trough near 5 °N, and a ridge along the equator. These features are seen on all three maps, though both Bathen's[4] and Robinson's[5] maps show another trough roughly between 160 °W and 180 °W near 3 °N. This trough does not appear in the available winter oxygen data nor in the maps of geopotential thickness.

In the north, all maps of geopotential anomaly at the surface relative to 500 decibars or greater reflect the subarctic cyclonic gyre (West Wind Drift, Alaska and Kamchatka Currents) by a low extending from the far west near the Kuril Islands (45 °N) eastward to the center of the Gulf of Alaska (about 55 °N, 145 °W). This has been illustrated for several years of data by Dodimead, Favorite, and Hirono[19]. The feature appears as a ridge on the saturation-depth map, somewhat twisted by the irregularity of the data, but clearly present. It does not appear on Bathen's[4] map, which shows troughs over much of the length of the ridge. This ridge is within the zone of a subsurface temperature maximum or a nearly uniform temperature structure extending into the pycnocline (see Figure 7 herein, Dodimead *et al.*[19], and Figure 40 in Reid[11]), and interpretation of mixed-layer depth from temperature alone can be misleading within that zone.

A ridge appears on the saturation-depth map along 25 °N-30 °N and also on the maps of Bathen and Robinson. It extends westward to about 135 °E (Figure 12) south of an isolated trough (centered at about 31 °N, 141 °E). This shape, in the far west, also bears a rough resemblance to the various maps of geopotential anomaly. That part of the ridge and the trough just to the north may reflect the presence of the Kuroshio Current, the Kuroshio return flow, and the subtropical countercurrent noted by Yoshida[20] and discused further by Masuzawa[21] and by White and Hasunuma[22]. All of the cited maps of geopotential anomaly show low values along about 25 °N west of about 150 °E, consonant with the ridge as seen on Figures 1 and 12, but none has shown the feature extending as far east as the maps of mixed-layer depth (Figures 1 and 12) show the ridge to extend.

We might see some simple relations between the 15 °N-20 °N trough and the 30 °N ridge in terms of wind-strength and direction, and fit these into schemes of surface flow, but the patterns do not everywhere fit so well. In the far north, where winter winds are strongest, the major features on Figure 12 seem to be dominated by the pattern of flow. Although winter winds and cooling do provide the deepest convective cells (as seen on Figure 5), these features appear to be the product of individual and localized storms, and do not result in a generally deep convection over the far northwestern area of greatest cooling and storms. It appears to be the flow field that dominates the pattern. A little farther south the deep trough along about 40 °N from about 155 °E to 170 °W (Figure 12) does seem to lie in the area of strong northwest winds shown by MacDonald[23] for January and February. This trough appears to be the direct result of convection by cooling and stirring: it does not correspond to the sea-surface circulation patterns recognized at present or to the geopotential anomaly calculated at the sea surface relative to 1000 decibars or deeper.

Wind-stirring must also affect the thickness of the upper layer. The long trough extending from about 15 °N in the west to 20 °N-25 °N or more in the east (Figure 12) bears some resemblance to the position of the maximum trade wind strength.[23,24] In particular, in the east the northeastward extension of the trough (past 30 °N, 140 °W) on all the maps of mixed-layer depths matches MacDonald's[23] wind fields very well indeed. And the ridge along about 30 °N, west of about 140 °W lies in MacDonald's[23] zone of minimum wind strength (the Horse Latitudes).

This resemblance between wind strength (and direction), depth of the mixed layer, surface current and geopotential anomaly is of course not coincidental. The winds not only stir but drive the ocean, but

so far we have not been able to understand these processes well enough to give a satisfactory accounting of the ocean-wide upper-layer flow and structure.

There are features other than the local wind strength, and the geostrophic balance of the large-scale flow, that affect the pattern. As discussed by Reid[11], some areas near Kamchatka and the Aleutian Islands (and probably near Alaska) have such accumulations of low-salinity (and thus very low-density) water at the surface that convection cannot penetrate very far down, even with a great amount of cooling. Instead of a very thick layer of cool water, we find a very thin layer of quite cold water, or surface ice, as off Kamchatka.

Discussion

There are several points to be made.

The 100% saturation-depth in summer corresponds to the winter mixed layer in much of the zone south of 40° latitude, particularly in the great anticyclonic gyre. This may indicate that, in summer, photosynthesis extends to greater depths within that gyre than around it.[3] Some evidence of this is available from the distribution of plant nutrients, which are consumed to much greater depths there than anywhere else.[25]

At high latitudes in winter, the upper layer is sometimes not quite saturated in oxygen. This may imply that cooling or mixing has not yet stopped, and colder, deeper mixed layers may follow later in winter.

Once equilibrium has been achieved in a homogeneous layer, transients, that is, local warming or freshening of the surface waters or horizontal advection of less dense water, may disturb the density structure and leave no clear record of previous convective depth. Oxygen saturation at depth, however, is not destroyed by these processes, and may leave a signal of the depth or density of a previous homogeneous layer. It is a quite independent quantity that may give us a better picture of the maximum thickness of the winter surface layer than we now have. ■

Acknowledgements

This paper represents one of the results of research supported by the Office of Naval Research and the Marine Life Research Program of the Scripps Institution of Oceanography.

References

1. Reid, J. L., 1980, "On the Use of Dissolved Oxygen Concentration as an Indicator of Winter Convection," (*EOS Transcripts: American Geophysical Union*), 61(46), (1980), 991.

2. Reid, J. L., Jr., "Distribution of Dissolved Oxygen in the Summer Thermocline," *Journal of Marine Research,* 20(2), (1962), 138-148.

3. Shulenberger, E., and J. L. Reid, "The Pacific Shallow Oxygen Maximum, Deep Chlorophyll Maximum, and Primary Productivity, Reconsidered," *Deep-Sea Research,* 28(9a), (1981), 901-919.

4. Bathen, K. H., "On the Seasonal Changes in the Depth of the Mixed Layer in the North Pacific Ocean," *Journal of Geophysical Research,* 77(36), (1972), 7138-7150.

5. Robinson, M. K., *Atlas of North Pacific Ocean Monthly Mean Temperatures and Mean Salinities of the Surface Layer,* Naval Oceanographic Office Reference Publication 2, (1976), 173 figures, 2 tables.

6. Weiss, R. F., "The Solubility of Nitrogen, Oxygen and Argon in Water and Seawater," *Deep-Sea Research,* 17(4), (1970), 721-735.

7. Scripps Institution of Oceanography, University of California, "Physical and Chemical Data, Boreas Expedition, 27 January-1 April 1966," *SIO Reference 66-24,* (1966), 164 pp. (unpublished data report).

8. Smyth, T. A., G. W. Arminini, and C. de Jong, "Oceanographic Observations at Ocean Station P (50°N, 145°W), Volume 66, 28 March-14 May 1975," Institute of Ocean Sciences, Patricia Bay, Victoria, B.C., *Pacific Marine Science Report 76-3,* (1976), 95 pp. (unpublished document).

9. Institute of Ocean Sciences, Patricia Bay, "Oceanographic Observations at Ocean Station P (50°N, 145°W), Volume 68, 20 June-17 September 1975," *Pacific Marine Science Report 76-14,* (1976), 217 pp. (unpublished document).

10. Japanese Oceanographic Data Center, "Preliminary Data Report of CSK, No. 34," Hydrographic Division, Maritime Safety Agency, Tokyo, Japan, *KDC* (Kuroshio Data Center) *Reference No. 31K004,* (1967), 33 pp.

11. Reid, J. L., "Northwest Pacific Ocean Waters in Winter," *Johns Hopkins Oceanographic Studies, 5,* (1973), 96 pp.

12. Scripps Institution of Oceanography, University of California, "Physical, Chemical and Biological Data, ZETES Expedition, Leg I, 11-24 January 1966," *SIO Reference 70-5,* (1970), 67 pp.

13. NORPAC Committee, *Oceanic Observations of the Pacific: 1955, the NORPAC DATA,* Berkeley and Tokyo, University of California Press and University of Tokyo Press, (1960), 532 pp.

14. Scripps Institution of Oceanography, University of California, "Physical and Chemical Data, Boreas Expedition, 27 January-1 April 1966," *SIO Reference 66-24,* (1966), 164 pp. (unpublished data report).

15. Kenyon, K. E., "The Shallow Salinity Minimum of the Eastern North Pacific in Winter," *Journal of Physical Oceanography,* 8(6), (1978), 1061-1069.

16. Reid, J. L., Jr., "On the Geostrophic Flow at the Surface of the Pacific Ocean with Respect to the 1000-Decibar Surface," *Tellus,* 13(4), (1961), 489-502.

17. Wyrtki, K., "Fluctuations of the Dynamic Topography in the Pacific Ocean," *Journal of Physical Oceanography,* 5(3), (1975), 450-459.

18. Reid, J. L., and R. S. Arthur, "Interpretation of Maps of Geopotential Anomaly for the Deep Pacific Ocean," *Journal of Marine Research,* 33(Suppl.), (1975), 37-52.

19. Dodimead, A. J., F. Favorite, and T. Hirano, "Salmon of the North Pacific Ocean, Part II: Review of Oceanography of the Subarctic Pacific Region," *Int. North Pacific Fisheries Commission Bulletin,* 13, (1963), 195 pp.

20. Yoshida, K., and T. Kodokoro, "A Subtropical Countercurrent in the North Pacific," *Journal of the Oceanographic Society of Japan,* 23(2), (1967), 88-91.

21. Masuzawa, J., "Water Characteristics of the North Pacific Central Region," *Kuroshio—Its Physical Aspects,* edited by H. Stommel and K. Yoshida, University of Tokyo Press, (1972), 95-127.

22. White, W. B., and K. Hasunuma, "Interannual Variability in the Baroclinic Gyre Structure of the Western North Pacific from 1954-1974," *Journal of Marine Research,* 38(4), (1980), 651-672.

23. MacDonald, W. F., *Atlas of Climatic Charts of the Ocean,* U.S. Department of Agriculture, Weather Bureau, W. B. No. 1247, (1938), 129 charts.

24. Wyrtki, K., and G. Meyers, "The Trade Wind Field and the Mean Annual Variation—Part I. The Mean Field and the Mean Annual Variation," *Hawaii Institute of Geophysics Report No. HIG-75-1,* University of Hawaii, (1975), 26 pp., 25 figures.

25. Reid, J. L., E. Brinton, A. Fleminger, E. L. Venrick, and J. A. McGowan, "Ocean Circulation and Marine Life," in *Advances in Oceanography,* edited by H. Charnock and Sir George Deacon, New York, Plenum Press, (1978), 65-130.

Dr. Joseph Reid is a Professor of Physical Oceanography at the Scripps Institution of Oceanography, where he has worked since 1951. His area of interest is the circulation of the world ocean, the characteristics of the waters and the areas and manner of their formation. He has carried out several oceanographic expeditions in the Pacific, Antarctic, and Atlantic oceans. In 1955 he proposed and coordinated the NORPAC Expedition, a program for collecting oceanographic observations over the entire North Pacific north of 20°N and carried out by 19 ships of the United States, Japan, and Canada.

"FRONTS-80"

—A Study of the North Pacific Subtropical Front

by

Pearn Niiler
School of Oceanography
Oregon State University

Introduction

In the upper ocean man's important activities occur in transportation, fishing and national defense. The upper one-hundred meters of the water column is the most changeable and complex part of the ocean, but today its many faces are also most susceptible to measurement and description. On the ocean surface, the effects of the sun, the storms, and man's own activities can be clearly seen, and signatures of many deep ocean circulation features are found. The upper ocean can now be studied simultaneously with remote sensing by satellites and rapid, in situ surveys by airplanes and ships. This paper is a description of a program called "FRONTS-80" in which the upper ocean temperature, salinity and flow were measured in great detail in the vicinity of the North Pacific Subtropical Front and what oceanographers learned about the relationship between satellite images of the ocean surface and the conditions in the subsurface ocean layers. It was principally sponsored by the Office of Naval Research, with participation of ships and oceanographers from National Aeronautics and Space Administration, National Oceanic and Atmospheric Agency and the Royal Canadian Navy. A schematic of the field activity is on Figure 1.

FRONTS-80 was motivated by the rather well documented observation that along a straight ship track the ocean mixed layer temperature and salinity can change abruptly (1–2 °C) in a very short distance (10–20 km); and that oceanographers do not understand why such large gradients, or fronts, occur or why these fronts are most often found in rather specific geographical locations. These questions can be answered by determining the relationship between ocean flow and thermohaline features on a variety of space and time scales and in FRONTS-80, an attempt was made to obtain such a data set in the eastern North Pacific. Table I lists the participants and when viewed together with Figure 1, the major components of the field program are apparent.

Across the entire breadth of the eastern North Pacific, a subtropical surface frontal area is located between 30 °N and 32 °N Latitude. The subtropical front is most clearly identified the year round by the horizontal, near-surface salinity distribution. In

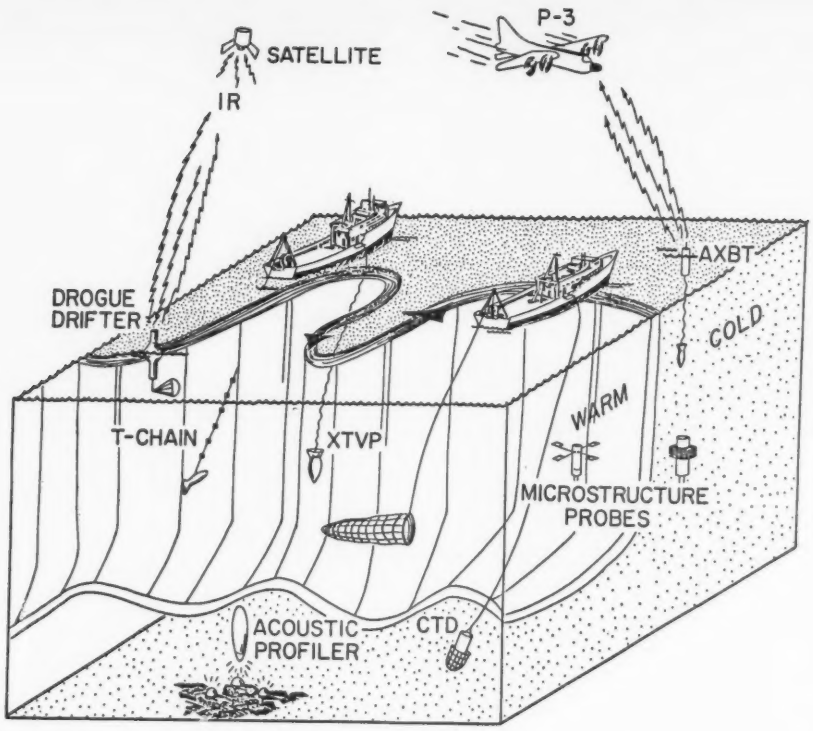

Figure 1. A schematic of the FRONTS-80 field program in the North Pacific Subtropical Front. This picture should be viewed together with Table I where the participants and techniques are identified.

winter, a surface temperature front also occurs along with the salinity front.[1] Figure 2 is a composite picture of the 100 m salinity, contoured from four separate synoptic surveys of the eastern North Pacific. At each dot on this figure, a hydrographic cast was made to at least 1000 m depth, and the separate surveys can be readily identified by an increasing density of observations within four distinct patterns. The largest scale survey was the earliest in February-March 1954.[2] Salinity gradients in this survey are concentrated in the vicinity of 31 °N Latitude circle, but clearly the north-south scale of the frontal pattern is not resolved. The January-February 1974 survey was centered at 32 °N, 155 °W, and here stations were placed 20 nautical miles apart in the north-south direction.[3] Such a map now resolves the north-south structure but leaves its 100 nautical mile east-west separation structures unresolved. The third survey, centered at 34 °N, 137 °W, was done in July-August 1976; and in this survey convoluted, two-dimensional features in the frontal pattern become vaguely apparent.[4] In FRONTS-80, which was done in January-February 1980, a 20 nautical miles x 20 nautical miles (n.m.) station spacing is employed, and a two-dimensional resolution of the field is finally obtained. Figure 2 shows how the oceanographers' view of the environment has evolved in the past three decades: the higher the resolution with which the ocean is sampled, the more interesting and significant the features found. But more importantly, the energetic, synoptic patterns in the ocean have been found to be surprisingly small and measuring them requires two-dimensional surveys with a very high degree of resolution. From these surveys we learn that the Pacific subtropical frontal area at any level above 1000 m contains an intense mesoscale or two-dimensional wave and eddy pattern in the thermohaline structures and that the flow field associated with these structures from time to time deforms the surface layers into intense fronts. During the FRONTS-80 field program we were able to describe the formation and evolution of one such

strong frontal zone and some of its salient features.

Ocean Variability in FRONTS-80

In December of 1979, bi-weekly Airborne Expendable Bathythermograph flights were begun from the Barbers Point Naval Air Station, Hawaii over a 3° x 3° grid centered over the subtropical frontal area at 31°N, 153°W. The mixed layer temperature patterns on January 17 and January 24 are shown on Figure 3(a) and 3(b), respectively. During this period, an elongated cold water tongue developed at 31°N, 153°W and, as mapped by subsequent surveys on the R/V *THOMAS WASHINGTON* (Figure 3(c)), this cold-water tongue developed strong frontal patterns

Table I. "FRONTS-80" Components and Investigators

COMPONENTS on Figure 1	INVESTIGATOR	INSTITUTION
Satellite Sea Surface Temperature "Satellite-IR"	R. Bernstein	Scripps Institution of Oceanography
	M. Van Woert	Scripps Institution of Oceanography
	R. Whitner	Scripps Institution of Oceanography
	T. Green	University of Wisconsin
	K. Sowinski	University of Wisconsin
Aircraft Expendable Bathythermograph "AXBT"	M. Miyake	University of British Columbia
Three-dimensional Thermohaline Stucture "CTD"	G. Roden	University of Washington
Multiship Expendable Bathythermograph	W. Emery	University of British Columbia
Satellite Tracked Drifters "Drifting Drogues"	P. Niiler	Oregon State University
Air-sea Interaction	C. Mooers	Naval Post Graduate School
Velocity and Hydrographic Fine-structure "Acoustic Profiler"	S. Hayes	Pacific Marine & Environmental Lab.
Expendable Temperature-Velocity-Pressure Profiles "XTVP"	T. Sanford	University of Washington
	E. Kunze	University of Washington
Doppler-Acoustic Velocity Profiles	L. Regier	Scripps Institution of Oceanography
	R. Davis	Scripps Institution of Oceanography
Towed Temperature Cross-Sections "T-Chain"	C. Paulson	Oregon State University
Temperature and Velocity Micro-structure "Microstructure"	R. Lueck	University of British Columbia
	T. Osborn	University of British Columbia
	T. Dillon	Oregon State University
	D. Caldwell	Oregon State University
Mesopelagic Fishes	M. Willis	Oregon State University
	W. Pearcy	Oregon State University

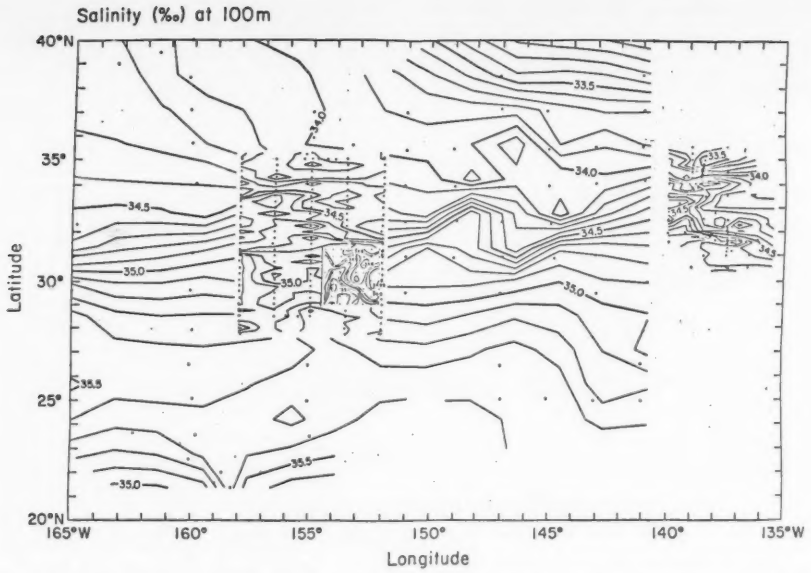

Figure 2. The distribution of 100-m depth salinity in the eastern North Pacific. The subtropical frontal area is between 30°-32°N and the subpolar frontal area is only apparent in the north-east corner of the picture. Successive surveys are done on higher resolution. The FRONT-80 area is the smallest insert centered at 31°N, 153°W.

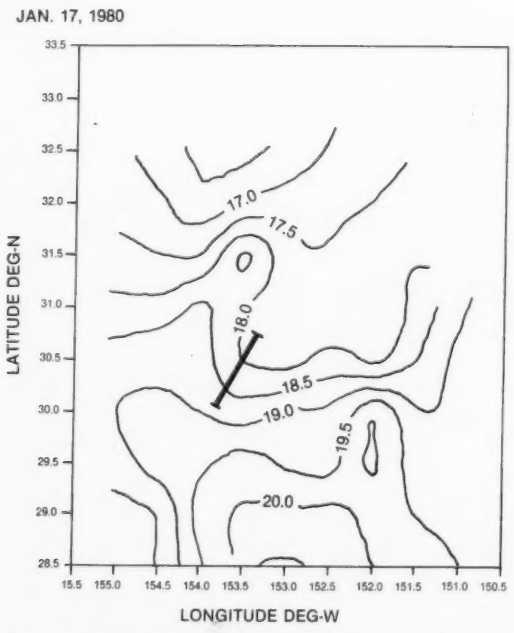

Figure 3a. Mixed layer isotherms drawn from AXBT temperature averaged between 30 m and 80 m depth on 17 January 1980. The heavy line is a continuous thermistor chain tow on 18 January and its data is displayed on Figure 6.

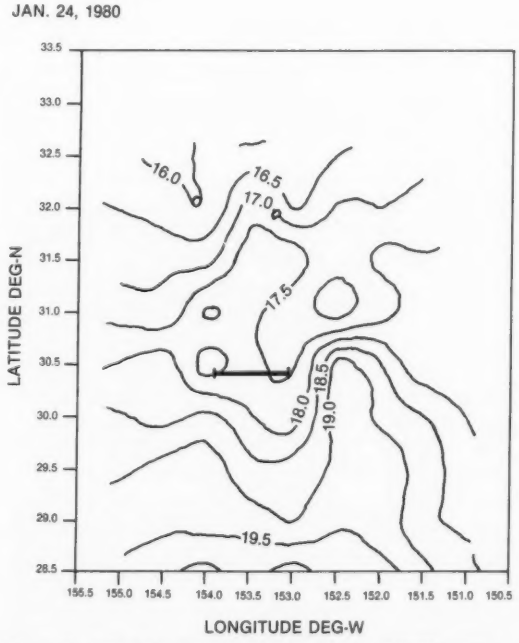

Figure 3b. Mixed layer isotherms drawn from AXBT temperatures averaged between 30 m and 80 m depth on 24 January, 1980. The heavy line is the location of an intensive XTVP survey between 21 January and 27 January, and its data are displayed on Figure 7.

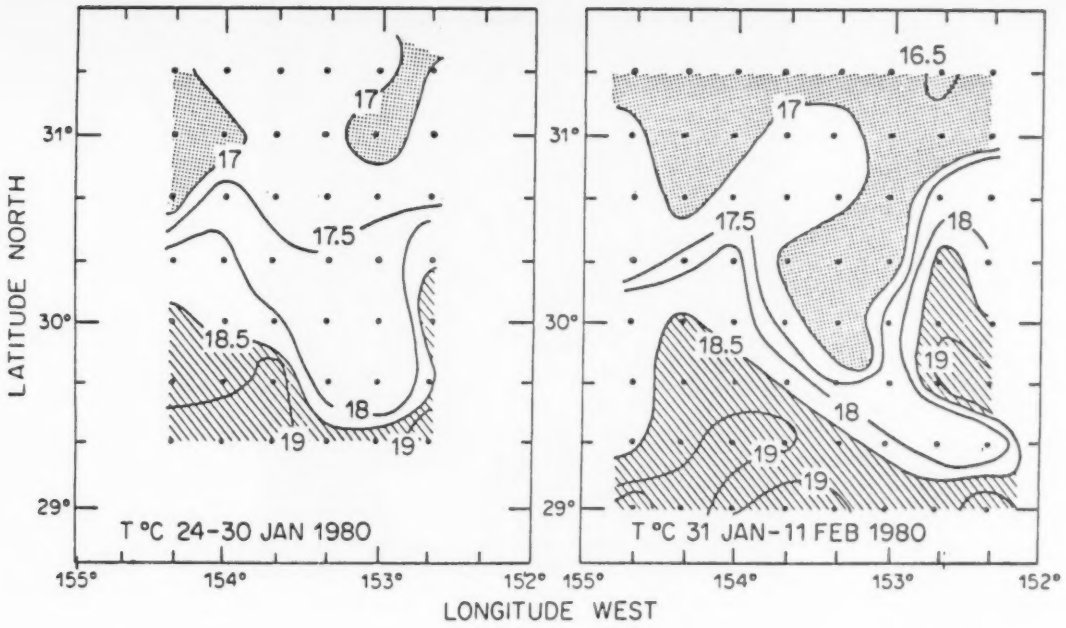

Figure 3c. The sea surface temperature patterns from the R/V **THOMAS WASHINGTON** *survey. Note the evolution of the 17-17.5°C water tongue through Figures 3a, b, c.*

on its western, southern and eastern flanks. On clear days in late January 1980, the satellite sea-surface radiation patterns from NOAA-6 Advanced Very High Resolution Radiometer (AVHRR), 3.7μ window revealed an identical developing cold water pattern and enhancement of surface temperature gradients. By the 7th of February, the pattern evolution subsided. During the ship survey, 10 satellite tracked drifters (drogued to 20 m depth) were released within this developing pattern. Three of these drogues which were placed on the cold side of the front traced out the stationary surface temperature pattern's broadest detail. Figure 4 is a summary of the ship survey, satellite radiometry and surface drogue data. On it the *red* contours are the dynamic topography of the ocean surface with respect to 1500 m, which is similar to a sea level isobaric weather map of the atmosphere.[5] The *blue* are the drogue tracks, and these closely follow the implied geostrophic flow patterns along the surface, geostrophic isobars. The AVHRR data is in enhanced grey tones. While much more detail is seen than is resolved by either the buoys or the implied geostrophic flow patterns, we clearly are viewing the same feature on the scale of 20 nautical miles in the subtropical frontal zone. Figure 5 is an enhanced satellite picture of sea surface temperature gradients, in which black is less than .1 °C/km and red are in excess of .250 °C/km. The mean value of temperature change computed across frontal zones in Figure 5 is 1.02 °C ± 0.25 °C, and the frontal width is 9.3 km ± 3.5 km.[6] Continuous tows and vertical finestructure profiles across some of these frontal features were done from the NOAA ship *OCEANOGRAPHER* and are reviewed below.

On Figure 3(a) is a track line of a temperature chain tow across a temperature frontal area on January 17. Figure 6 is a display of continuous temperature traces along this track. On either side of the frontal area, the water column between 8 m and 88 m is vertically homogeneous (the temperature is the same) while in the frontal zone (of 10 km width) the water column is stratified. Nearly all tows across frontal zones, of which the above is one example, show vertical stratification. This phenomenon could not occur without very strong relative flow, or vertical shear of horizontal currents which would bring warm water (or cold water) to the frontal area at a faster rate than vertical mixing would eradicate a vertical gradient. Therefore, in the *colored* areas of Figure 5 we also expect to see vertical stratification of

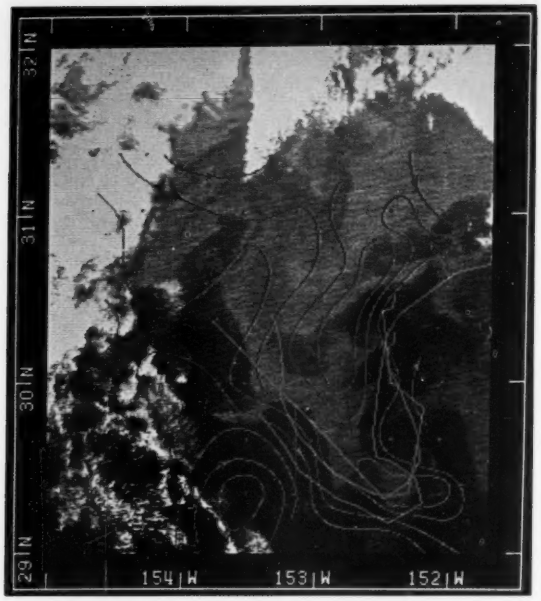

Figure 4. The surface dynamic topography with respect to 1500 db (red) (31 January-11 February, 1980) track of surface drifters (20 January-14 February, 1980) and AVHRR (3.7μ) (9 February, 1980). Note how closely the buoys follow the frontal zone as inferred from the satellite data and the dynamic topography.[6]

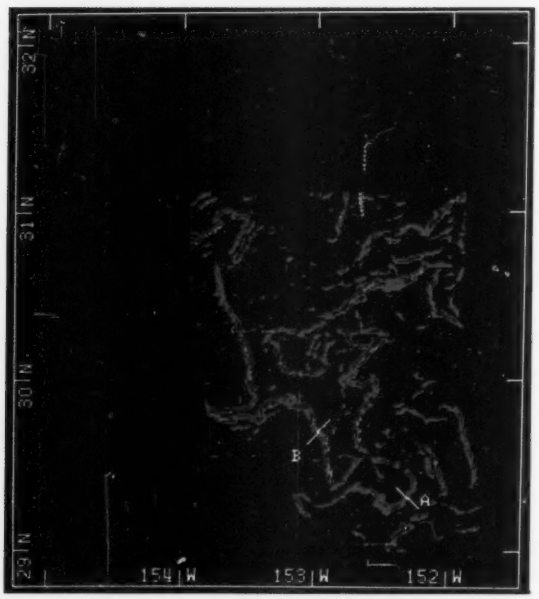

Figure 5. Magnitude of the temperature gradient based on satellite data. Temperature gradient between 0.1°C/km and 0.175°C/km is green, 0.175°C/km and 0.250°C/km is blue and 0.250°C/km and the maximum value 0.386°C/km is red.[6]

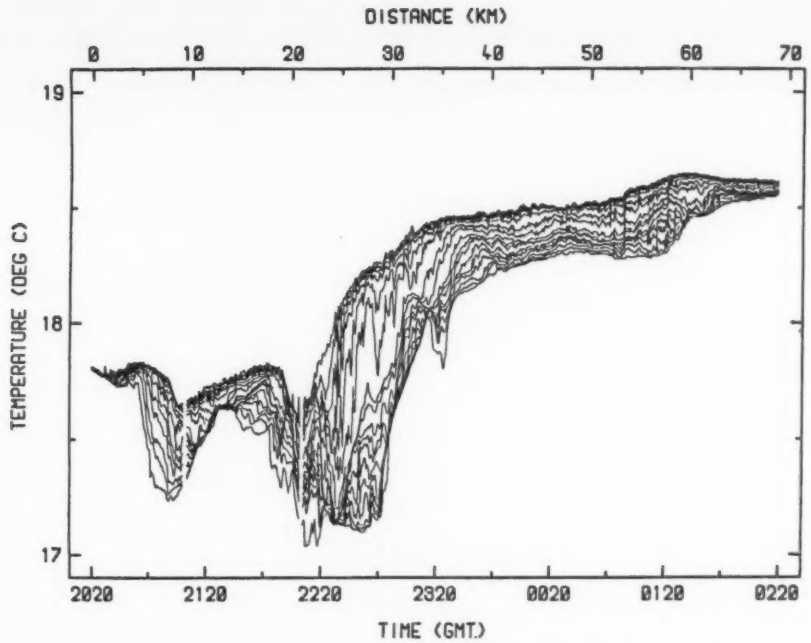

Figure 6. A frontal structure observed with a towed thermistor chain. The thermistors were distributed between depths of 8 m and 88 m. The observations were taken on 17 and 18 January 1980. (See Figure 3a for the tow track relative to the AXBT image of surface temperature.)

0.5°C – 1.0°C over the upper 100 m water column and a "well mixed" layer elsewhere.

The vertical shear of horizontal currents was measured with an acoustic doppler velociometer and expendable shear profiler (XTVP). On Figure 3(b) is a repeated track line of XTVP drops across a well developed frontal current zone between January 21 and January 27 at the rapidly developing southern end of the cold tongue. During this time the dynamic topography and drifters showed a strong southward flow, and by February 9th a strong surface gradient developed there in the AVHRR picture (Figure 5). Figure 7 is the horizontal kinetic energy as a function of distance across a strong current area. An east-west frontal pattern at depth is found across this track, and it is due to the dynamic topography gradient. Figure 7 shows that, within the strong current, energy of inertial motions was propagating down from the surface at a rate four times larger than elsewhere in the area. The strong mesoscale flows which apparently cause surface frontal concentration can also trap or release strong internal, near-inertial wave energy in the upper ocean.

The AVHRR data presents the best two-dimensional horizontal resolution that we can presently obtain of the sea surface conditions. From Figure 4 we can easily see that this area is quite rich in interleaving patterns. In the cooler water north of the front, considerable vertical interleaving is also found. Vertical layers of water masses are seen in a temperature, sound velocity, and density profile in Figure 8, with both temperature and salinity inversions especially between 40 m and 120 m depth intervals. After a strong storm, these layers are mixed vertically, only to reappear a few days later. Figure 9 is a microstructure profile north of the subtropical front. In addition to wind mixing during storms, we see that salt can be transferred vertically both by salt fingering and double diffusive processes. The horizontal interleaving process sets up a variety of conditions for vertical turbulent transports of heat and salt.

A Summary

Physical oceanographers cannot do controlled experiments at sea, rather they observe the natural variability of the waters where a variety of processes operate in concert. With each new data set, more of

Figure 7a. Rotary horizontal kinetic energy in J/m³ plotted against longitude across the front. Clockwise with depth (downward-propagating) energies are plotted as solid circles and triangles and the anti-clockwise (upward-propagating) energies as open circles and triangles. The circles are from profiles taken within 12 hours of each other on 21 January, while the triangles are from later profiles, mostly on 24-27 January. Intensification of downward-propagating energy is seen on the western edge of the deep frontal zone (see Figure 7b) in the form of a peak rising by a factor of 4 above the background level with a half-energy width of 10 km. There is no corresponding intensification in the upward-propagating energy.

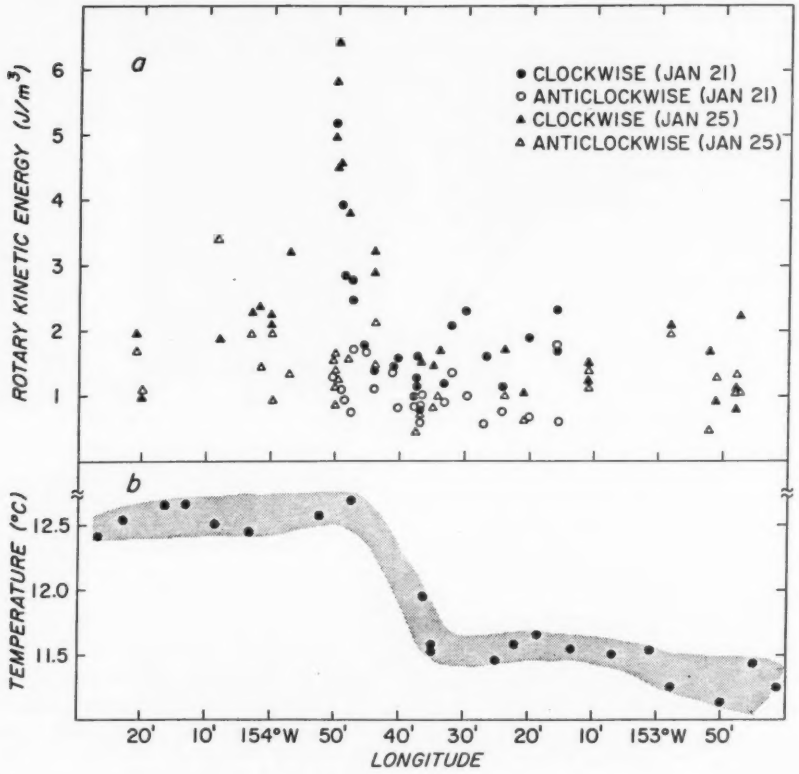

Figure 7b. Temperature averaged over 180-300 m vs. longitude from the 19 January, XBT section. The front is well defined as a temperature jump of 1.0°C, corresponding to a sigma-t jump of .6°/₀₀ between 153°35' and 50' W. The front did not significantly change position or intensity over the period of XTVP measurements. (See Figure 3b for the location of the track relative to the AXBT image of surface temperature).

this natural variability is mapped, and some features in it are also understood in terms of rather broad physical principals. The FRONTS-80 data set, some of which was reviewed here, has increased our knowledge of the ocean's frontal areas in a number of important ways.[7]

First, the subtropical frontal regions of the Pacific were viewed concurrently through an AVHRR satellite sensor and in situ observations through 1500 m of the water column. Both techniques mapped the intensification of a frontal zone on a 20–30 n.m. resolution over a four week period. The inversion technique for obtaining sea surface temperature from the 3.7μ (of 11μ) band radiometer signal can now provide relative temperatures to ± .25 °C over a spatial scale of 2.5 km. A strong relationship between horizontal and vertical temperature gradients in this frontal zone is suggested by the results.

Secondly, the flow patterns were measured by Lagrangian drifters, doppler-acoustic logs and XTVP's. Large inertial-internal waves were found in

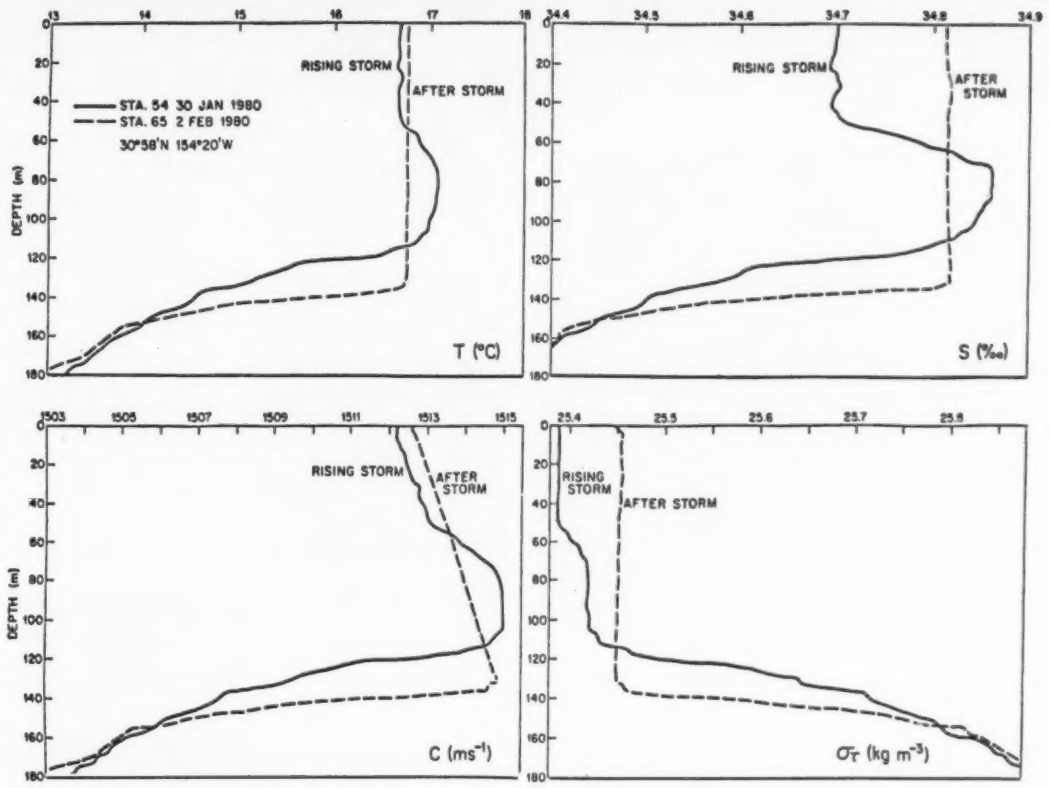

Figure 8. Profiles of temperature (T), salinity (S), sound velocity (C) and density (σ_t) during a rising storm (solid lines) and after the storm (dashed lines).[5]

strong frontal currents. The acoustically-determined current profiles which averaged 30–50 km horizontal areas rotate clockwise with depth through the mixed layer. The month-long drogue drift is nearly 30° to the right of the monthly averaged wind. The drogues in the cold side of the front do not cross the frontal area while those on the warm side move to the south. This implies sinking of water on the northern side and rising to the south. On a weekly time scale, the frontal pattern is traced out by drogue paths, and strong surface jets are found in areas where surface fronts are forming.

Thirdly, the vertical-horizontal mixing processes in the frontal area are strongly coupled because horizontal interleavings are vertically mixed by storms. Salt is also transferred vertically by salt fingering. Drogue tracks show that the horizontal kinetic energy of surface fluctuations, and horizontal mixing by eddy process, increase rapidly south of the subtropical front. New and rapid survey tools were used for the first time which allowed vertical profiles of high resolution CTD and current shear to be obtained from a moving ship every 1–2 km.

There are many pieces to the puzzle of why the subtropical front occurs and why its intensification tends to be most often located in a rather well defined latitude band. With the FRONTS-80 data the investigators are busy computing the rates of horizontal and vertical mixing, the strengths and shears of horizontal circulation that maintain this front, and are following the evolution of the frontal scales of variability via remote sensing through many winter seasons. In FRONTS-80 we discovered that we had barely 'scratched the surface' of a fascinating and complex ocean phenomena. ■

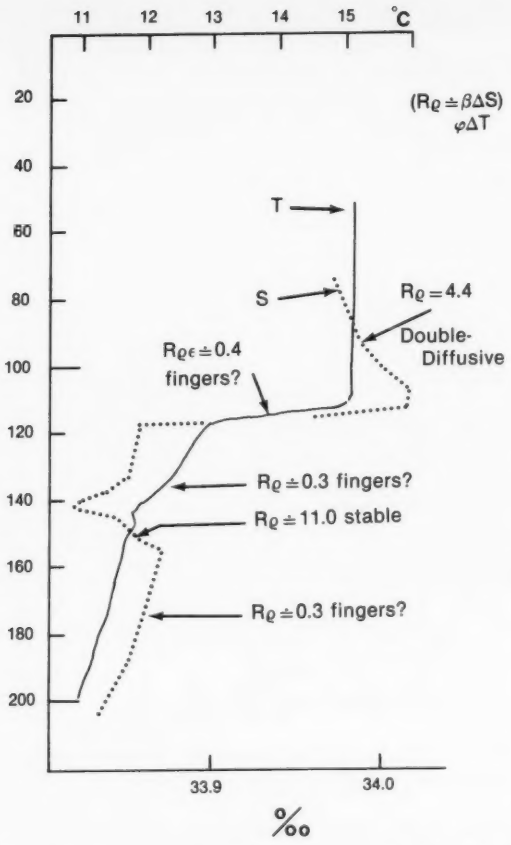

Figure 9. Temperature and salinity finestructure profiles north of the front (33°56°N). R_ρ is the stability ratio $|\beta\frac{\Delta S}{\Delta z}|/|\alpha\frac{\Delta T}{\Delta z}|$, where β and α are the density gradients with respect to salinity and temperature, respectively, and Δ is a change over Δz of one meter. In laboratory situations a low value of R_ρ implies proper conditions for the formation of salt fingers.

References

1. Roden, G. I., "On the North Pacific Temperature Salinity and Sound Velocity and Density Fronts and Their Relation to Wind and Energy Flux Field," *Journal of Physical Oceanography, 5*(4), (1975) 557-571.

2. McGary, J. W. and E. D. Stroup, "Mid-Pacific Oceanography, Part III, Middle Latitude Waters, Jan.-March, 1954," Special Scientific Report, U.S. Fish and Wildlife Service, No. 180, (1956) 173pp.

3. Roden, G. I., "On the Subtropical Frontal Zone North of Hawaii during Winter," *Journal of Physical Oceanography, 10,* (1980) 342-362.

4. Lynn, R. (1976) (private communication).

5. Roden, G. I. "Mesoscale Thermohaline Sound Velocity and Baroclinic Flow Structure of the Pacific Subtropical Front during the Winter of 1980," *Journal of Physical Oceanography, 11*(5), (1981) 658-675.

6. van Woert, M., "The Subtropical Front: Satellite Observations during FRONTS-80," (1982), (in press, *Journal of Physical Oceanography*).

7. Paulson, C. A. and P. P. Niiler (editors), "Fronts-80: Preliminary Results from an Investigation of the Wintertime North Pacific Subtropical Front," Oregon State University, School of Oceanography, Ref. 81-2, (1981).

Dr. Pearn Niiler is a professor of oceanography at Oregon State University. His research interests are in both theoretical and observational general ocean circulation and how air-sea interaction and ocean turbulence influence its large-scale features. Most recently his studies have been of the circulation of the mixed layer in the eastern Pacific Ocean and the transport and mesoscale eddy field of the Kuroshio in the western Pacific Ocean.

conrad award

Dr. Berman Honored

The Navy's highest honor for scientific achievement, the Captain Robert Dexter Conrad Award, was presented to Dr. Alan Berman, former Director of Research for the Naval Research Laboratory (NRL), in a ceremony in Washington, D.C. on 18 June. The award was presented on the eve of Dr. Berman's departure from the Laboratory to become the Dean of the Rosenstiel School of Marine and Atmospheric Science at the University of Miami.

The award, a medal and certificate, was presented by the Honorable Melvyn R. Paisley, Assistant Secretary of the Navy for Research, Engineering and Systems, on behalf of the Secretary of the Navy. In presenting the award, Secretary Paisley delivered a citation commending Dr. Berman for his "accomplishments as a brilliant physical scientist, as an astute administrator, as a charismatic leader, and as a respected advisor to the leaders of the Nation."

The Conrad Award is presented annually to an individual for outstanding scientific achievement of significance to the Navy. It commemorates the service of Captain Robert Dexter Conrad, who was one of the primary architects of the Office of Naval Research that was established in 1946 to support research at universities and research institutions on a permanent basis. Dr. Berman is the 26th recipient.

Under Dr. Berman's guidance, NRL has, among other significant accomplishments, developed several complete space systems. The efforts included the design and fabrication of satellites, the development of ground systems, data processing and data dissemination. NRL has also played a major role in the development of advanced materials technology and high performance electronic systems and devices. Dr. Berman's personal research specialties are underwater acoustics, oceanography and signal processing.

In September 1980, the President conferred upon Dr. Berman the rank of Distinguished Executive of the Senior Executive Service in recognition of his performance as Director of Research at the Navy laboratory. He was also awarded the Department of the Navy Superior Civilian Award in 1969 for his leadership in operations which located the sunken submarine *USS SCORPION,* and in 1973 the Department of Defense Distinguished Civilian Service Award, the highest award that may be given to a civilian by the Secretary of Defense.

Dr. Berman was Director of Columbia University's Hudson Laboratories before coming to NRL as its director in 1967. ■

Finestructure: Oceanic "Kinks and Wiggles"

by

Michael C. Gregg
Applied Physics Laboratory
University of Washington

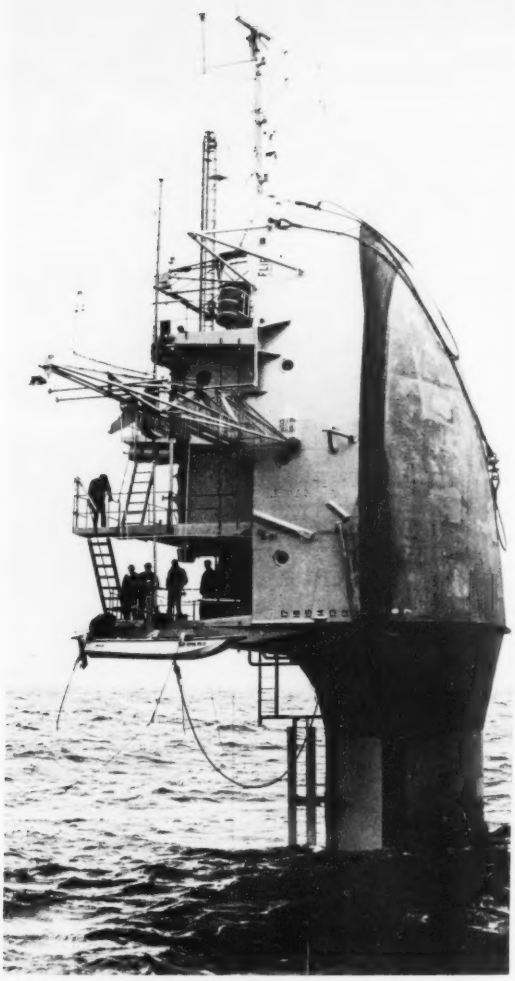

FLIP (floating instrument platform)

Introduction

Many people who have gone to sea on naval or oceanographic ships during the past 40 years have wondered about the origin of the meter-scale 'kinks and wiggles' evident in temperature records obtained with the Bathythermograph (BT) or its successor, the Expendable Bathythermograph (XBT). These features are now referred to as the finestructure of the ocean. By combining finestructure observations with similar profiles of velocity (Figure 1) and with measurements of the centimeter-scale microstructure, much has been learned about the processes that produce the "kinks and wiggles."

The finestructure is a range of length scales lying between the smaller structures directly involved in irreversible mixing and the larger features that characterize the mesoscale variability. The scale at which mixing takes place is determined by the viscosity of water and the intensity of turbulent stirring in particular mixing events. For the mixing of heat in the ocean, the variability of the turbulent intensity produces a range of sizes from about 10 cm to 5 mm, over which the mixing is most intense. These scales

Acknowledgements

Tom Sanford, Eric Kunze and Eric d'Asaro of the Applied Physics Laborabory, University of Washington provided valuable help in the preparation of this article.

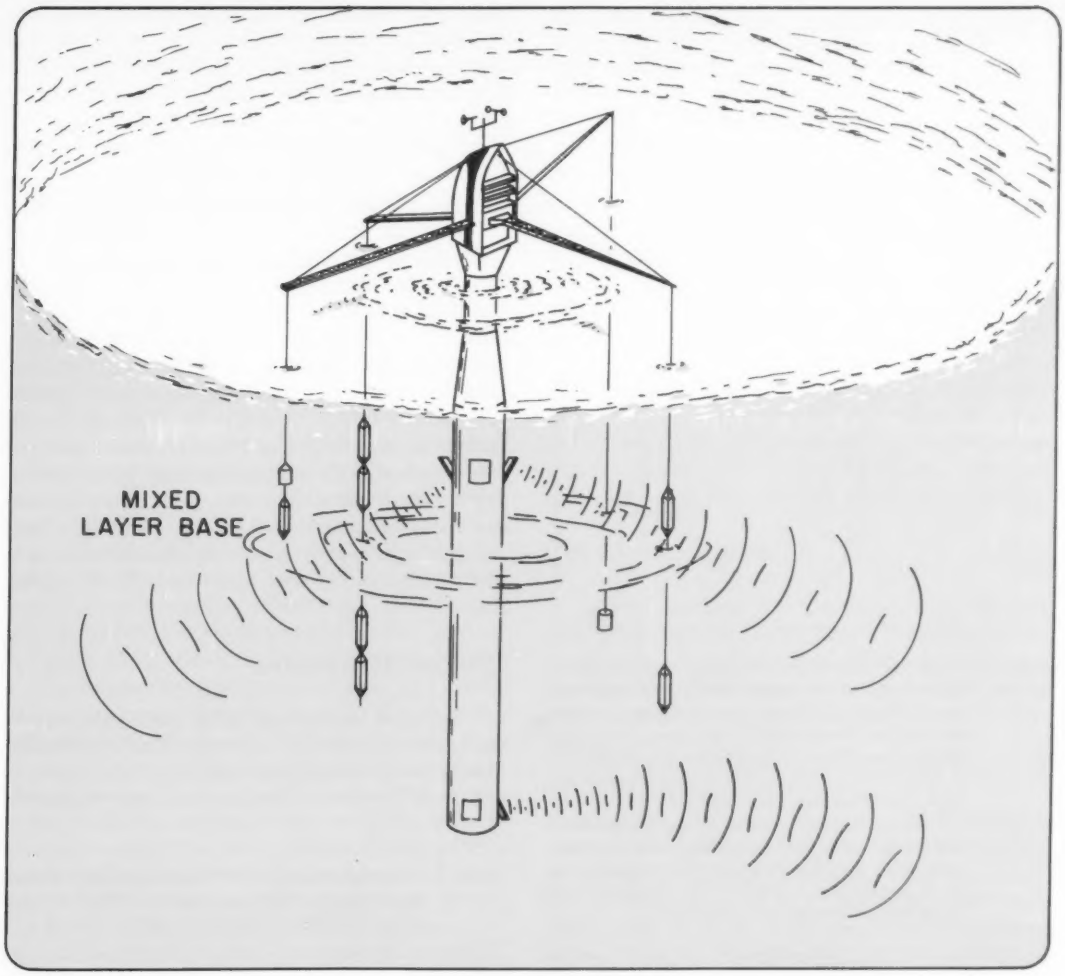

FLIP with instrument booms extended

are referred to as the microstructure. Since no significant mixing takes place over distances larger than 1/2 m, that scale is taken to define the small-scale boundary of the finestructure range. The largest size of finestructure is rather vague, but is at least several hundred meters in the vertical.

Although the microstructure is at least approximately isotropic, i.e., it has similar vertical and horizontal scales, the finestructure is strongly affected by the stratification of the ocean and has horizontal scales which are long compared to those in the vertical. The aspect ratio, a subject of current research interest, is estimated to vary from 10:1 to 1000:1.

Three general classes of processes produce finestructure: small-scale turbulence, internal wave strain and double diffusion. Although all three are random processes in the ocean, the intensity of internal wave strain appears to be the most uniform. By contrast, the occurrence of turbulent mixing is highly intermittent in time and is patchy in space. Furthermore, the dominant mechanisms by which the turbulence is generated vary with proximity to the surface or bottom and possibly with position within the mesoscale field. At present, double diffusion is the most enigmatic; it is known to be important in frontal regions, but its role in the main thermocline of the central oceans is unclear.

The cartoon in Figure 2 shows some of the mechanisms that produce finestructure, together

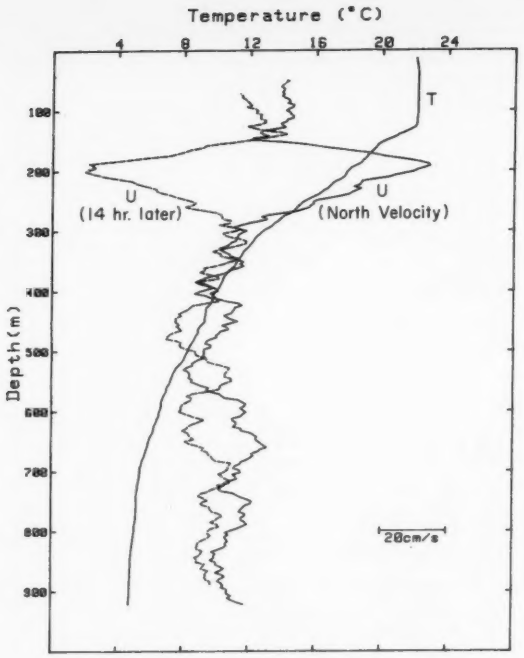

Figure 1. Profiles of temperature and velocity obtained with an Expendable Current Profiler (XCP). The temperature record shows many fluctuations in gradient over scales of meters to tens of meters. These are referred to as finestructure. The velocity structures are primarily due to low frequency internal waves, known as inertial motions. The dotted profile was taken approximately one-half an inertial period after the solid curve, showing a reversal in most of the velocity structures, which identifies them as inertial. These data were kindly supplied by T. Sanford and E. Kunze of the Applied Physics Laboratory, University of Washington.

with schematic temperature profiles through the resultant structures. This figure will be referred to in discussions of the processes. However, first it is useful to consider the instruments operated to observe finestructure and the statistics used to describe the observations.

The Observation of Finestructure

Since observational techniques provide the 'window' through which any physical process is viewed, it is important to have an understanding of their capabilities and limitations. A wide variety of dropped and towed instruments are used to study finestructure. Most contain a single set of sensors, and are dropped or towed through the ocean to obtain records of temperature and possibly also salinity. A few combine these approaches and are cycled in depth while being towed; these are termed 'tow-yos' and yield cross sections of the measured fields. Another approach to obtaining cross sections is to tow vertical arrays that have many closely-spaced sensors.

Dropped Instruments

Dropped instruments differ principally in how freely they fall through the water. The wire-lowered Conductivity-Temperature-Depth (CTD) system is the most common profiling instrument used by

Figure 2. Cartoon showing the major processes forming finestructure and the temperature structures they produce. Specific processes are discussed in the text.[5]

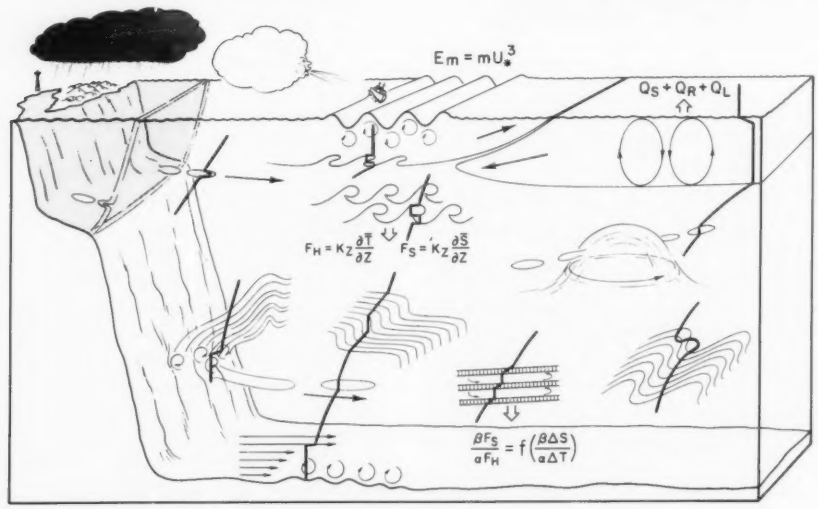
$E_m = mU_*^3$
$Q_S + Q_R + Q_L$
$F_H = K_Z \frac{\partial \bar{T}}{\partial Z}$
$F_S = K_Z \frac{\partial \bar{S}}{\partial Z}$
$\frac{\beta F_S}{\alpha F_H} = f\left(\frac{\beta \Delta S}{\alpha \Delta T}\right)$

oceanographers for studying finestructure. The standard units are manufactured commercially and are lowered from research ships using hydrographic winches. Typically, the data are transmitted at a rate of 30 samples per second up a conducting cable. Lowering rates of 1/2 to 1 m/s produce a depth spacing of 1.5 to 3 cm. The data words have a sensitivity of 16 digital bits, corresponding to 27 μ S/m in electrical conductivity and .00013 °C in temperature.

The major limitation of the CTD for finestructure work is the smearing of the data to scales of several meters by the heaving of the ship, which is transmitted to the sensors by the hydrographic cable. A secondary limitation is the difficulty of obtaining accurate salinity data over scales of several meters and smaller. Determination of salinity is inherently difficult because it must be extracted from simultaneous measurements of temperature and conductivity. Since the conductivity signal is often dominated by the thermal contribution, this requires taking the small difference of two large numbers. Such a procedure is very sensitive to even minor errors, particularly in sensor calibrations. The effect of both limitations is to obscure the small-scale part of the finestructure, where the sharper features occur.

The Expendable Bathythermograph (XBT) falls freely, with speeds ranging from 2 to 4.5 m/s, depending upon the model. A thin wire serves as a data link to the ship. To date, these devices have not included pressure sensors, but the regularity of the fall rate is used to determine depth as a function of time since launch. The low sensitivity, about .01 °C, and the slow response time of the temperature probe limit the XBT to a resolution of several meters. If the units are not given special calibrations, the standard error is about 0.2 °C, which precludes lateral mapping of most finescale features.

Expendables that also measure electrical conductivity or sound speed to obtain salinity have been tested, but so far they have not proved useful in studying finestructure.

During the past several years it has also been possible to measure velocity profiles with an expendable probe. The Expendable Current Profiler (XCP) measures the voltage induced by the ions in seawater moving through the earth's magnetic field. The technique, which provides a vertical resolution of several meters and a sensitivity of about 1 cm/sec, is inherently a relative and not an absolute measurement; additional information, such as the surface velocity, is required if the profiles are to be made absolute. The great advantage of the XCP is its capacity for performing repeated profiles to study spatial or temporal evolution of velocity structures, such as that shown in Figure 1.

To obtain better performance than available with expendables, yet avoid the problems inherent with wire-lowered instruments, oceanographers have developed free-fall instruments that move smoothly through the water and can resolve the structures to the centimeter scale. Some drop through the full water column and record their data internally on magnetic tape. Due to the time required to recover the instruments aboard ship, only a few drops per day can be made, and very little can be determined about the temporal evolution of structures or their horizontal extent. For work in the upper few hundred meters of the ocean, lightweight profilers using data links contained in loose tethers have been developed to permit rapid sampling to the centimeter scale. Others are now operational that can operate remotely, sliding up and down a mooring wire and recording the evolution of the profile for months.

Towed Instruments

Horizontal tows of single sensors yield relatively little information due to the large horizontal-to-vertical aspect ratio of finestructure. The most useful approaches have been to tow vertical arrays containing large numbers of temperature sensors or to do towyos with a CTD.

The Naval Research Laboratory has developed the use of thermistor chains to a fine art. One of their chains (Figure 3) has an array of 180 thermistors spaced 1/2 m apart. Each sensor is sampled 20 times per second; corresponding to a horizontal spacing of 12.5 cm for a tow speed of 2.5 m/s. The sensitivity is .0003 °C. By means of an elaborate motion-compensation system the chain has been towed in sea state 4 with rms depth fluctuations of only 2 cm. Since the tow speed is faster than the evolution of much of the finestructure, thermistor chains provide a good approximation to a synoptic picture over horizontal scales of several hundred meters.

The major difficulty with chains occurs at vertical scales of several meters, as is the case with the CTD, and is due to the difficulty of reconstructing the profile from measurements taken with so many different sensors. In the seasonal thermocline, where tow chains are the most useful, a typical vertical gradient is .06 °C/m, corresponding to an average difference of only .03 °C between thermistors 1/2 m apart. This is barely above the accuracy of calibration baths and requires the use of relative calibrations based on the observed data.

The other approach to towed measurements is to let the ship drift or steam slowly while cycling a CTD

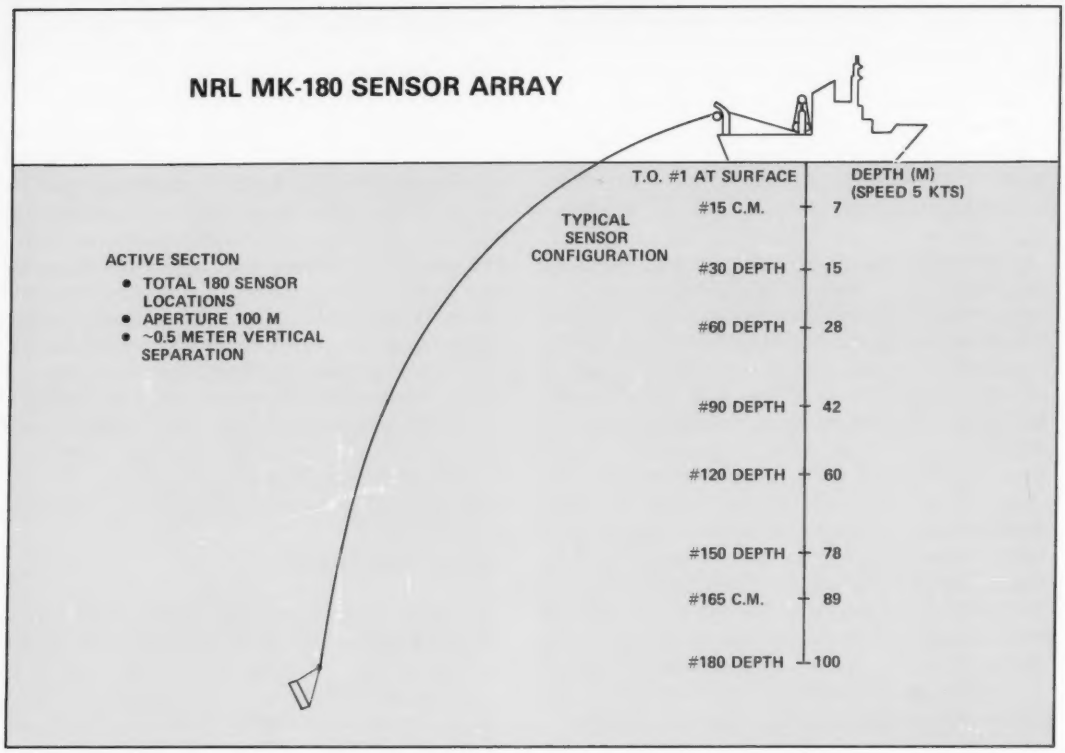

Figure 3. Schematic of the Naval Research Laboratory (NRL) towed thermistor chain. This version of the chain has 200 sensor locations which span a total aperature of 100 m. Six of the sensors are pressure gauges. This figure was kindly supplied by E. E. Rudd and B. S. Okawa of NRL.

up and down. At speeds greater than 1 m/s, bodies designed specifically for towing, rather than the standard CTD package, are required. The advantage of this approach is that only one set of probes is involved, avoiding the relative calibration problem experienced with chains. This is particularly important in obtaining salinity, due to the difficulty of maintaining stable calibrations with conductivity cells. On the other hand, much greater horizontal interpolation is required than with chains, since successive tow legs are often spaced relatively far apart compared to the finestructure scales.

Statistical Description

Oceanic temperature, salinity and velocity profiles usually have strong average gradients, upon which the finestructure variability is superimposed. Consequently, the temperature at a location **x** and time t can be expressed as the sum of an average and a fluctuating part

$$T(\mathbf{x}, t) = \overline{T(\mathbf{x})} + T'(\mathbf{x}, t) \qquad (1)$$

where the overbar represents the time average and the prime denotes the fluctuating component. As pointed out by Osborne Reynolds during the last century, this separation is only unique if the averaging period, P, is chosen so that there is little variability with periods between P and the dominant period of the fluctuations. Another way of stating this is that a 'spectral gap' should separate the average and fluctuating components in a Fourier decomposition of a temperature time series. For finestructure work, P must be chosen to be longer than the period of the slowest internal waves, which are also referred to as inertial motions. This period is given, in hours, by 12/sin l, where l is the latitude. Thus, at 30° the inertial period is 24 hours, but at lower latitudes it becomes much longer.

Most commonly, the separation into mean and fluctuating components is made by making a collection, or ensemble, of profiles at one location over an

interval of at least an inertial period. Subtracting the average value at each depth yields an ensemble of the fluctuating parts of the records, each of the form

$$T'(z, t) = T(z, t) - \overline{T(z)}. \qquad (2)$$

Due to observational limitations, there has not yet been a mapping of the temperature field that is accurate over all important length scales or is complete in space and time. Consequently, the statistics used to describe finestructure are elementary. The primary measure of the intensity of the finestructure is the variance, $\overline{(T')^2}$, and the power spectrum, which is formed from a Fourier decomposition of the records. If the spectrum is taken of a collection of spatial records, then it yields the distribution of variance as a function of wavenumber, which is the reciprocal of the length scale.

Figure 4 shows schematic spectra of ensembles of temperature and velocity profiles similar to those in Figure 1. In this case, however, the records have been differentiated so that the spectra represent the wavenumber distribution of the variances of $\frac{dT'}{dZ}$ and $\frac{dU'}{dZ}$. Both spectra have nearly identical shapes, indicating that the processes responsible for temperature and velocity variability are probably similar. The spectra are nearly flat for wavenumbers less than 0.1 cycles per meter, corresponding to length scales longer than 10 m. They "fall off" between 0.1 and 2 cpm, reaching a local maximum in the microstructure range at wavenumbers between 5 and 100 cpm. The level of the spectra in the microstructure range is highly variable compared to the more uniform levels at lower wavenumbers. Much of the sharp finestructure evident in records such as Figure 1 has wavenumbers in the "roll off" region and is surprisingly uniform in spectral level and slope.

Another simple statistic useful for describing finestructure is the probability of obtaining a particular temperature difference over a vertical separation, ΔZ,

$$\frac{\Delta T}{\Delta Z} = \frac{T(Z+\Delta Z) - T(Z)}{\Delta Z}. \qquad (3)$$

A higher order of statistical approach is the study of the lengths, or times, over which fluctuations are coherent. For example, if a collection of simultaneous temperature profiles is made at different positions, the horizontal coherence as a function of horizontal separation is defined to be

$$R(Z, \Delta X) = \frac{\langle T'(X, Z)\, T'(X+\Delta X, Z)\rangle}{\langle (T'(Z))^2\rangle}. \qquad (4)$$

This is used in determining the aspect ratio of finestructure.

These statistics are used to obtain quantitative descriptions of finestructure that can be compared with predictions from analytical and numerical models of particular processes.

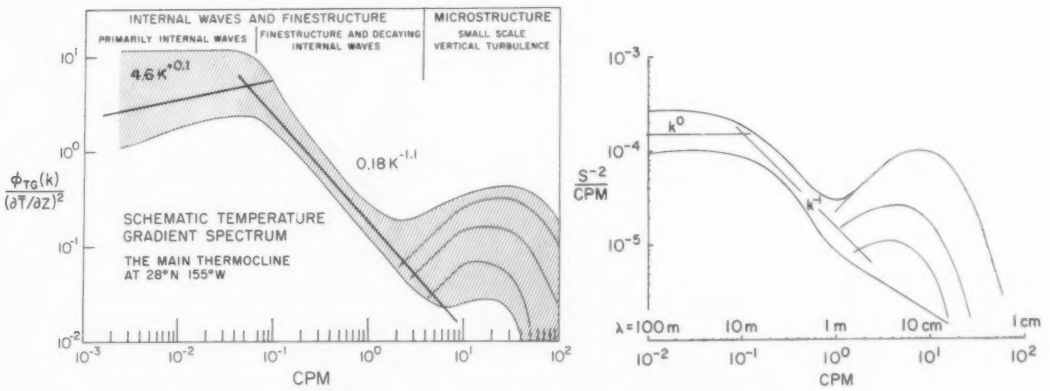

Figure 4. Schematic spectra of the vertical temperature gradient, $\partial T'/\partial Z$, and the vertical gradient of horizontal velocity, $\partial U'/\partial Z$. Both have similar shapes over a wide band of wavenumbers.[4, 7]

Processes Forming Finestructure

Some of the finestructure is formed irreversibly by mixing processes and will persist after the mixing ceases, until it is altered or destroyed by another event. Two basic processes are responsible for forming irreversible finestructure: three-dimensional turbulence and double diffusion. The turbulence may be produced by many mechanisms, depending upon local conditions, but it has some characteristics that appear to be universal with turbulence in laboratory tanks and other environments, such as the atmosphere. The major interest of oceanographers is to determine the conditions under which the turbulence is generated and the resultant net changes to the temperature, salinity, and velocity fields. Double diffusion can occur only in places where the temperature and salinity gradients occur in the proper relationship to each other, unlike turbulence, which occurs everywhere in the ocean. Internal waves play a role in both of these mixing processes; they generate turbulence throughout most of the ocean but may inhibit double diffusion. In addition, internal waves produce reversible finestructure by straining the temperature field. Unlike the products of mixing, this finestructure would disappear if the internal wave field vanished.

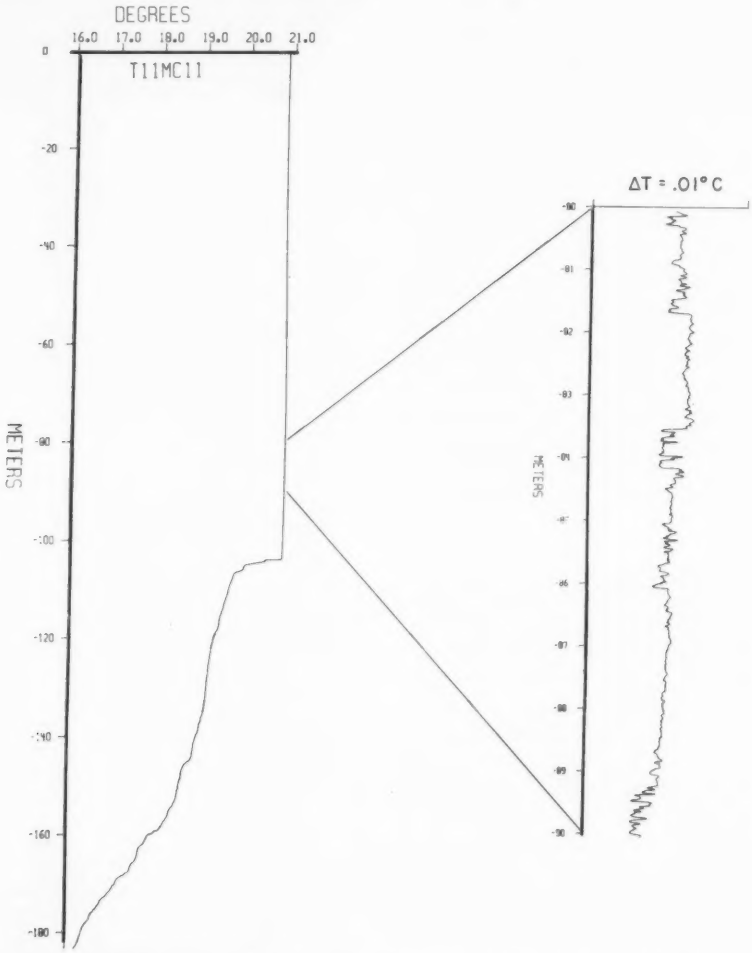

Figure 5. A well-mixed surface layer formed by cooling at the sea surface. Although the net temperature difference across the 100-m-deep layer was less than .01°C, detailed microstructure measurements show fluctuations of several millidegrees throughout.[5]

Small Scale Turbulence: Overturns and Blini

The basic stratification of the ocean is produced by global differences in the character of air-sea interactions, which results in a wide variation in the density of the surface water. In polar regions the dominant effect of the exchange upon the ocean is the cooling of the surface water, which produces high densities. The Weddell Sea in the Antarctic has surface densities greater than those formed anywhere else; hence, that water sinks to the bottom and spreads out over the sea floor. In the tropics, air-sea exchanges add heat to the upper ocean, producing low density surface water, which remains on the surface and is transported to higher latitudes by the mean circulation.

For a mixing event to occur, the local stratification must be overturned. At the sea surface this can be accomplished by the presence of cool air, which produces dense water that can sink to depths of hundreds of meters (top right in Figure 2), or by wind-generated turbulence (top center in Figure 2). The resultant surface mixed layers can have nearly isothermal average profiles and extend tens to hundreds of meters below the surface. However, detailed profiles always show millidegree temperature fluctuations within these layers (Figure 5).

Near the sea floor, hydrothermal activity, such as the vents found on spreading ridges, can also produce convective mixing, but this occurs over a much smaller geographical extent than does convective cooling of the surface. More widespread is the formation of bottom mixed layers by tidal currents (Figure 2, bottom left) and internal waves breaking on continental and island slopes (Figure 2, left edge and Figure 6).

Well away from the sea surface or bottom, turbulence is generated when kinetic energy is released from the internal wave field or from the mean flow. This can happen by two mechanisms: shear instability and advective overturning. The former occurs when the vertical shear, dU/dZ, becomes large with respect to the stratification. The criterion for this is that a dimensionless parameter, known as the Richardson number, be less than 1/4, i.e.,

$$Ri = \frac{N^2}{(dU/dZ)^2} < 1/4 \qquad (5)$$

where $\varrho(Z)$ is the density and $N^2 = \frac{-g}{\varrho}\frac{d\varrho}{dZ}$ is a measure of the stratification, termed the stability frequency. Shear instabilities sometimes form a sequence of overturning vortices (shown schematically in the upper center of Figure 2). This particular form, known as the Kelvin-Helmholtz instability, has been thoroughly studied in laboratory tanks. Advective overturning occurs when the water particles of large-

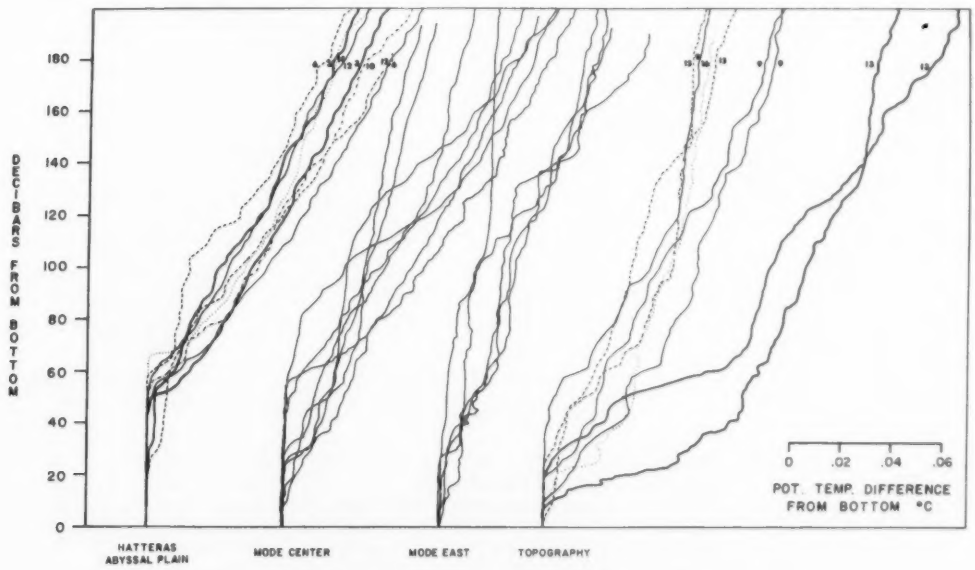

Figure 6. Variations in the thickness of the bottom well-mixed layer in the Western North Atlantic basin.[9]

amplitude internal waves are carried forward of the wave crest, much like the roll-over and breaking of surface waves near shore (Figure 2, lower right). Although many overturns have been observed with high-resolution profilers, little is known about the relative importance of these two mechanisms, due to the lack of time histories of individual events.

However generated, once the turbulence in a breaking event decays, a patch of water is left behind which has a more homogenous profile than before. If the mixing went to completion, the mixed patch would have a nearly isothermal profile. In practice this is rarely the case, and the patch is only partially mixed before the turbulence decays. The mixed patch, which may have a vertical scale of tens of centimeters to as much as 10 m, is then distorted by the internal wave field and in addition, spreads laterally as it collapses gravitationally.

A collapse has not been fully documented but is inferred from measurements of laboratory events and 'snapshots' from tow-yo temperature maps. An example of such a snapshot made in the near-surface water is shown in Figure 7. Two days after the storm that produced the profile in Figure 5, which was well-mixed to 100 m, the surface water was separated into distinct layers at some sites. The layers were 50 m thick. Stations C and D had two of these layers, while Station B had three, and Station A remained as a single 100-m-thick surface layer with a 50-m-thick layer below. It was possible to trace the lenses laterally for at least 20 km. The same surface water occurred at B, C, and D, while the surface water at A was the same as the middle layer at B.

The spreading is driven by the horizontal pressure gradients created by the presence of the mixed patch itself. For a mixing event occurring in the thermocline, the pressure gradient is due to the difference in density of the water within the mixed layer compared to the undisturbed profile (Figure 8). If the density profile is initially linear and the mixing event goes to completion, the horizontal density difference across the layer, as a function of distance z from the center of the layer, is

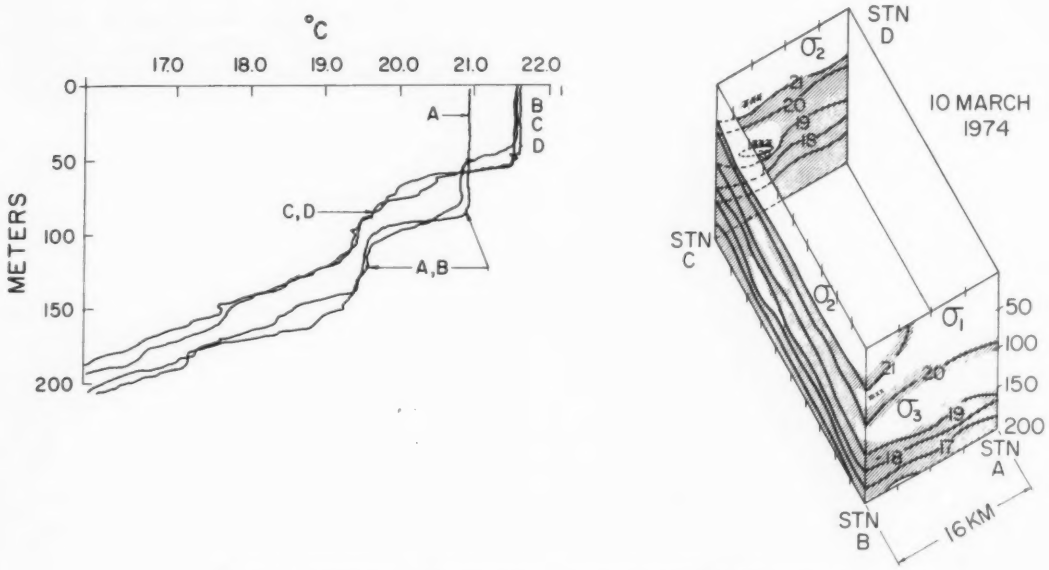

Figure 7. "Snapshot" of near-surface interleaving structures following a storm. In the isometric view, homogenous water is clear and the high-gradient regions are shaded. The profile at A had a 100-m-thick well-mixed surface layer (also see Figure 5) and a less homogenous 50-m-thick layer below that. At Station B there were three successive 50-m-thick layers, the bottom two of which were the same as those at Station A. The upper layer at Station B had the same water as the surface layers at Stations C and D. XBT profiles between the stations showed the boundary of the upper water to be between A and B.[3]

$$\Delta\varrho\,(Z) = -\frac{\overline{d\varrho}}{dZ}\,Z \qquad (6)$$

where $\overline{d\varrho}/dZ$ is the initial density gradient. (This difference is shown as the separation of the dotted and solid density curves in Figure 8.) The corresponding horizontal pressure gradient at the vertical center of the mixed layer can then be obtained from the hydrostatic equation

$$\Delta P = -g\int_{\frac{h_0}{2}}^{0}\Delta\varrho(Z)dZ = -g\frac{\overline{d\varrho}}{dZ}\,\frac{h_0^2}{8}. \qquad (7)$$

Laboratory studies have shown that the initial spreading velocity, U_0, can be accurately estimated by using the Bernoulli equation for incompressible, frictionless flow. This yields

$$\frac{1}{2}\,\varrho\,U_0^2 = \Delta P = -g\frac{\overline{d\varrho}}{dZ}\,\frac{h_0^2}{8}$$

or (8)

$$U_0 = \frac{h_0\,N}{2}\,.$$

Since N = 0.01 radians/sec is a typical value for the upper ocean, U_0 = cm/sec for h_0 = 10 m and U_0 = 1/2 cm/sec for h_0 = 1 m. Although these values are comparable to typical internal wave velocities, the velocity signature of a collapsing mixed region has not yet been observed.

Since the patches are believed to become roughly circular and to be very thin in relation to their horizontal extent, the Russian word for pancake, "blini," is often used to describe them.

If turbulent mixing were the dominant process forming the finestructure and if the mixing went to completion in each patch, the profiles of temperature, salinity, and density would have the appearance of "stair steps." The individual patches would be marked by sharp boundaries, forming the treads of the stair-steps, which would be thin in relation to the more homogenous sections forming the risers. In addition, the smooth change in the temperature-salinity relation found in undisturbed profiles would become discontinuous due to the mixing.

Although a 'sheet and layer' model of the thermocline has been used as the basis for analytical models of finestructure, observations show that only rarely is the mixing of sufficient intensity and duration to produce stair-step profiles. One example of a distinct stair-step was found very close to the island of Bermuda and has at least six distinct well-mixed layers in a 75-m-thick section (Figure 9). A more typical profile, which is characteristic of large regions in

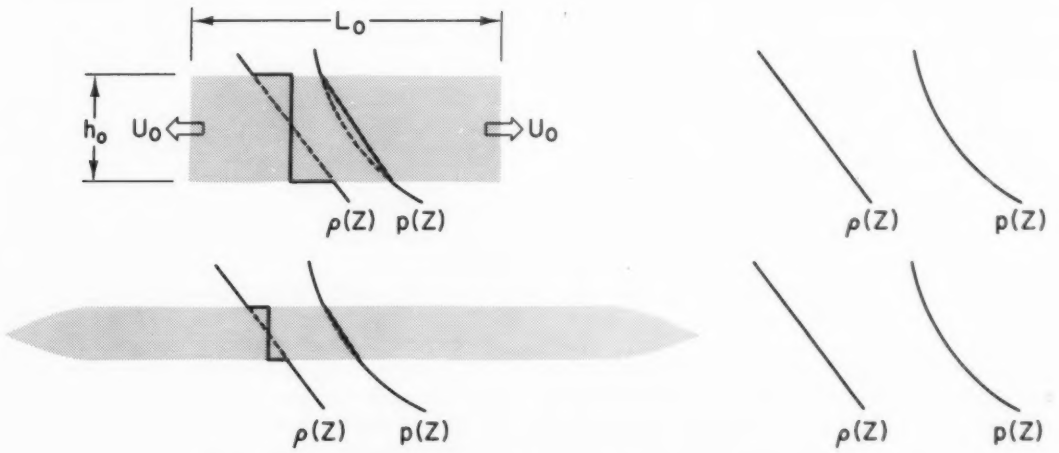

Figure 8. Schematic of the gravitational collapse of a fully mixed region in the thermocline, which is initially h_0 meters high and L_0 meters across. The initial density profile, $\varrho(Z)$, was linear, as shown at the right. The spreading motion is driven by the horizontal pressure gradient, which results from the mixing. This gradient is shown by the separation of the dotted and solid pressure curves, p(z), through the layer.

the mid-ocean, is also shown in Figure 9. In the upper plot the mixed regions are clearly shown when $\frac{\Delta T}{\Delta Z}$ is formed, while in the lower plot the distinction between sheets and layers is not at all clear.

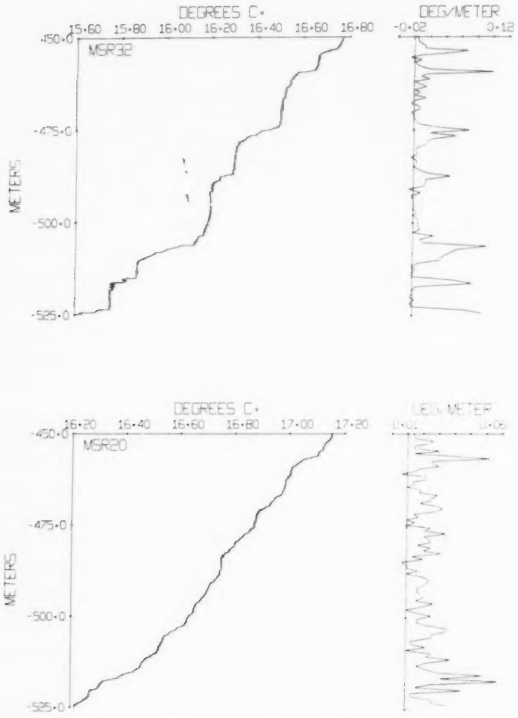

Figure 9. Temperature profiles taken near the island of Bermuda. The upper record was taken a few km from shore and had distinctive stair-step structures extending over a 75-m span. The well-mixed layers are clearly defined by the variability in $\Delta T/\Delta Z$ (shown on the right for ΔZ = 0.8 m). Accompanying microstructure observations showed that intense mixing was occurring in this section. The lower profile was taken farther off shore and is typical of the main thermocline. The finestructure is irregular and does not admit a separation into high and low gradient sections. Microstructure measurements showed low levels of turbulent mixing.[10]

A comparison of the degree of 'mixedness' of the profiles can be made more quantitative by comparing histograms of $\frac{\Delta T}{\Delta Z}$. If the differencing scales, ΔZ, is less than or equal to the scales of the layers, the histograms should exhibit a large fraction of values with very low mean gradients. The histogram formed from the 'steppy' record shows that the lowest bin is the most probable; 26% of the profile can be considered to be well-mixed (Figure 10, left). By contrast, a large number of typical records have a most probable value that is about 1/2 the mean gradient (Figure 10, right), with only 8% of the record in the smallest positive bin. Thus, in the typical profile, even if all of the finestructure is due to turbulent mixing events, only a small percentage of the overturns mix to completion.

Lateral tracing of mixed regions in the thermocline has been attempted by using tow-yos to follow their high-gradient boundaries. This has proved to be very difficult, due to the internal wave field, which displaces and distorts the patches. The displacement can be dealt with by plotting $\frac{\Delta T}{\Delta Z}$ vs T, or $\frac{\Delta \varrho}{\Delta Z}$ vs ϱ along a collection of saw-tooth profiles. This reflects the spreading of the collapsing mixed regions along isopycnal surfaces and not across them. However, the distortion of the wave field makes it very difficult to identify patch boundaries for more than a few hundred meters. Better techniques for observing changes in the temperature-salinity relation through these partially mixed regions are required.

Internal Waves and Reversible Finestructure

Internal waves displace water particles from the positions they would occupy if the waves were not present. The displacement of one particle is the sum of many nearly periodic motions. Motions with dominant frequencies near the high frequency limit of the internal wave band, i.e., f = N, are primarily vertical, since the buoyant force restores the displaced water to its original position. Near the low frequency limit, i.e., f_i = (sin l)/12 (cycles per hour), the motions are primarily horizontal, due to the dominant role of the Coriolis force in restoring displacements. At intermediate frequencies, i.e., $f_i << f << N$, displacement have appreciable components in both the horizontal and vertical directions. Typical rms amplitudes are 7 m in the vertical and 1 km in the horizontal.

Except when breaking events occur, internal waves produce no mixing; hence, the scalar fields act as passive "tags" on the water particles, and it is possible to infer a great deal about the displacement field $\eta(\mathbf{x}, t)$ by mapping scalar fields. Due to the difficulties of measuring salinity, the temperature field is the one most commonly used, although the density field would be the most desirable.

Since length scales of a meter and greater are involved in internal wave displacements, molecular diffusion is negligible and the heat equation can be written as

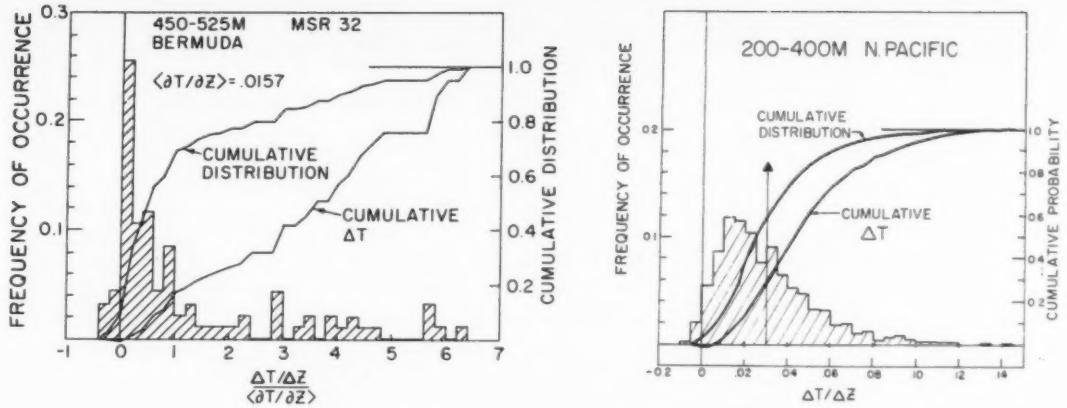

Figure 10. Histograms of ΔT/ΔZ. The plot on the left was formed from the record shown in the upper half of Figure 9. The plot on the right was made from a collection of profiles taken in the North Pacific, which were similar to the data in the lower half of the previous figure. The stair-step Bermuda record has a preponderance of values in the lowest bin, while the typical data have a most probable value that is about half the mean gradient (shown by the arrow).[10]

$$\frac{\partial T}{\partial t} + \mathbf{u} \cdot \nabla T = O. \tag{9}$$

Using the separation of the temperature field into mean and fluctuating components, equation (1), and the observed fact that the major effect of internal waves on the temperature field is due to vertical motions, this equation becomes

$$\frac{\partial T'}{\partial t} + w \frac{\partial \overline{T}}{\partial Z} = O \tag{10}$$

where w is the vertical velocity.

Integrating the above equation gives

$$T' = -\eta \frac{\partial \overline{T}}{\partial Z} \tag{11}$$

where

$$\eta = \int_o^t w dt$$

is the displacement.

The above relation permits the vertical displacement field to be determined simply from observations of temperature fluctuations. This has been done with collections of CTD profiles and with horizontal sections from tows of thermistor chains. Figure 11 shows the temperatures recorded by an 80-m section of the NRL thermistor chain operated just below the base of the mixed layer. Sections in which the traces are widely spaced are regions of high temperature gradient, and hence of large temperature differences between nearby thermistors. Convergent temperature traces occur where the profile is weakly stratified and adjacent probes have nearly the same temperature. Records such as this one are converted to a displacement cross section by first computing the average temperature for each thermistor. Then the displacement at the ith sensor is computed using

$$\eta_i = \frac{T_i - \overline{T_i}}{\left(\frac{T_{i-1} - T_{i+1}}{Z_{i-1} - Z_{i+1}}\right)} \tag{12}$$

Clearly, if some of the temperature variability is due to irreversible finestructure, the procedure will give incorrect answers, a limitation that may be serious for vertical scales of several meters or less.

Conversion of equation (11) to a power spectrum yields a simple relation between $\Phi_\eta(k)$, the spectrum of vertical displacement, and $\Phi_T(k)$, the temperature spectrum

$$\Phi_\eta(k) = \frac{\Phi_T(k)}{\left(\frac{\partial \overline{T}}{\partial Z}\right)^2} . \tag{13}$$

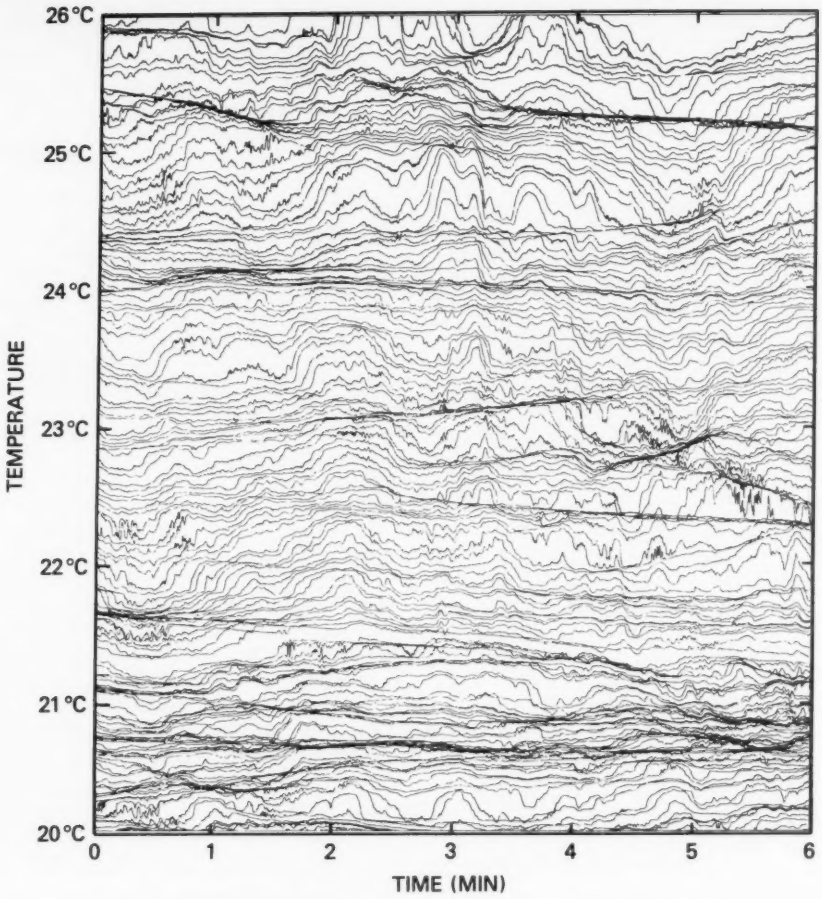

Figure 11. Temperature traces from the topmost 80 m of the Naval Research Laboratory (NRL) chain. The speed was 2.5 m/s, corresponding to 150 m/min. Regions of large gradient are shown by increased distances between traces, while low gradient sections appear with large separations. (The plot was kindly supplied by E. E. Rudd and B. S. Okawa of NRL.)

The above relationship was used in the construction of the model internal wave spectrum by Garrett and Munk[1,2], which has been found to be a remarkably good first approximation to the observed internal wave spectrum. The spectral levels have not been found to vary by more than a factor of four throughout the ocean, except for more intense levels found on the equator.

A simple linear relationship such as equation (11) does not provide a mechanism for forming the meter-scale irregular kinks and wiggles which are so pervasive in observed profiles. For these features to be produced by internal wave displacements, it is necessary that adjacent isothermal surfaces be 'squeezed' much closer together or moved farther apart than their average separations. This straining of the profile over scales of meters or less is inherently nonlinear, and thus is not included in a simple relationship such as equation (6), which provides no description of the *difference* in displacements over distances of a few meters.

Initially, oceanographers generally assumed that most of the finestructure kinks represented the boundaries between mixed or partially mixed blini. However, Lazier[3] pointed out that repeated temperature profiles made in a lake showed the kinks migrating vertically through the temperature field with time. This can only be due to internal waves with frequen-

cies that are intermediate between the stability frequency and the inertial frequency propagating at an angle to the horizontal. An example from the ocean is shown in Figure 12.

Consider the two isotherms shown schematically in Figure 13. The lower isotherm has an equilibrium position Z_1' and is shown to be displaced η_1 so that it appears at $Z_1 = Z_1' + \eta_1$. The upper isotherm has an equilibrium position at Z_2', which is a distance y above the first isotherm, and is displaced η_2 from its equilibrium position. The instantaneous separation is $Z_2 - Z_1 = \delta$ and the temperature gradient between Z_2 and Z_1 is $(T_2 - T_1)/\delta$; by comparison, the mean temperature gradient has been assumed to be $(T_2 - T_1)/y$. Thus, if $\delta/y < 1$, the instantaneous gradient between Z_2 and Z_1 will be greater than the mean gradient; and if $\frac{\delta}{y} > 1$, the instantaneous gradient will be less than average.

The probability of having simultaneous displacements η_1 and η_2 for isotherms having an equilibrium separation y has not been measured. The simplest assumption is that this function is similar to a joint Gaussian distribution

$$P(\eta_1, \eta_2/y) = \frac{1}{[2\pi Z^2(1-r)]^{1/2}} \exp\left[-\frac{\eta_1^2 + \eta_2^2 - r\eta_1\eta_2}{2Z^2(1-r^2)}\right] \quad (14)$$

where r(y) is the correlation function (it equals 1 for $y = 0$) and Z is the rms displacement for a single isotherm. This function is smooth and symmetrical; if it is integrated to produce the probability density for only one isotherm it becomes the familiar 'bell' curve.

Desaubies and Gregg[4] inverted equation 14 to give $P(y/\delta)$, the probability density of observing any pair of isotherms having an equilibrium separation y, given a pair of sensors separated by δ. Unlike equation 14, $P(y/\delta)$ is not symmetric, but is highly skewed. Using the mean gradient to form $P(\frac{\Delta T}{\delta})$ gives a quantity that can readily be compared with the measured temperature differences. It was found that the derived function reproduces the essential features of the histograms of open ocean data (Figure 9, right), including the skewness, which results in a maximum at 1/2 the average gradient and a long tail extending to high gradients.

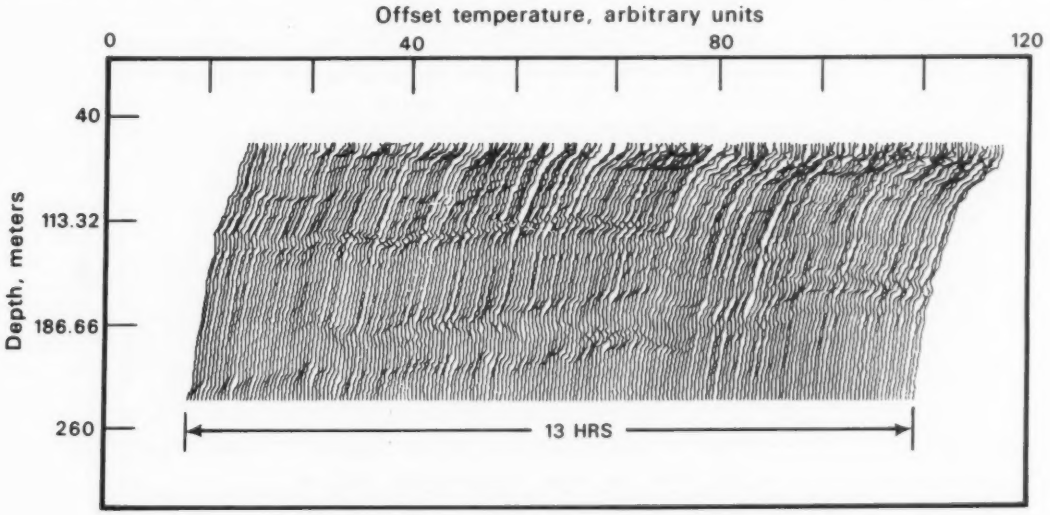

Figure 12. A 13-hour long time series of temperature profiles. Successive profiles have been offset for display. High gradient features can be seen to migrate vertically with time. The movement is upward with respect to temperature, as well as pressure, indicating that the features must be due to internal wave strain.[11]

This approach does not prove that most of the meter-scale fluctuations are in fact due to internal wave strain, but does show that such a result is consistent with what is known of the displacement field.

Double Diffusion

Although the thermal contrast of warm water at the surface and cold water near the bottom provides

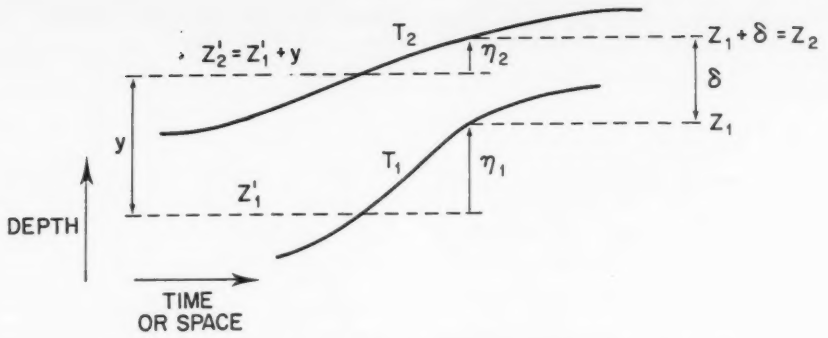

Figure 13. Schematic showing the positions of two isotherms, T_1 and T_2. The isotherms have been displaced by η_1 and η_2 from their equilibrium positions, Z_1' and Z_2', respectively. The instantaneous gradient measured between Z_1 and Z_2 is $(T_2 - T_1)/\delta$, which is greater than the average gradient, $(T_2 - T_1)/y$.[4]

the dominant stratification of the ocean, the role of salinity is not negligible. Temperature and salinity can have three possible relationships in a stably stratified profile: (A) warm, high salinity water over colder, less saline water; (B) warm, low salinity water over colder, more saline water and; (C) cold, low salinity water over warm, high salinity water. For a two-layer system, these possibilities are shown as A, B, and C in the temperature-salinity diagram of Figure 14. Both A and B are found over large fractions of the ocean, while C occurs in some coastal regions or in local structures near fronts.

The molecular diffusivity of heat in water is about 100 times greater than the diffusivity of dissolved salt. Consequently, if a two-layer fluid system is formed, the temperature profile will be rapidly altered by diffusion, while that of salt will be changed only a small amount. For case A, warm salty over cold fresh, the rapid heat flux across the interface will destabilize the stratification of the interface by producing water that is relatively cool and salty just above the interface and water that is relatively warm and fresh immediately below it (dotted curves in Figure 14, left). Since the altered water above the interface is more dense than the water below, it will sink. Similarly, the water just below the interface will rise. The combined effect produces a pattern of cells of alternately descending and rising fluid that are termed salt fingers. Case A is therefore called the "salt finger regime."

In case B, both the temperature and salinity fields stratify the profile so the differential rates of diffusion do not produce any instabilities. Hence, this case is termed diffusively stable.

In case C the thermal diffusion produces water on the top side of the interface that is relatively warm and fresh; hence, it is less dense than the water above it. A similar result occurs with the the cool and salty water produced on the lower side of the interface, which becomes more dense than the water below it. In this case two convecting cells are established, one above the interface and one below. For want of a better name, case C is termed the "diffusive regime."

Both of the diffusively unstable motions act to transport heat and salt much more rapidly than would be the case for simple molecular transport along the mean gradients. The salt fingering regime accomplishes this by the fluid motions in the fingers, while the diffusive regime uses a combination of molecular diffusion across a very sharp interface, which is kept thin by the "sweeping" action of the convective cells and the vertical component of the convective motions. In thermodynamic terms these regimes are dissipative structures. Salt fingers are more efficient than the diffusive regime. Both act to transport heat in such a way that there is an upward flux of buoyancy; hence, water below the interface becomes more dense and that above becomes less dense.

Experiments performed in sufficiently deep laboratory tanks reveal that both double diffusivity regimes produce convective motions that are self limiting. Lateral diffusion across the salt fingers reduces their density contrast so that the fingers have lengths of 1 to 20 cm, depending upon the initial conditions. However, below and above the interface the convective motions persist, producing thick well-mixed layers. The new boundaries of these layers in turn become sites of salt fingering, resulting in a full stair-step profile (Figure 2, bottom center). A similar result occurs for the diffusive regime.

Double diffusion ceased to be a laboratory curi-

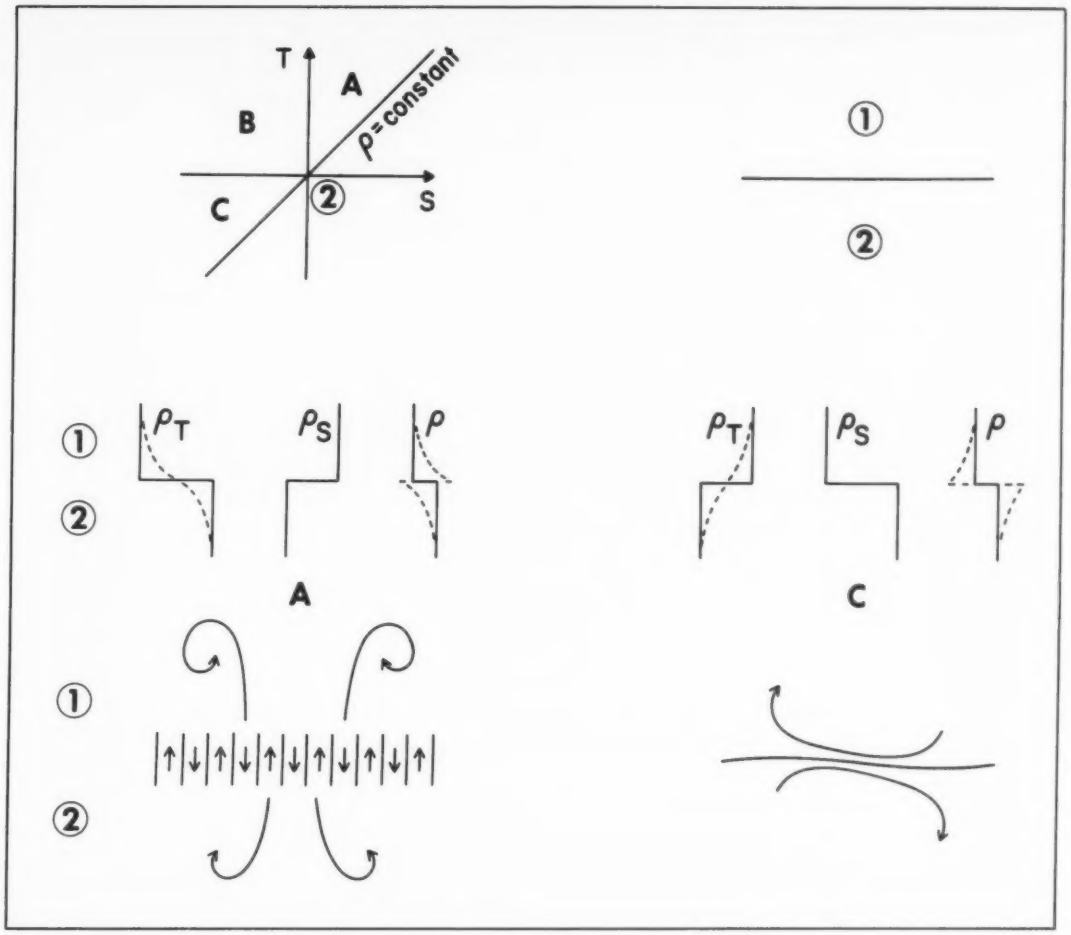

Figure 14. Schematic of the two types of double-diffusive convection for a two-layer profile. The temperature-salinity diagram (upper left) shows the possible temperature and salinity ranges of the upper fluid, 1, with respect to the lower, 2. Those ts combinations that are above the ϱ = CST. line are statically stable. Two of the three types of temperature-salinity relations above the line are diffusively unstable; A (warm, saline over cool, fresh) and C (cool, fresh over warm, saline). The third possibility is diffusively stable; this is B (warm, fresh over cool, saline). In case A, the more rapid diffusion of heat across the interface (dotted line) compared to the salt diffusion produces salt fingers across the interface.

osity with the discovery of thick sections of oceanic profiles containing very distinct stair steps, as shown in Figures 15 and 16. The example in Figure 15 was found in the Mediterranean Sea; others have been discovered in restricted regions of the North Atlantic and the Caribbean. Optical observations have revealed the distinctive signatures of salt fingers on the interfaces between layers, while horizontal sections have traced layers for tens of kilometers. Figure 16 shows a 150-m-thick section from the Arctic Ocean, over which temperature increases with increasing depth. The steps are signatures of the diffusive regime.

Although broad areas of the upper ocean are potentially sites for salt fingering, layers such as those in Figure 15 have been found at only a few

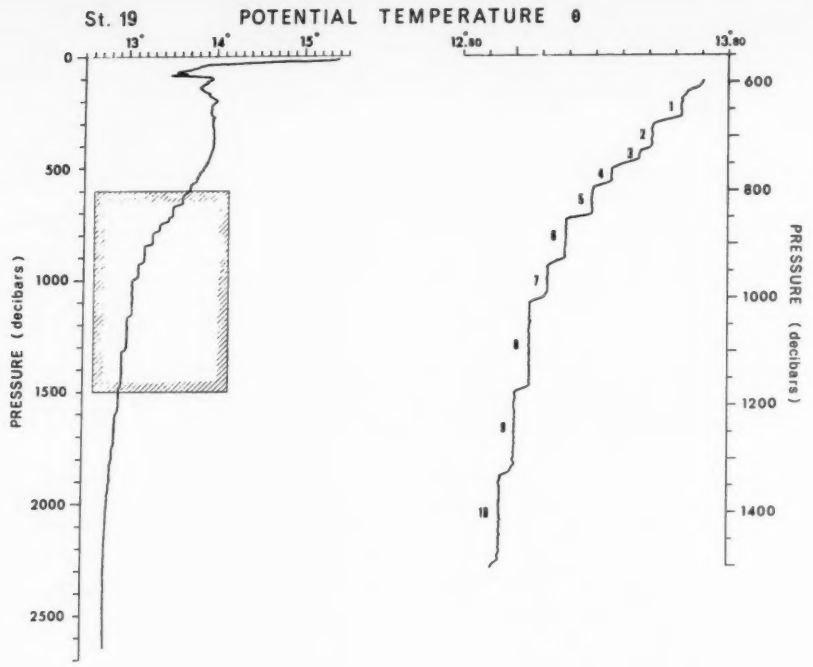

Figure 15. A sequence of 10 distinct layers in the Tyrrhenian Sea which were formed by salt fingering.[12]

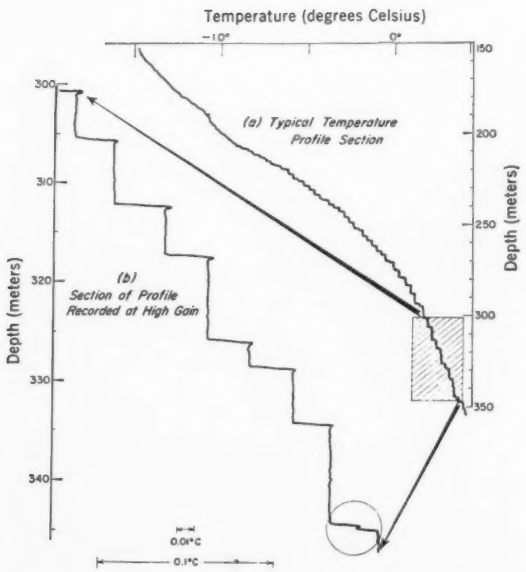
Temperature (degrees Celsius)
(a) Typical Temperature Profile Section
(b) Section of Profile Recorded at High Gain
Depth (meters)
Depth (meters)

Figure 16. A sequence of steps of increasing temperature with increasing depth formed by the diffusive regime in the Arctic Ocean.[13]

sites. The reason for this is not known, but disruption of the fingers by internal wave motions is suspected. The amount of ocean that is unstable to the diffusive regime is much more limited; only a few places have thick temperature inversions such as the one in the Arctic. However, both facets of double diffusion have been found to play a major role in lateral mixing across fronts that have temperature and salinity contrasts.

Laboratory experiments have been done to simulate the horizontal gradients across fronts. Two fluids with different diffusivities are placed on opposite sides of a vertical barrier (Figure 17). Each side is established with the same density profile so that there will be no horizontal pressure gradients when the barrier is removed. However, it is found that intruding tongues promptly form, with salt fingers and diffusive steps on the interfaces between adjacent tongues. The density fluxes due to double diffusion create horizontal pressure gradients, which drive the intruding motion.

Lateral gradients similar to the laboratory situation are formed across fronts in the ocean. CTD towyos reveal the presence of multiple interleavings across most fronts, which are similar to those in

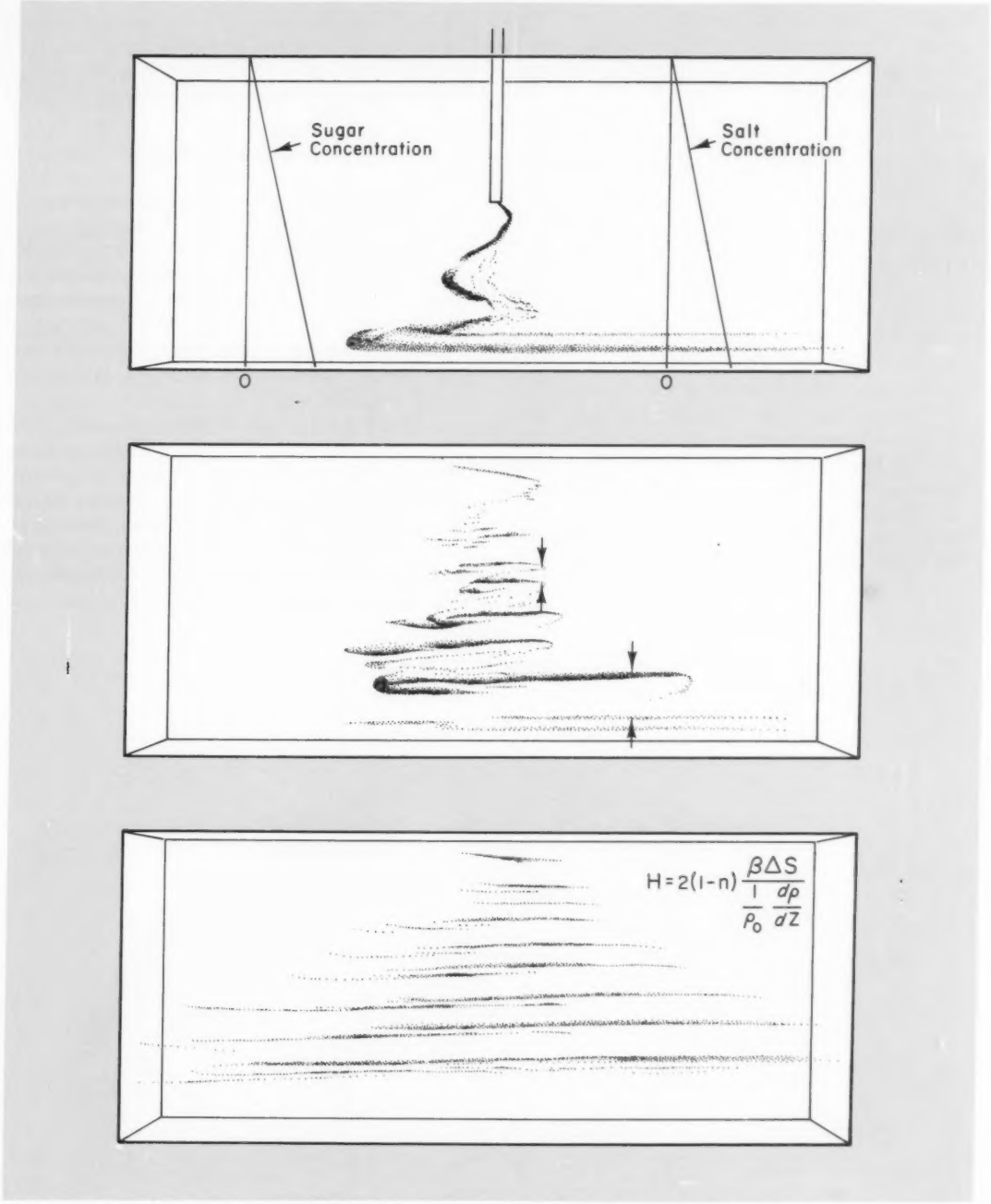

Figure 17. The formation of interleaving tongues of water driven by double diffusion. Two fluids having the same density profile, but different diffusivities, are established on opposite sides of a vertical barrier. After the barrier is removed, layers form, which have salt fingers and small diffusive steps on alternating boundaries. This is believed to be similar to the lateral processes occurring across oceanic fronts.[14]

Figure 17. The scale of these intrusions varies from about 1 meter to tens of meters and seems to be in rough agreement with the scales predicted by the laboratory experiments.

Because salt fingers are more efficient than the diffusive regime, they produce greater density fluxes. Consequently, cold, fresh intrusions, which have fingers on their lower boundaries, become more buoyant and rise vertically across constant density surfaces. Likewise, the salt fingers on the upper boundaries of warm, saline intrusions cause the intrusions to become less buoyant and to sink across density surfaces as they move laterally. Such motions can produce large lateral and vertical fluxes in frontal regimes. Figure 18 shows a three-dimensional map of such a tongue sloping across density surfaces.

Finestructure due to tongues intruding across fronts dominates the temperature and salinity fields in many oceanic regions, particularly in coastal locations and in the open ocean transitions between major circulation gyres. Figure 19 shows the frontal zones where strong interleaving may be expected in the upper waters of the North Pacific. It remains to be determined how many of the intrusions are formed by double diffusion and how many result from other processes, such as instabilities in long waves along the front, and are then modified by double diffusion.

Future Directions

The present view of finestructure is based on a very limited observational data base. Much remains to be done to understand the processes that produce the fluctuations and their significance in the hierarchy of ocean physics. The work has two major thrusts: more complete observational programs to follow the evolution of particular events, and systematic surveys to assess geographical and, perhaps, seasonal variability.

Measurements made to date, even during intensive programs in limited geographical regions, have not included many important aspects of the features being studied. For example, when mapping has been done using a CTD tow-yo or tow chain, the measurements usually have not resolved temperature and salinity to the meter scale. Hence, it has not been

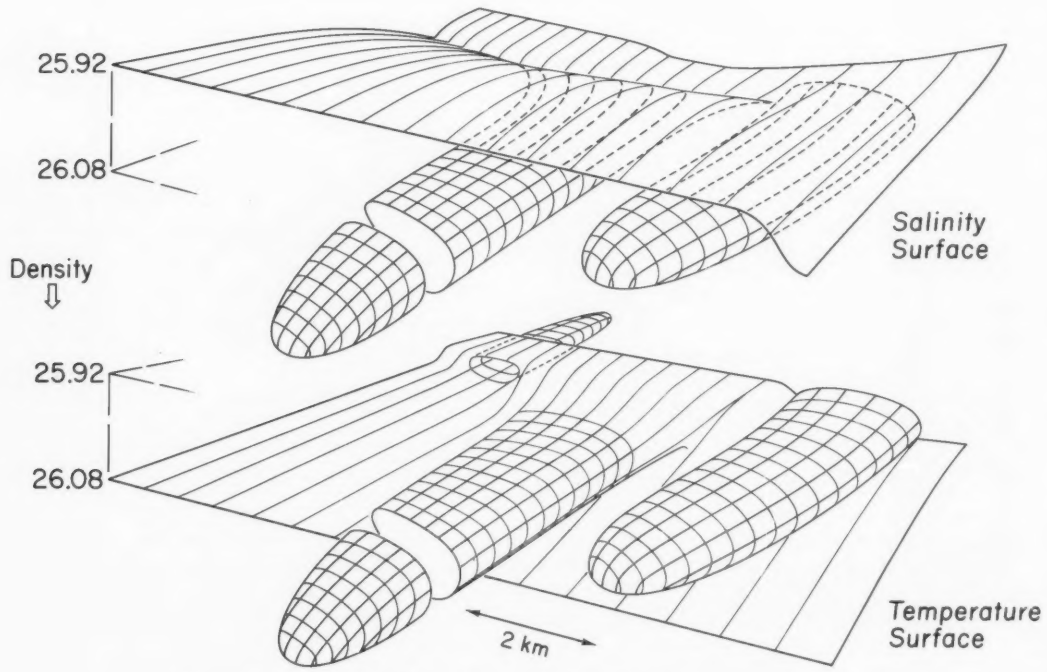

Figure 18. Isometric views of the temperature and salinity surfaces across a temperature-salinity front. Density was used as the vertical axis, instead of pressure or depth, to remove internal wave displacements. The vertical dimension of the major tongue was about 10 m.[15]

possible to study variability in the temperature-salinity relation, nor to estimate the weak horizontal pressure gradients. Even though velocity profiles have been obtained with the XCP during some of these programs, uncertainty in depth and temperature calibrations has precluded detailed comparisons. When maps of specific features have been made, such as Figures 7 or 18, they have included neither sufficient information about the larger environment nor the temporal evolution of the mapped structures. Without more complete information, it is not possible to make accurate estimates of force balances or of the net changes produced in the large-scale fields.

The global significance of finescale processes is a statistical problem. Once the net effect of individual processes is defined by local experiments, it will be necessary to measure how frequently, and with what intensity, the different processes occur over representative geographical locations. For example, a time history of three-dimensional maps similar to Figure 18 could yield the net fluxes of heat and salt across a front due to the formation of one interleaving tongue. However, it is not feasible to do such detailed measurements to follow all of the tongues on even a small section of a single front. The detailed results must be extrapolated using less detailed survey data.

Although the focus of this discussion has been on our understanding of the role of finestructure in ocean physics, there are other related effects in biological and chemical variability and acoustic transmission. One of the most important interactions with biology is the effect of finestructure on spatial distribution patterns. Plankton do not occur randomly but tend to be concentrated in distinct patches. At least some of these patches occur on the high density gradients associated with the "kinks" in XBT traces. Understanding the history of the kinks may aid in deciphering why they are a favorite environment for plankton. Variations in sound speed produced by finestructure affect the propagation of acoustic energy having wavelengths comparable to or smaller than the finestructure. Thus, finestructure will affect the propagation of standard sonar frequencies. Since some of the intrusive tongues have sound speed fluctuations of several m/s, the effects will often be strong. Knowledge of the general regime, e.g., "Is the site in a frontal zone?" will help in understanding acoustic conditions. ■

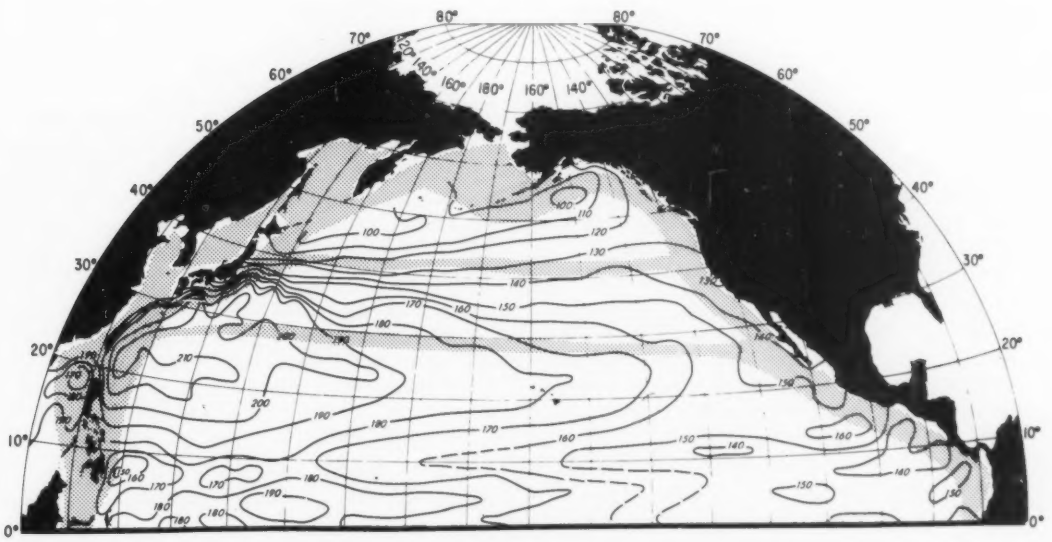

Figure 19. Solid lines show the dynamic topography of the North Pacific.[16] The shaded zones indicate the major near-surface fronts, where interleaving finestructure may be expected.

References

1. Garrett, C. and W. Munk, "Space-time Scales of Internal Waves: a Progress Report," *Journal of Geophysical Research,* 80 (1975), 291-297.

2. Garrett, C. and W. Munk, "Space-time Scales of Internal Waves," *Geophysical Fluid Dynamics,* 2 (1972), 225-264.

3. Lazier, J. R. N., "Temporal Changes in Some Fresh Water Temperature Structures," *Journal of Physical Oceanography,* 8 (1973), 226-229.

4. Desaubies, J. Y. F. and M. C. Gregg, "Reversible and Irreversible Finestructure," *Journal of Physical Oceanography,* 22 (1980), 541-556.

5. Gregg, M. C. and M. G. Briscoe, "Internal Waves, Finestructure, Microstructure, and Mixing in the Ocean," *Reviews of Geophysics and Space Physics,* 17 (1979), 1524-1548.

6. Gregg, M. C., "Variations in the Intensity of Small-scale Mixing in the Main Thermocline," *Journal of Physical Oceanography,* 7 (1977), 436-454.

7. Gargett, A. E., P. J. Hendricks, T. B. Sanford, T. R. Osborn, and A. J. Williams, III, "A Composite Spectrum of Vertical Shear in the Upper Ocean," *Journal of Physical Oceanography,* 11 (1981), 1258-1271.

8. Gregg, M. C., "Fine and Microstructure Observations during the Passage of a Mild Storm," *Journal of Physical Oceanography,* 6 (1976), 528-555.

9. Armi, L. and R. C. Millard, Jr., "The Bottom Boundary Layer of the Deep Ocean," *Journal of Geophysical Research,* 81 (1976), 4983-4990.

10. Gregg, M. C. and T. B. Sanford, "Signatures of Mixing from the Bermuda Slope, the Sargasso Sea, and the Gulf Stream," *Journal of Physical Oceanography,* 10 (1980), 105-127.

11. Pinkel, R., "Upper Ocean Internal Wave Observations from Flip," *Journal of Geophysical Research,* (1975), 3892-3910.

12. Molcard, R. and A. J. Williams, III, "Deep Stepped Structure in the Tyrrhenian Sea," *Memoires Societe Royale des Sciences de Liege,* 6e serie, tome VII (1975), 191-210.

13. Neal, V. and S. Neshyba, "Thermal Stratification in the Arctic Ocean," *Science,* 166 (1969), 373-374.

14. Ruddick, B. R. and J. S. Turner, "The Vertical Length Scale of Double-diffusive Intrusions," *Deep-Sea Research,* 26A (1979), 903-913.

15. Gregg, M. C., "The Three-Dimensional Mapping of a Small Thermohaline Intrusion," *Journal of Physical Oceanography,* 10 (1980), 1468-1492.

16. Wyrtki, K., "The Dynamic Topography of the Pacific Ocean and Its Fluctuations," Report HIG-74-5, (1974), Hawaii Institute of Geophysics.

Dr. Michael Gregg is Research Professor at the University of Washington and Principal Oceanographer at the University's Applied Physics Laboratory. For ten years Professor Gregg has been a principal investigator for the Office of Naval Research. His area of research is small scale mixing processes. For five years Professor Gregg was a U.S. Naval Officer assigned to the Division of Naval Reactors, U.S. Atomic Energy Commission.

research notes

Progress in Synthetic Seismogram Modeling

Office of Naval Research principal investigator Dr. Donald Helmberger at the California Institute of Technology Seismological Laboratory has developed a new method for predicting distortions of waves which reflect off of or transmit through irregular boundaries. The technique is the numerical evaluation of the Kirchhoff-Helmholtz integral. The potential and the normal derivative of the potential on the surface are chosen assuming that the incident wave is a high frequency pulse and that the boundary is locally flat. These assumptions allow one to specify the boundary values with simple analytical functions. The integral is evaluated by breaking the surface into elements and, following Huygen's principle, summing the response of each element appropriately in time to get the potential at the observation point. For both reflected and transmitted problems, the computed solution of this method compares well with existing analytical high frequency solutions. Thus, the method enables one to predict the effects of 3-dimensional structures on both reflected and transmitted high frequency pulses. ■

(J. Michael McKisic, ONR)

Accomplishments in Semiconductor Wafer Polishing Leads to Better Yield and Lower Cost Devices

The introduction of damage into surfaces of semiconductor wafers during polishing has been of concern to device manufacturers for the past two decades. Although considerable empirical progress has been made in the development of acceptable procedures for polishing Si and Ge wafers, the reduction or elimination of residual polishing damage within near surface zones of III-V and II-VI semiconductors has not been satisfactorily addressed, and severe problems remain, both in relation to the growth of epitaxial layers and in device processing. Unfortunately, wafer polishing methods used to date are "recipes" largely absent of scientific understanding.

Drs. Thomas Magee and Robert Ormond of Advanced Research and Applications Corporation (ARACOR) have recently conducted with the support of the Office of Naval Research an in-depth analysis of semiconductor surfaces using high resolution transmission electron microscopy (TEM). They have found that a conventionally polished semiconductor wafer has defects known as dislocation nesting and line looping to depths as great as 15 micrometers beneath the surface. These defects are typically of a size commensurate with the lithographic resolution required of very high speed integrated circuit type devices. As such, they cause devices to operate at less than specified performance, reduce yield, and raise cost.

Starting with a non-contract hydroplane polisher developed at Lincoln Labs, the ARACOR group improved the machine to incorporate precisely controlled wafer spin rates, increased the polisher-to-wafer gap, and devised optimum etchant fluids whose viscosity is no longer critical to the process. Using these new techniques, the polished wafer surfaces are now nearly featureless and have no detectable evidence of dislocation nesting, looping dislocations, and/or polishing traces. Surface defect features remaining are equal to those in the bulk of the crystal thereby indicating that the new non-contacting or hydroplane polishing procedure introduces no additional damage to the crystal wafer. These results will be widely publicized and are expected to significantly improve the reproducibility and yield of high performance electronic devices. ■

(Max Yoder, ONR)

DEPARTMENT OF THE NAVY
OFFICE OF NAVAL RESEARCH
ARLINGTON, VA 22217

OFFICIAL BUSINESS
PENALTY FOR PRIVATE USE, $300

POSTAGE AND FEES PAID
DEPARTMENT OF THE NAVY
DOD 316
CONTROLLED CIRCULATION RATE
PRINTED MATTER
CONTROLLED CIRCULATION
PUBLICATION